THE UNIVERSITY OF CHICAGO

DISCOVERY OF ANTI-METASTATIC THERAPIES GUIDED BY THE PHYSIOLOGICAL SUPPRESSOR RAF KINASE INHIBITORY PROTEIN

A DISSERTATION SUBMITTED TO
THE FACULTY OF THE DIVISION OF THE BIOLOGICAL SCIENCES
AND THE PRITZKER SCHOOL OF MEDICINE
IN CANDIDACY FOR THE DEGREE OF
DOCTOR OF PHILOSOPHY

COMMITTEE ON CANCER BIOLOGY

BY
ALI EKREM YESILKANAL

CHICAGO, ILLINOIS
MARCH 2019

To my loving partner, for tirelessly picking up the pieces, gluing them back together, and putting a smile on it.

"You may encounter many defeats, but you must not be defeated. In fact, it may be necessary to encounter the defeats, so you can know who you are, what you can rise from, how you can still come out of it."

- Maya Angelou

"When you can't change the direction of the wind — adjust your sails."

- H. Jackson Brown Jr

"There is nothing noble about being superior to some other man. The true nobility is in being superior to your previous self."

- Hindu proverb

"Lighten up on yourself. No one is perfect. Gently accept your humanness."

- Deborah Day

TABLE OF CONTENTS

LIST OF FIGURES

LIST OF TABLES

ACKNOWLEDGMENTS

I would like to thank Dr. Marsha Rosner, for her patience, guidance, and support throughout my graduate education. For me, she has always been an example of endless scientific curiosity, dedication to high quality work, and commitment to mentorship. She taught me how to ask the right questions and not to be afraid of finding the answers outside of my comfort zone. Her encouragement helped me do things I thought I could never do, like programming, and made me the scientist I am today. Thank you for creating many opportunities for me to shine and grow as a scientist and as a person.

I would also like to acknowledge my committee members Dr. Xiaoyang Wu, Dr. Yingming Zhao, and Dr. Geoffrey Greene. Their valuable input was instrumental in the making of this dissertation. In the moments when I was lost in my own science, they have shown me that there is always another way. I would also like to thank Dr. Kay Macleod, for telling me to stop worrying right when I needed to hear it.

I would like to thank Dr. Gary Johnson, Casey Frankenberger, and Daniel Rabe for their technical and intellectual support early on in my project. Dr. Gary Johnson and his team developed the multiplexed inhibitor bead / mass spectrometry (MIB-MS) method that generated the high-thoughput kinome data that jump-started my project and he continues to be a valuable collaborator for the Rosner Lab. Daniel Rabe generated almost all of the cell lines I used in this study and was very helpful as an upperclassman in the same graduate program. Casey spearheaded the early phases of this study before I joined the lab and generated some of the preliminary data. But more importantly, as a bioinformatician, his code samples and analyses were great resources for my development as a programmer.

I would like to acknowledge my labmates, who made the lab a stimulating environment for me everyday. To Suzana Gomez, who taught me every lab technique I know, and never failed to point out all the "cookie violations" I made in the lab. To Joseph Wynne, Jiyoung Lee, and Nykia Walker for being great resources to bounce ideas off of about any and every aspect of life. To Maria Smith, Ethan Steinberg, and Siqi Sun for providing me with an

extra pair of hands when I needed it (even on the weekends). To Peter Yang, who not only contributed to the findings of this study with his technical support, but also managed to always lighten up the mood with his well-timed jokes. And finally, to Payal Tiwari, who has walked the life of a graduate student alongside me. As a colleague, Payal's problem solving skills and work ethic were instrumental in establishing the efficacy of our anti-metastatic treatment in animal studies (Chapter 3). As a friend, her honesty made me a better person every day, and her daring nature inspired me to take on new challenges.

I would also like to thank my friends who all enriched my life as a graduate student in a unique way. To my friends in my a cappella group The Histones, who always took me seriously and yet taught me how not to take myself too seriously. Our weekly rehearsals and hangouts were instrumental in energizing me to carry out the work described in this project. To my best friend Athena, for knowing me better than I do, and also for being the best study buddy I could have ever asked for. To Marguerite, for showing me how to be couragous enough to rise up and start over (and for introducing me to the best anime shows ever created).

I would like to thank my father Ahmet and my mother Sibel Yesilkanal, for being brave enough to let me follow my dreams at the age of 14, even if it meant not seeing their son for years at a time. I can always feel their support and unconditional love from across the ocean. To my sister, who is eight-years younger, but eight-years wiser than me. I have always aspired to her self-confidence and discipline, and tried to channel her attitude toward life as I carried out this work.

Finally, I would like to thank Matthew, who single-handedly braved all my frustrations, disappointments, mistakes and continuously cheered me on in my journey as a graduate student. With his endless love, support, and optimism, he provided me with everything I needed to get through the tough days and cherish the good days. He taught me how to be proud of myself and believe in myself at times when doing so seemed very difficult. Without his presence in my life, this work would have been impossible. This is why I am dedicating

this work to my partner Matthew Vincent Joannou.

ABSTRACT

Metastatic progression of tumors is the major cause of death in patients with triple negative breast cancer (TNBC). However, since metastasis is a multi-step process, unraveling its complexity is a major challenge. One effective way of tackling this question is to study natural blockers of the metastatic process, metastasis suppressors, and identify the mechanisms by which they regulate metastasis. Raf kinase inhibitory protein (RKIP, also known as PEBP1), a protein that regulates kinase activity, is a physiological suppressor of TNBC metastasis. Although RKIP inhibits the activity of Raf-1, other kinase targets of RKIP in tumors are not known. To address this question, we used a mass spectrometry approach involving inhibitor-conjugated beads to identify kinases that are down-regulated by RKIP in human TNBC xenograft tumors. Our results identified a network of stress kinases targeted by RKIP, including kinases that have not been previously reported as RKIP targets. By using a high-throughput invasion assay, we developed a low-dose multi-drug cocktail of kinase inhibitors targeting stress MAP kinases p38, JNK, MLK, and MEK. This combination treatment mimicked RKIP's anti-metastatic role in cultured cell, as well as xenograft and syngeneic models of TNBC. In order to unravel the effect of this stress network on metastatic gene expression, we conducted an RNA-seq analysis comparing metastatic xenograft tumors to non-metastatic RKIP-overexpressing tumors. Genes downregulated by RKIP in these tumors were enriched in motility and invasion related gene sets, and their expression was induced under stress conditions. Several of these genes were directly regulated by BACH1, a pro-metastatic factor targeted by RKIP. Interestingly, the same genes were negatively correlated with RKIP expression across multiple TCGA cancer types and with other metastasis suppressor genes within the breast cancer cohort, highlighting the clinical relevance of the RKIP-network. Elucidating RKIP function at a systems level reveals the interplay between key metastatic signaling cascades, particularly in relation to cell motility and invasion. Our findings suggest that a low-dose, multi-drug combination therapy that targets a network of stress kinases is a viable anti-metastatic therapy for TNBC patients.

CHAPTER 1

BACKGROUND

1.1 Clinical problem of metastasis

Metastasis is the process by which tumor cells leave their primary site and spread to the rest of the body. In most cases, multiple organ dysfunction or failure due to the aggressive metastatic spread of the tumor is the cause of lethality in cancer patients [14]. When cancer patients present with a late-stage metastatic tumor at the clinic, their prognosis is generally poor, regardless of the type of cancer. Moreover, the metastatic phenotype correlates with resistance to treatment and recurrence, which can partially be attributed to tumor cells' ability to escape and seed in new parts of the body. In recent years, studies have shown that metastasis is a much more dynamic process than previously imagined, by which tumor cells continually move in and out of tissues that can even result in seeding of tumor cells back into their primary site long after the primary tumor has been removed [20]. Circulating tumor cells can be detected in a patient's blood even decades after the patient has been deemed cancer-free [64], increasing the possibility of a late relapse. Similarly, residual cancer cells after the initial treatment of the primary tumor can stay dormant in distant tissues for up to 25 years and become reactivated later, causing patients to succumb to the disease [49, 1]. Developing therapies that block the metastatic process is, therefore, an urgent clinical need.

Blocking metastasis, however, is challenging because it involves multiple steps, each of which is mediated by diverse signaling events within the tumor cell as well as its microenvironment [10]. In order to metastasize, a tumor cell needs to gain migratory capabilities, invade through its surrounding tissue, intravasate into blood or lymph vessels, extravasate from circulatory vessels, and colonize at new tissue sites [99]. Tumor cells also need to prepare the metastatic niche prior to successful seeding and colonization [75]. Each of these steps involves different cell-cell, cell-matrix interactions and signaling pathways, rendering it difficult to sort out the mechanisms regulating metastasis. Reaching a comprehensive

understanding of how metastasis works and elucidating the key signaling mechanisms and cell types that mediate this process is essential for development of effective anti-metastatic therapies.

Current clinical approaches to treating late stage metastatic disease is systemic treatment with chemotherapy. Chemotherapeutic treatment, however, is known to induce more aggressive and more metastatic phenotype either by selecting for resistant tumor cell populations [11] or by actively reprogramming tumor cell transcriptome / kinome to take on a resistant phenotype [43]. This ultimately results in relapse and a rapid progression of the disease. If the further dissemination of cancers can be stopped with a targeted anti-metastatic therapy, the remaining tumors can potentially be treated as local diseases. More importantly, it is hypothesized that inhibiting metastatic pathways and cellular mechanisms can benefit overall survival in patients [90]. Anti-metastatic treatments also have the potential to sensitize resistant tumor cells to standard-of-care systemic treatments such as chemotherapy, radiotherapy, and other targeted agents [33, 90]. However, anti-metastatic treatment options are limited and require identification of new targets as well as development of novel combinations of inhibitors. This study will lay out a framework for identifying new therapeutic approaches to metastatic disase.

Developing combinatorial treatments are key to effective treatment of metastasis and improved outcome, since tumor cells have mechanisms of overcoming single-agent targeted therapies. In most cases, targeted agents have a "whack-a-mole" effect on cancer cells which activate alternative growth, survival, and metastasis pathways that will render tumors resistant to the initial treatment [37]. Combinations of multiple targeted agents or different treatment modalities (targeted, non-targeted, local, systemic etc.) should, therefore, be considered in developing anti-metastatic therapies against cancers.

1.2 Metastasis suppressors

How do we deconvolute a cellular phenomenon as complex and multi-step as metastasis? One effective way of investigating metastasis is by studying the natural inhibitors of this process – metastasis suppressors. Metastasis suppressors are a group of physiological proteins that function to block metastatic progression of tumors. Unlike tumor suppressors, metastasis suppressors do not affect initiation and growth properties of the primary tumors, but rather inhibit the dissemination mechanisms of tumor cells such as invasion through tissue, intravasation/extravasation, and metastatic colonization. Understanding the details of the regulation and function of metastasis suppressors can create therapeutic opportunities to either restore or mimic the role of these proteins in metastatic cancers. Furthermore, metastasis suppressors and their functional gene networks can be used as prognostic and predictive markers in the clinic for metastatic progression and survival.

Zhao and colleagues recently curated a database of 194 experimentally validated metastasis suppressor genes in humans based on literature-based evidence [113]. 161 of these genes were protein-coding, and 33 of them are microRNAs. 83 of the metastasis suppressor genes have been also reported as tumor suppressors in the TSGene database [114, 112], suggesting that almost half of these genes have dual functions and their roles as tumor vs. metastasis suppressor should be experimentally clarified. Nevertheless, there are over 50 genes that play a role in blocking one or more steps in the metastatic progression without influencing the overall growth of the primary tumor. Zhao and colleagues also identified the biological pathways enriched for these 194 suppressors to be related to epithelium / tissue morphogenesis, epithelial proliferation, cell surface and platelet signaling, and cell death, though some of these findings are affected by the tumor suppressor functions of the genes included in the analysis. Signaling and gene regulatory networks modulated by each metastasis suppressor gene are not completely understood and of continuous research. To this date, most commonly studied metastasis suppressor genes are NME1/2, BRMS1, CD82, PEBP1, KISS1,

CDH1, NDRG1, MTSS1, SERPINB5, and CD44, each implicated in at least 7 different cancer types [113].

1.3 RKIP as a metastasis suppressor

Raf Kinase Inhibitory Protein (RKIP), also known as phosphatidylethanolamine binding protein 1 (PEBP1), is a highly conserved protein that functions as a metastasis suppressor in multiple solid cancers [31, 22]. RKIP's role as a metastasis suppressor was initially described in prostate cancers. Fu and colleagues demonstrated with their comparison of metastatic prostate cancer cell lines to non-metastatic cell lines that expression levels of RKIP is a determinant factor for the metastatic phenotype [31]. RKIP is commonly lost or downregulated in cancers that have reached the metastatic state. Low RKIP expression correlates very strongly with metastatic phenotype in the majority of cancers including prostate, breast, pancreatic, lung, cervical cancers and gliomas [53, 58, 59]. Due to this negative association between RKIP and metastasis, RKIP has been implicated as a powerful predictive biomarker for metastatic risk in patients, as well as a prognostic marker for metastasis-free and overall survival in many solid tumors [53]. Experimentally, over-expressing RKIP blocks invasion in vitro and metastatic progression in vivo [31, 22], without affecting growth properties of the primary tumor. At the molecular level, RKIP directly or indirectly suppresses the activity of multiple signaling pathways known to be crucial for metastasis, such as the RAF-MEK-ERK cascade [105, 21, 96] , NFκB signaling [106], G protein-coupled receptor signaling [57], and GSK3βsignaling [2]. RKIP-related gene signatures can also be utilized to identify cancer patients at highest risk [6, 30, 56, 94, 22] . These clinical and experimental findings establish RKIP as a suppressor of invasion, intravasation, extravasation and metastasis.

1.4 Triple Negative Breast Cancer and RKIP: a model for metastatic disease

Breast cancers are clinically caterogized into multiple subtypes based on the hormone receptor and human epidermal growth factor receptor 2 (HER2) status. Each of these subtypes has different clinical features, rates of progression, and prognostic outcomes, and therefore, considered a distinct entity [8, 52, 76]. Triple negative breast cancer (TNBC), as the name suggests, is the subtype that lacks estrogen receptor (ER) and progesterone (PR) receptor expression, and HER2 amplification. TNBC constitutes about 15-20% of all breast cancer cases and are highly aggressive with high metastatic potential. In terms of molecular profiling, approximately 80% of TNBC tumors overlap with the basal-like molecular subtype [28]. Since TNBC is missing all three clinical targets, hormonal therapies (e.g. selective estrogen receptor modulators, aromatase inhibitors) as well as HER2-targeting treatments (e.g. herceptin) are ineffective against TNBC. Instead, TNBC is treated with non-targeted treatments including surgery, radiation, and chemotherapy [5]. TNBC patients are at a much higher risk for metastasis compared to similary staged other subtypes with most relapses occuring within 5 years of initial treatment. Therefore, there is an urgent need for understanding disease progression and developing targeted treatment options for TNBC patients.

The highly metastatic nature of TNBC and the availability of multiple cell lines and mouse models makes TNBC a good system in which to study mechanisms of metastasis. More importantly, RKIP has a robust anti-metastatic phenotype in TNBC models and RKIP-based gene signatures can stratify TNBC patients for metastatic risk. [30, 56]. RKIP expression is usually lost in these poor-prognosis tumors, correlating with the highly metastatic phenotype [58, 59, 3, 24]. Previous work from the Rosner laboratory demonstrated that RKIP blocks multiple steps of the metastatic process both in vitro and in vivo. For example, exogenous expression of RKIP in TNBC cell lines results in significant reduction in invasion without any effect on growth [22]. In xenograft models, RKIP blocks intravasation of tumor cells as

well as later stages of metastasis such as extravasation and colonization. Therefore, studying RKIP function in TNBC not only allows for the investigation of the metastatic networks regulated by RKIP, but also identifies potential therapeutic targets in TNBC.

1.5 Molecular functions of RKIP

At the molecular level, RKIP functions as an inhibitor of kinase activity. It was originally identified as a direct binding partner for RAF kinase, and multiple studies have since shown that RKIP interferes with the activation of the RAF-MEK-ERK cascade [105]. Subsequently, it was revealed that it can modulate other signaling pathways such as NFκB-related pathways [111]. RKIP itself can act as a substrate for kinases, and phosphorylation of certain residues can alter RKIP's binding properties. Most notably, phosphorylation of Ser153 residue by PKC switches RKIP's binding from Raf to GRK2 [57], resulting in PKA activation. The mechanism by which this phospho-switch occurs involves a novel salt bridge theft that enables the promotion or disruption of peptide interactions to provide specificity at protein interfaces [87, 88]. This illustrates RKIP's potential role in sensing active signaling networks and modifying the cellular kinome through new protein interactions.

RKIP is an inhibitor of the classic RAF-MEK-ERK signaling cascade. The MAP kinase network consists of 6 main axes: (1) ERK1/2, (2) p38s, (3) JNKs, and (4) ERK5, (5) ERK3/4, and (6) ERK7/8 (reviewed in detail by Dhillon et al. [23]). Among these MAPKs, activation and function of ERK5/6/7/8 are the least understood and outside the scope of this study. Each MAPK axes consists of three levels, where MAPKs are activated by MAP2Ks (e.g. MEK1/2, MKK4, MKK7, MKK3, MKK6), which themselves are activated through phosphorylation by MAP3Ks (e.g. Raf, MEKK, Tpl2, MLK, TAK, ASK, TAOK). The ERK1/2 axis is induced by growth factors and mitogens, whereas p38 and JNK axes are activated by cytokines and stress stimuli.

A yeast two-hybrid assay that utilized the kinase domain of Raf-1 as bait originally identified RKIP as a Raf binding protein [105]. High RKIP concentrations are able to interfere

with MEK binding, preventing MEK activation [104]. Under physiological conditions, RKIP inhibits Raf-1 subsequent to Raf-1 membrane translocation but prior to phosphorylation of downstream targets such as MEK and ERK [96]. RKIP-binding to subdomains I and II of the Raf-1 kinase domain blocks phosphorylation of residues Ser338 by PAK and Tyr340/341 by Src, both of which are required for activation of Raf-1 upon growth factor stimulation [60]. Enhanced Raf-1 activation in RKIP-depleted cells enabled increased DNA synthesis and cell proliferation at lower EGF concentrations, effectively enhancing the sensitivity of the system to stimuli [96].

RKIP also plays a role in protein kinase C (PKC)-induced Raf activation. Our previous work showed that PKC phosphorylates RKIP at serine residue 153 (S153) in neuronal cells, and this phosphorylation leads to dissociation of RKIP from Raf-1 and subsequent activation of MEK and ERK [21]. This exemplifies RKIP's ability to mediate cross-talk between different signaling cascades. The role of S153 phosphorylation in regulating RKIP inhibition of Raf/MAPK signaling has now been demonstrated in a variety of cell types [22, 36]. Our lab has generated S153E mutants of RKIP, which were intended to mimic the phosphorylation of this cite. However, experimental evidence showed that S153E mutant RKIP acts as a constitutively active version of RKIP [22], which is more robust in inhibiting Raf-1, particularly in vitro.

1.6 Microenvironmental functions of RKIP

RKIP's anti-metastatic function is at least partially mediated through its effect on the tumor microenvironment. Our previous studies demonstrated that RKIP over-expression in metastatic TNBC mouse models robustly blocks recruitment of tumor-associated macrophages (TAMs) into the tumors through a mechanism dependent upon the chemokine CCL5 [30]. TAMs are known to be critical components of metastatic progression in solid tumors, as macrophages can enhance tumor cell invasion and intravasation, and promote tumor angiogenesis [70]. More broadly, using species-specific RNA sequencing in a xenograft TNBC

mouse model, Bainer et al. demonstrated that gene expression in metastatic breast tumors is widely correlated with gene expression in local stroma of both mouse xenografts and human patients [6]. Moreover, changes in stromal gene expression elicited by tumors that do or do not express RKIP is a better predictor of breast cancer subtype and patient metastasis-free survival than tumor gene expression. These findings show that understanding microenvironmental functions of RKIP can open new prognostic and therapeutic avenues.

1.7 Mechanisms of RKIP downregulation and strategies for recovering RKIP expression

Similar to tumor suppressors, inactivation of metastasis suppressors is a common step in a cancer's progression into a metastatic disease. RKIP expression is lost or diminished in metastatic cancers. However, mutations or deletions in the PEBP1 gene in human cancers are rare, suggesting that RKIP is silenced through non-genetic mechanisms [103]. In prostate cancers, RKIP expression is reduced by increased promoter methylation and histone deacetylation, as well as SNAIL-mediated transcriptional suppression [7]. RKIP gene promoter has been reported to be methylated in other cancer types as well (reviewed by Yesilkanal and Rosner [103]), but it does not always predict survival independently [50], or global demethylation by 5-AzaC does not always recover RKIP expression [7]. In breast cancers, RKIP expression does not negatively correlate with SNAIL [103], nor is it recovered by histone deacetylase inhibitor treatment [55]. Certain miRNAs (e.g. miR-27a, miR-23a, miR-224) have been reported to inhibit RKIP expression in lung, prostate, and breast cancers (reviewed in [103]), while increased proteosomal degradation can account for loss of RKIP in hepatocellular carcinoma [66]. Taken together, these findings suggest that regulation of RKIP expression is a complex process involving multiple factors in a cell- or tissue-dependent manner.

1.8 Computational approaches to understand RKIP function and significance

Computational strategies are extremely useful in identifying critical signaling pathways and targetable factors, especially when powered by patient-derived data. Using known biological interactions (or experimentally-derived interactions) as filters is a powerful method while building networks because it improves signal-to-noise ratio [44]. RKIP, as a selective metastasis suppressor, is a potent filter for generating statistical correlations focused on the metastatic process.

To systemically identify downstream mediators of RKIP, Rosner and colleagues have employed integrated approaches that combine statistical/computational analysis of breast cancer gene expression data and experimentally-validated gene interactions. Dangi-Garimella et al. first experimentally identified a pro-metastatic signaling cascade involving Myc/LIN28/let-7 as an RKIP target [22]. Then, Yun et al. used this RKIP/let-7 interaction as a computational filter to connect the RKIP signaling cascade to previously-described bone metastasis signature genes [109, 48]. Specifically, they used statistical and machine learning approaches involving gene set analysis (GSA) and Random Forest (RF) on a compilation of publicly-available microarray gene expression data from patient tumors. With this method, they identified HGMA2 and BACH1 as likely mediators that connect RKIP signaling to downstream bone metastasis genes MMP1 (matrix metalloproteinase 1), OPN (osteopontin), and CXCR4 (chemokine C-X-C motif receptor 4). Yun et al. then validated down-regulation of HMGA2 and BACH1 by RKIP and let-7 experimentally in vitro and in vivo. Thus, these studies used patient gene expression data to generate hypothetical signaling networks that were then validated experimentally. The key biomarkers identified can also serve as therapeutic targets to mimic the anti-metastatic action of RKIP.

Exploring and expanding RKIP-regulated gene networks using patient-derived expression data also allow for developing predictive and prognostic gene signatures that have mechanistic

relevance to specific patient cohorts. After identifying RKIP-regulated signaling networks in tumors and their microenvironment, the Rosner group generated several RKIP pathway-based gene signatures for predicting metastasis-free survival of breast cancer patients [6, 30, 56, 94, 109]. The biomarkers used in these gene signatures span a wide range of metastatic processes such as extracellular matrix remodeling, epigenetic regulation, tumor-associated macrophage recruitment, and reprogramming of stromal gene expression by tumors. While these signatures facilitate the identification of patients who would benefit from RKIP-like regulation, the challenge has been to come up with therapeutic treatments that either mimic or reactivate RKIP functionally in tumor cells.

With the completion of TCGA and ease of access to clinical sequencing data from multiple studies, building clinically relevant hypothetical gene networks and signatures is becoming less challenging. Gene signatures built on experimentally validated mechanistic gene-gene interactions can (1) help identify/stratify patients for guided/personalized treatment, (2) be used as biomarkers for predicting drug efficacy or sensitivity in patients, (3) be combined with machine learning methods for drug discovery or drug repurposing for a particular biological function. Conceptually, novel anti-metastatic therapies can be discovered as long as the therapeutic approach being tested is able to target genes in patients identified as high risk by RKIP-related gene signatures. In parallel, therapeutic treatments that mimic RKIP's anti-metastatic functions would be more effective in patients who are at high risk for metastasis based on their RKIP pathway signature score.

In sum, RKIP is an important suppressor of metastasis that would be most effective if induced in metastatic cells. However, even in the absence of RKIP protein, it is possible to leverage RKIP targets and patient data to identify novel targets such as specific kinases that, if inhibited together, can mimic the anti-metastatic properties of RKIP and make tumors more homogeneous and more susceptible to conventional cytotoxic therapy.

1.9 Summary of outstanding questions

Metastasis is a complex event, but its details can be unraveled by studying its physiological suppressors. RKIP is a metastasis suppressor that functions as an inhibitor of kinase signaling in healthy cells, but its expression is decreased or silenced in metastatic cancers. Mechanisms by which RKIP expression is lost depends on the tumor type. In TNBCs, these mechanisms are unclear, making it challenging to reactivate or reintroduce RKIP into metastatic cells. Therefore, in this study we are following an alternative approach where we leverage what we know about RKIP's anti-metastatic function in order to develop anti-metastatic therapies. Our approach is to identify kinomic and genomic networks regulated by RKIP and develop combinatorial targeted therapies to mimic RKIP's downstream effect in cancers. Since RKIP's molecular role in the cell is to modulate signaling pathways, we hope to employ kinase inhibitors which are readily available and easy to use to modulate the same pathways.

However, this approach requires a systems level understanding of kinase networks and the downstream metastatic genes targeted by RKIP. Cross-talk between different cascades within the network need to be identified in order to reprogram the entire network. These feedback mechanisms will be important in answering questions such as (1) which kinases should be targeted? (2) how many inhibitors do we need to mimic RKIP? (3) how can we monitor the efficacy of a treatment at the molecular level? and finally (4) what are the downstream effector genes that mediate metastasis and does the RKIP-mimicking treatment reduce the activity of these genes? We hope that by answering these questions we will not only uncover key metastatic signaling networks that are targeted by RKIP, but also have new therapeutic options for metastatic disease, particularly in triple negative breast cancer.

CHAPTER 2

MATERIALS AND METHODS

2.1 Cell lines

MDA-MB-231 (MB231), MDA-MB-436 (MB436), MCF10A, 184A1, and 293T cells were recived from American Type Culture Collection (ATCC®). E0771-LMB (LMB) cells were received from Robin Anderson [46]. M6C cells were received from Jeffrey Green [41]. MDA-MB-231-BM1 (BM1) cells were obtained from Andy Minn, but they were originally generated by Massague and colleagues [48]. BM1, MB436, LMB, and M6C cells were cultured in DMEM media with 10% FBS, penicillin (50U/ml), and streptomycin (50μg/ml). MCF10A and 184A1 cells were grown in DMEM/F-12 (50/50) with 10% FBS and penicillin-streptomycin. The cells were used in experiments within 15 passages after their arrival in the laboratory.

2.2 Small molecule inhibitors

For in vitro and in vivo studies, JNK inhibitor SP600125, MEK inhibitor Trametinib (GSK1120212), and MLK inhibitor URMC-099 were purchased from APExBIO (Cat No A4604, A3018, B4877, respectively). p38 inhibitor SB203580 was purchased from Selleckchem (Cat No S1076) for the in vitro experiments. For in vivo studies, water soluble SB203580 hydrochloride was purchased from APExBIO (Cat No B1285).

2.3 Signaling studies in vitro

In order to study the changes in stress kinase signaling upon stress in the presence of RKIP, or small molecule inhibitors of the MAPKs, cells were plated at sub-confluence. Once they reach roughly 70% confluence, they were starved overnight (16-24 hours) in serum-free media, and then induced with either anisomycin (Sigma-Aldrich, Cat No A9789) at 25 ng/ml or

100 ng/ml final concentration, or by 2% or 10% serum for 30 minutes to activate MAPK pathways. In studies with small molecule inhibitors of the MAPK pathway, all inhibitors were re-suspended in DMSO and used at indicated concentrations. The cells were pre-treated with the inhibitors in serum-free media for 30 min after overnight starvation, immediately before induction with anisomycin or serum for 30 minutes. In this case, the inducing agent was directly added to the pre-treatment media that already had the inhibitors, or the pre-treatment mediate was replaced by fresh media containing the inducer and the inhibitors. This is to ensure the inhibitors are present during induction of the MAPK pathways. Upon induction for 30 min, the cells were washed three times with cold PBS and immediately lysed in RIPA buffer for protein collection.

2.4 Protein isolation and Western blots

Cultured cells were washed with cold PBS and lysed in RIPA buffer with protease inhibitors (Millipore Sigma, Cat No 539134) and phosphatase inhibitors (GoldBio, Cat No GB-450). Tumor samples were snap-frozen in liquid nitrogen, pulverized, and lysed in RKIP buffer with protease and phosphatase inhibitors. All samples were sonicated 3 x 10 seconds at 35% power and centrifuged at max speed for 15 minutes at 4^{o}C. Supernatant was collected and the protein concentration is measured using Bradford assay. All samples were boiled in 6X Laemmli buffer immediately after protein concentration measurement.

For Western blots, equal amounts of protein, ranging from 10ug to 50ug, across all samples were used. Blots were blocked for 1 hour at ambient temperature with either Odyssey® Blocking Buffer (LI-COR Biosciences, Cat No 927-40010, diluted 1:1 with PBS) or with 5% BSA in TBS-T. Then, blots were incubated with primary antibodies at 4^{o}C over-night, and with secondary antibodies at ambient temperature for 1 hour. Finally, blots were treated with ECL reagent (Pierce ECL Western Blotting Substrate, Thermo Scientific, Cat No 32106) when HRP-conjugated secondary antibodies are used and developed under the Chemilumescence channel of the LI-COR® Fc Imaging System. Blots with fluorescent secondary anti-

bodies were imaged under 700nm or 800nm channels of LI-COR® Fc.

Primary antibodies used:

Phospho-RSK2 (Ser227) (Cell Signaling, 3556)

Phospho-ATF2 (Thr71) (Cell Signaling, 9221, no longer available)

Phospho-SEK1/MKK4 (Ser257/Thr261) (Cell Signaling, 9156)

Phospho-TAOK3 (Ser177) + Phospho TAOK2 (Ser181) + Phospho-TAOK1 (Ser181) (Abcam, ab124841)

MLK3 (Cell Signaling, 2817)

Phopsho-p44/42 MAPK (ERK1/2)(Thr202/Tyr204) (Cell Signaling, 9101)

Phospho-MSK1 (Thr581) (Cell Signaling, 9595)

Phospho-SAPK/JNK (Thr183/Tyr185) (Cell Signaling, 9251)

p44/42 MAPK (ERK1/2) (Cell Signaling, 9107)

SAPK/JNK (Cell Signaling, 9252)

Phospho-p38 MAPK (Thr180/Tyr182) (Cell Signaling, 4511)

Phospho-AKT1 (S129) (Abcam, ab133458)

Phospho-MKK3 (Ser189)/MKK6 (Ser207) (Cell Signaling, 12280)

Phospho-c-Jun (Ser73) (Cell Signaling, 3270)

Phospho-p70 S6 Kinase (Thr389) (Cell Signaling, 9205)

MLK3 (Abcam, ab51068)

MLK3 (Santa Cruz, sc-166639)

Phopsho-MLK3 (T277/S281) (Abcam, ab191530)

DOCK4 (Santa Cruz, sc-100718)

Casein Kinase 2β(Santa Cruz, sc-12739)

Casein Kinase 2α(Santa Cruz, sc-9030)

TAOK1 (Abcam, ab197891)

TAOK1/PSK2 (Santa Cruz, sc-136094)

TAOK2 (Santa Cruz, sc-47447)

TAOK3 (Abcam, ab150388)

α- Tubulin (Santa Cruz, sc-8035)

Secondary antibodies used:

Goat anti-Mouse IgG (LI-COR, IRDye® 800CW, 926-32210)

Goat anti-Mouse IgM (LI-COR, IRDye® 800CW, 926-32280)

Goat anti-Rabbit IgG (LI-COR, IRDye® 680RD, 926-68071)

Goat anti-Rabbit IgG, HRP conjugate (EMD Millipore, AP187P)

Goat anti-Mouse IgM, HRP conjugate (Invitrogen, 31440)

Goat anti-Mouse IgG, HRP conjugate (Sigma Aldrich, A4416)

2.5 Transient transfection with siRNAs

Prior to transfection, the cells were plated in 6-well plates and grown to ∼70% confluence. siRNA vectors were used at a final concentration of 50nM per well of cells. The vectors were incubated with 10µl of Lipofectamine 3000 (Invitrogen, Cat No L3000-015) in OPTI-MEM media (Gibco, Cat No 31985062) for 15-30 minutes. The DNA-lipid complex was, then, added onto the cells in a drop-wise fashion. Cells were incubated with the siRNAs for at least 24 hours before harvesting for experimental use. All experiments were performed 24-72 hours post-transfection. All siRNA constructs were purchased from Dharmacon.

Individual siGENOME human TAOK1 siRNA, Dharmacon, D-004846-02-0005)

Individual siGENOME human TAOK2 siRNA, Dharmacon, D-004171-13-0005)

Individual siGENOME human TAOK3 siRNA, Dharmacon, D-004844-02-0005)

siGENOME Non-Targeting siRNA Pool #1, Dharmacon, D-001206-13-05)

2.6 Generation of stable cell lines with lenti-viral constructs

293T cells were plated in T-75 plates and were grown to ∼70% conlfuence prior to transfection. 1 hour prior to transfection, the media was replaced with fresh media. Lenti-

viral vectors were incubated with 3rd generation viral packaging vectors (pCMV-VSV-G, pMDLg/pRRE, pRSV-Rev) and LT-1 (Mirus, Cat No MIR-2305) in OPTI-MEM media for 30 minutes as described by the provider's instructions. This transfection mix was, then, added onto the 293T cells in a drop-wise fashion. Virus containing media was collected 24-48 hours after transfection. Cellular content and debris was removed by centrifugation and the supernatant was filtered through 0.45μm PES syringe (Millex, Cat No SLHP033RS) to remove any remaining cells in the media. Polybrene was added to the media at the final concentration of 8 ng/ml to facilititate viral transduction of the target cell line. The target cell lines were transduced with the virus-containing media for 24-48 hours. At the end of the transduction period, cells were washed, trypsinized, and re-plated for selection. Transduced cells were exposed to high concentration antibiotic selection (3μg/ml puromycin) up to 2 weeks (approximately 3 passages).

All lenti-viral procedures were carried out following Biosafety Level 3 (BSL3) practices in BSL2 tissue culture hoods according to institutional biosafety rules. Viral waste generated during the transfection/transduction process was decontaminated with 10% bleach prior to disposal.

2.7 Boyden chamber invasion assay

Each Boyden chamber membrane (Fisher Scientific, Cat No 353097) was coated with a thin layer of BME (200ul of 0.25mg/ml stock, or total of 50ug of BME per membrane) and incubated at 37°C for 1 hour. Cells were trypsinized and centrifuged at 500 x g for 5 minutes followed by two rounds of PBS washes to remove remaining serum-containing media. Then, the cells were resuspended in serum-free media and diluted to the desired concentration for plating onto the Boyden chambers. Each Boyden chamber received 20,000 – 100,000 cells in 300 ul serum-free media, depending on the cell line. 10% serum was used as the chemoattractant for these assays. For the experiments testing the effect of MAPK inhibitors on invasion, the cells were resuspended in drug-containing serum-free media immediately.

After 16-24 hours, the membranes were stained with Calcein AM (Fisher Scientific, Cat No 354217) for 1 hour at 37°C in dark to stain for live cells. Cells that are in the top chamber were removed from the membrane with a wet cotton swab. Cells in the bottom chamber were dissociated from the membrane by incubating in cell dissociation buffer (Trevigen, Cultrex® Cat No 3455-096-05) in a shaker at 37°C for 1 hour. Finally, Calcein AM signal was measured in Perkin Elmer Victor X3 plate reader as a read-out of invaded cells.

2.8 High-throughput chemotactic invasion assays

For testing anti-invasive drug combinations, IncuCyte® ClearView 96-Well Chemotaxis plates (Essen BioScience) were used. 2000 cells per well were embedded in 2mg/ml BME and plated onto the chemotaxis plate following the manufacturer's instructions. Media containing 2% FBS was used in both top and bottom chamber to maintain cell viability over 72 hours or more. 200 ng/ml human EGF (Bio-Techne, 236-EG-01M) was used the chemotactic agent in the bottom chamber, and the control wells only had the vehicle for the chemotactic agent.

This assay is more accurate when nuclear-labeled cells are used. Therefore, we generated BM1-mKate2 (nuclear red) cells using IncuCyte® NucLight Red Lentivirus Reagent (Essen BioScience, Cat No 4478) following the manufacturer's instructions. After transduction, cells with the highest nuclear red signal intensity (top 25%) were sorted by FACS.

Chemotaxis module in IncuCyte® can accurately count the number of cell in the top chamber and the bottom chamber of the ClearView plates separately. Invasive capability of the cells in the presence of various small molecule inhibitors was measured as the percentage of cells that moved to the bottom chamber over the period of 72 hours. The formula used for this calculation is (number of cells in the bottom chamber)/(number of cells in the bottom chamber + number of cells in the top chamber) x 100. The total number of cells in the top and bottom chambers is used as read out of proliferation, which was important in determining drug combinations that blocked invasion without affecting growth properties of the cells.

2.9 Proliferation assays

For proliferation assays, 1,000 – 20,000 cells (depending on the cell line) were plated in 96-well plates and quantified over 5 days in IncuCyte by measuring confluence in Phase-Contrast images taken every 4 hours. For experiments testing the effect of MAPK inhibitors on proliferation, the cells were plated in 100µl per well and allowed to adhere overnight. Then, 100µl growth media containing 2X drug was added directly on top of the initial media.

2.10 3D Proliferation Assays

For 3D proliferation experiments, we used Cultrex®3D Basement Membrane Matrix, Reduced Growth Factor (Trevigen, Cat No 3445-005-01, Lot No 37353J16, Lot concentration: 15.51 mg/ml, referred to as BME). For all experiments, the cells in growth media were mixed with BME at the final concentration of 2mg/ml. For 3D proliferation assays, 100µl of the cell/BME mixture was dispensed into each well of a 96-well plate. Upon solidification of BME, 100µl of growth media was added on top of the solidified gel. For experiments where the cells were treated with inhibitors, the inhibitors were prepared in the growth media at 2X of their desired final concentration and added after the gel is solidified to assure 1X final concentration. The growth of the cells was monitered in IncuCyte® Zoom or S3 models for the indicated duration of time.

2.11 Scratch wound assays for migration

Migration assays are conducted using IncuCyte's "Scratch wound" module. 20,000 – 30,000 cells were plated on IncuCyte® ImageLock Plates (Essen BioScience, 4379). Once the cells reached 100% confluence, the wells were scratched with IncuCyte® WoundMaker (Essen BioScience, 4493) following the provider's instructions, washed with PBS twice, and supplied with fresh growth media. For experiments testing the effect of MAPK inhibitors on cell

migration, fresh growth media containing the inhibitors at the desired final concentration was added onto the cells after the PBS washes. Wound-healing process was monitored over 72 hours in IncuCyte, and wound density was measured over time as a read-out of cell migration.

2.12 RNA isolation and gene expression analysis by qRT-PCR

Cells were washed with cold PBS twice and lysed in TRI Reagent (Zymo Research, Cat No R2050-1-200). RNA was isolated using Direct-zol^{TM} RNA MiniPrep (Zymo Research, Cat No R2052). 4ug of total RNA from each sample was converted to cDNA using High Capacity cDNA Reverse Transcription Kit (Applied Biosystems, Cat No 4368813). Primer pairs used for this study are listed in tables 2.1 and 2.2:

2.13 Chromatin Immunuprecipitation (CHIP) assays

BM1 cells were crosslinked with 10% formaldehyde for 10 min and quenched with 0.125 mM glycine for 3 min. Cell were then lysed for sonication at 80% output for 4 x 10 seconds with a 10 second pause inbetween each cycle. The lysate was pre-cleared with IgG (Santa Cruz, sc-2028) for 1 hour at 4^{o}C and the supernatant was precipitated with antibodies against BACH1 (AF5776, R&D System), or IgG (normal mouse IgG, Santa Cruz, sc-2025) overnight at 4^{o}C. Primers for ChIP quatitative RT-PCR are in Table 2.3.

2.14 Animal studies

The primary animal model used in this study was mouse models of TNBC. Mice were procured and housed by the Animal Resources Center and handled according to the Institutional Animal Care and Use Committee at the University of Chicago. Athymic nude mice were purchased from Harlan Sprague Dawley and C57Bl/6 mice were purchased from the Jackson Laboratories. C3-1-TAg-REAR mice were received from Jeffrey Green and maintained

Primer pair		Primer sequence
Hs_PEBP1	Forward	GCTCTACACCTTGGTCCTGACA
	Reverse	AATCGGAGAGGACTGTGCCACT
Hs_NFATC2	Forward	GATAGTGGGCAACACCAAAGTCC
	Reverse	TCTCGCCTTTCCGCAGCTCAAT
Hs_ROCK1	Forward	GAAACAGTGTTCCATGCTAGACG
	Reverse	GCCGCTTATTTGATTCCTGCTCC
Hs_ROCK2	Forward	TGCGGTCACAACTCCAAGCCTT
	Reverse	CGTACAGGCAATGAAAGCCATCC
Hs_ADAM10	Forward	GAGGAGTGTACGTGTGCCAGTT
	Reverse	GACCACTGAAGTGCCTACTCCA
Hs_ADAM17	Forward	AACAGCGACTGCACGTTGAAGG
	Reverse	CTGTGCAGTAGGACACGCCTTT
Hs_EPC1	Forward	CCAGACATGCAGTACCTCTACG
	Reverse	GCTGTTTCTGCATGAGTGCCAG
Hs_PIKFYVE	Forward	CTGAGTGATGCTGTGTGGTCAAC
	Reverse	CAAGGACTGACACAGGCACTAG
Hs_DOCK4	Forward	GCATGTGGATGATTCCCTGCAG
	Reverse	GGAGGTGATGTAACACGACAGG
Hs_DOCK5	Forward	GCTTCTGAGCAACATCCTGGAG
	Reverse	TCCTTCTCAGCAGCCGTTCCAT
Hs_ARL13B	Forward	GAACCAGTGGTCTGGCTGAGTT
	Reverse	GTTTCAGGTGGCAGCCATCACT
Hs_DDR2	Forward	AACGAGAGTGCCACCAATGGCT
	Reverse	ACTCACTGGCTTCAGAGCGGAA
Hs_ITGA1	Forward	CCGAAGAGGTACTTGTTGCAGC
	Reverse	GGCTTCCGTGAATGCCTCCTTT
Hs_RAPGEF2	Forward	CTCGGATCAGTATCTTGCCACAG
	Reverse	AGGTTCCACTGACAGGCAATGC
Hs_RAPGEF6	Forward	AGACAGATGAGGAGAAGTTCCAG
	Reverse	GACCTCATAGGCACTGGAGACA
Hs_APC	Forward	AGGCTGCATGAGAGCACTTGTG
	Reverse	CACACTTCCAACTTCTCGCAACG

Table 2.1: List of Human primers used in this study

in-house.

For primary tumor growth experiments, 2 x 10^6 BM1 cells, 5 x 10^5 LMB cells, and 1 x 10^6 M6C cells were injected orthotopically near the mammary fat pad of athymic nude, C57Bl/6, and C3-1-TAg-REAR mice, respectively. Tumor growth was monitored over time by caliper measurements of the width and length of tumors. Tumor volumes were calculated with the formula:

$$volume = \big(\pi/6\big) \times length \times 2\big(width\big)$$

Primer pair		Primer sequence
Mm_PEBP1	Forward	ACTCTACACCCTGGTCCTCACA
	Reverse	TGAGAGGACAGTGCCACTGCTA
Mm_NFATC2	Forward	ACTTCACAGCGGAGTCCAAGGT
	Reverse	GGATGTGCTTGTTCCGATACTCG
Mm_ROCK1	Forward	CACGCCTAACTGACAAGCACCA
	Reverse	CAGGTCAACATCTAGCATGGAAC
Mm_ROCK2	Forward	GTGACCTCAAACAGTCTCAGCAG
	Reverse	GACAACGCTTCTGAGTTTCCTGC
Mm_ADAM10	Forward	TGCACCTGTGCCAGCTCTGATG
	Reverse	GATAGTCCGACCACTGAACTGC
Mm_ADAM17	Forward	TGTGAGCGGTGACCACGAGAAT
	Reverse	TTCATCCACCCTGGAGTTGCCA
Mm_EPC1	Forward	CTGCCAGGCTTCAGTGCTAAAG
	Reverse	ACTGACAGCCTGCTTTCCTACG
Mm_PIKFYVE	Forward	TCTTCTGCCCAGTCCAGCAATG
	Reverse	ACAGAACATGCTCGGACACTGG
Mm_DOCK4	Forward	GATAGGAGAGGTGGATGGCAAG
	Reverse	CGCCTTGAGATGCAGATCGTAG
Mm_DOCK5	Forward	GAGCCGACAGTCTCCTCACATT
	Reverse	CTGCCTGGTTTTGAAGGTGCTG
Mm_ARL13B	Forward	ACCAGTGGTCTGGCTGAGATTG
	Reverse	CATCACTGTCCTTCTCCACGGT
Mm_DDR2	Forward	TCATCCTGTGGAGGCAGTTCTG
	Reverse	CTGTTCACTTGGTGATGAGGAGC
Mm_ITGA1	Forward	GGCAGTGGCAAGACCATAAGGA
	Reverse	CATCTCTCCGTGGATAGACTGG
Mm_RAPGEF2	Forward	GCCGAATGGCATCAGTCAACATG
	Reverse	CAACATCCAGCACTGTGGCGTT
Mm_RAPGEF6	Forward	ACAGAGTGAGCCAGGTGCTTCA
	Reverse	CACTCACTTCCTCAGTTGGTCC
Mm_APC	Forward	GTGGACTGTGAGATGTATGGGC
	Reverse	CACAAGTGCTCTCATGCAGCCT

Table 2.2: List of Mouse primers used in this study

The mice were sacrificed when the tumors reached approximately $1cm^3$.

For metastasis assays $1x10^5$ luciferase-expressing BM1 cells (BM1-luc) were injected into the left ventricle of the heart to allow for systemic distribution of these bone-tropic tumor cells. $5x10^5$ LMB cells and $1x10^6$ M6C cells were injected into the tail vein. Mice were monitored for 3-6 weeks (depending on the model) for tumor development. At the earliest sign of respiratory problems, or paralysis of the limbs, the experiment was ended and the mice were euthanized. Tumor burden was measured at the end of the study via Xenogen IVIS® 200 Imaging System (PerkinElmer) for BM1-luc tumors. For LMB and M6C tumors, tumor burden was measured by counting overt surface metastases in the lungs after perfusion

Primer pair		Primer sequence
Hs_ROCK1	Forward	CAGCCTCACTCTCCCATTTT
	Reverse	TCCAGCCTTTCCTCTGCTAA
Hs_PIKFYVE	Forward	CTGGACTCCTTCTGCCTGAG
	Reverse	AAGACTCCGCCCTCTGTTTT
Hs_DOCK4 (upstream)	Forward	ATTTGCCTGGAGTGGAAGTG
	Reverse	CTGTATCCAGGGGGATGATG
Hs_DOCK4 (downstream)	Forward	TAAGCCCTAGCTCCTGGACA
	Reverse	AGGGGTCACAAACACTCCTG
Hs_RAPGEF2	Forward	AAAAATGCCAAGAAGGGGTTA
	Reverse	CACTCATCTAGACAGACCCCTGA
Hs_RAPGEF6	Forward	CGCCACAGTTCATTCACACT
	Reverse	GCGAAGGGTTGTTTGCTAGA

Table 2.3: List of Human primers used for the CHIP assay quantitative RT-PCR

and formalin fixation, as well as counting tumors in cross-sections of the lungs after H&E staining (described below).

For the in vivo studies involving MAPK inhibitors and the 4-drug MAPKi combination treatment, small molecule inhibitors were resuspended under sterile conditions. Since not all of the inhibitors were water-soluble, all inhibitiors were initially resuspended in DMSO at the volumes that will result in less than 5% final DMSO concentration. p38 inhibitor SB203580 and the MLK inhibitor URMC-099 were further diluted to the desired concentration with 50%PEG-400 (Sigma, Cat No 91893) + 50%saline. JNK inhibitor SP600125 and MEK inhibitor Trametinib were diluted in corn oil (Sigma, Cat No C8267). For the 4-drug combinatorial treatment, dissolving all of the inhibitors in the same solvent was challenging. Instead, all inhibitors were dissolved in their own solvent at 4X higher concentration then the desired final concentration. Then, SB203580 and URMC-099 were mixed at 1:1 ratio, reducing the concentration for each drug down to 2X. Similarly, SP600125 and Trametinib were mixed at 1:1 ratio. These dual combination solutions were then filtered through 0.22 μm PES filter syringes to assure sterility. Each mouse received 50μl of each dual combination on the same day, resulting in a total of 100μl of drug mix (2 injections per mouse) with each drug at their desired 1X final concentration. Final concentration for SB203580, URMC-099, SP600125, and Trametinib in the 4-drug MAPKi combination was 10 mg/kg/day, 10

mg/kg/day, 10 mg/kg/day, and 0.5 mg/kg/day, respectively. All injections were intraperitoneal.

For the tumor growth experiments with the MAPK inhibitors, tumors were allowed to reach the size 50-100 mm^3 size before the MAPKi treatment began. Then, the mice were treated with the respective MAPKi treatment (or the control) for up to 3 weeks. Tumor size was monitored twice a week with a caliper. For the metastasis assays the tumor cells were treated with the 4-drug MAPKi combination at the in vitro doses for 24 hours prior to injections to allow for anti-metastatic reprogramming of the cells. Homing to metastatic tissues upon intracardiac or teil vein injections can take up to 48 hours. To ensure that the reprogrammed tumor cells do not revert back to their untreated state in the circulation, we pre-treated the mice with the MAPKi combination 2-6 hours before tumor cell inoculation as well. After the inoculation, the mice were treated with the inhibitors daily for up to 3 weeks until the experimental endpoints discussed above were reached.

2.15 Tissue fixation and Immunohistochemistry

Tumor tissues were fixed in 10% formalin upon dissection for 72 hours and then transferred into 70% Ethanol for long-term storage. Mouse lungs were perfused with PBS before formalin fixation step to allow for tissue expansion and high quality histological analysis. Fixed tissues were embedded in paraffin and sliced into 5µn sections prior to immunohistochemical analysis. All immunohistochemisty for this body of work was performed by the University of Chicago Human Tissue Resource Center staff. Briefly, tissue sections were stripped of the paraffin through xylene treatment and rehydrated with a Ethanol-to-water gradient washes. Then the sections were incubated in antigen retrieval buffer at 97^oC for 20 minutes. Immunohistochemical analysis of macrophage infiltration within the tumor tissues was performed by using primary antibodies agains mouse macrophage marker F4/80. Both primary and secondary antibody treatments were carried out at room temperature in a humidity chamber. After secondary antibody incubation, the slides were developed using Elite Kit (Vector Lab-

oratories, Cat No PK-6100). Finally slides were counterstained with hematoxylin and bluing reagent and mounted with a cover glass.

For the detection of tissue morphology as well as tumor populations within the lung, lung sections underwent hematoxylin&eosin (H&E) staining. The sections were deparaffinized and rehydrated as described above, immersed in hematoxylin, rinsed in warm distilled water, and treated with eosin.

Stained slides were scanned at 10X on Nikon Eclipse Ti2 Inverted Microscrope System. Macrophage infiltration of the tumors was quantified on FIJI (ImageJ) software using the IHC Image Analysis Toolbox plugin (available at https://imagej.nih.gov/ij/plugins/ihc-toolbox/index.html). For each tissue, five randomly-selected fields were exposed to same quantification parameters and the average signal from all five fields was used to compare macrophage infiltration between different tumor tissues.

2.16 MIB-MS analysis

Multiplexed inhibitor beads - mass spectrometry analysis on BM1-VC and BM1-RKIP tumors was conducted in collaboration with Dr. Gary L. Johnson and his team at the University of North Carolina at Chapel Hill. Tumors were grown in athymic nude mice as described previously. Once the tumors reached the size of $\sim$300mm^3, they were isolated, flash-frozen in liquid nitrogen, and shipped to the Johnson Laboratories in Chapel Hill. Preparation of the lysate for the MIB-MS analysis, and the mass spectrometry were all performed by Dr. Johnson's team as described by Duncan et al. [25].

2.17 RNA-sequencing of tumors

To compare the transcriptomes of metastatic BM1-VC and non-metastatic BM1-RKIP tumors, 2 x 10^6 cells were injected orthotopically. When tumors reached approximately 500mm^3 size (about 3-weeks post inoculation), we harvested the tumors and flash-froze

them in liquid nitrogen. Tumor samples were pulvarized immediately, and lysed in TRI Reagent® (Zymo Research, Cat No R2050-1-200). RNA was extracted using the Direct-zol™ RNA MiniPrep Kit (Zymo Research, Cat No R2052) following the manufacturer's instructions under RNAse-free conditions. In order to prevent contamination of the RNA samples by genomic DNA, the samples were treated with DNAse-I (Zymo Research, Cat No E1011-A) for 15 min at ambient temperature on the RNA extraction column. Total RNA was eluted in RNAse/DNAse-free water (Zymo Research, Cat No W1001-30) and submitted to the University of Chicago Genomics Facility for further analysis.

RNA quality assessment, library preparation, and sequencing of the tumor RNA samples were all performed by the Genomics Facility staff following the facility's standardized protocols. Quality of the samples were assessed using Bioanalyzer and the samples were determined to be of high quality with an average RNA integrity number (RIN) of 8.6. For the RNA-seq analysis we had 7 control tumors and 5 RKIP-overexpressig tumors, so we chose to generate an individual oligo dT selected, mRNA directional library for each tumor sample without any pooling scheme. All 12 samples were run on the same lane in HiSEQ4000 to generate 50 base-pair long single-end reads.

Bioinformatic analysis of the RNA-seq results were all carried out using the web-based bioinformatics platform Galaxy (usegalaxy.org). Raw "*.fastq" files were uploaded to the Galaxy servers via a file transfer protocol (FTP) software. The reads were analyzed for GC content using FastQC and trimmed to remove adaptor sequences using Trim Galore!. The reads, then, were mapped to the human genome (hg19) using RNA STAR. In all samples, 70-75% of the reads were uniquely mapped. The resulting "*.bam" files were used to count reads per gene with featureCounts. Finally, read counts were normalized and analyzed for differential expression between Control and RKIP-overexpressing samples using DESeq2. Principle component analysis on the normalized read counts demonstrated two distinct clusters of samples, separated by the RKIP status.

2.18 The Cancer Genome Atlas Analyses

For the analysis of patient data, normalized RNA-seq results were accessed through the cBioportal data base (www.cbioportal.org)[34, 13]. For every TCGA cancer type, the provisional data sets were used for analysis (tagged "TCGA, Provisional" on cBioportal). List of genes that correlate with RKIP and BACH1 were also downloaded directly from cBioportal, as the data base already has these correlation matrices generated for each TCGA cancer type. Oncotype and expression heatmap plots were directly generated by cBioportal. Prior to generation of these plots, z-score threshold of 0.5 was arbitratily chosen to classify patients into high vs. low expressors for a particular gene of interest. For example, if a patient's tumor sample has an RKIP expression level that has a z-score higher than 0.5, then the sample was deemed "RKIP-high", and if the z-score was below -0.5, the sample was deemed "RKIP-low". If the z-score falls within -0.5 and 0.5, then the sample was considered as "Intermediate", or "Other". Both Pearson and Spearman correlations were used in determining gene-gene correlations and a coefficient cut-off of 0.3 was chosen arbitrarily for both correlation metrics.

The clinical metadata regarding the TCGA breast cancer data set was downloaded from cBioportal. The clinical information on breast cancer patients does not contain TNBC status information. So we assigned TNBC vs. Non-TNBC status to breast cancer samples by considering immunohistochemistry-based assessment of ER, PR, and HER-2 expression. If the sample was negative for all three of these parameters by IHC, the sample was deemed "TNBC". Otherwise, the sample was considered as "Non-TNBC". A total of 115 cases were identified as TNBC with this method.

Pam50 subtype information for the TCGA breast cancer samples was downloaded using the R packaged "TCGAbiolinks" [19] (. For this analysis, only those samples with a Pam50 annoation were considered (there were only 512).

2.19 Gene Set Enrichment Analyses

Functional gene set enrichment analysis of the differentially expressed genes in the RNA-seq data as well as the genes that correlate with RKIP and BACH1 was performed using the web-based interface of the Metascape software [97] (metascape.org). For the identification of pathways and processess enriched in the input gene lists, both "Gene Ontology" (GO) and "Kyoto Encyclopedia of Genes and Genomes" (KEGG) categories were considered. Minimum overlap of 5 genes and an enrichment score of 1.5 was chosen as the enrichment parameters. Adjusted p-value cut-off of 0.05 was chosen as the significance threshold.

CHAPTER 3

LESSONS LEARNED FROM RKIP: ROLE OF STRESS NETWORKS IN CANCER METASTASIS

3.1 Abstract

Late stage cancers are extremely difficult to treat because there are very few systemic treatment options against metastatic disease. At the metastatic stage, tumor cells are more resistant to the standard chemotherapeutic treatments. Particularly in late stage triple negative breast cancers the only line of treatment is chemotherapy, but a high proportion of these patients either do not respond to the treatment or relapse within 5 years. Therefore, there is an urgent clinical need for novel therapeutic approaches that can target the metastatic stage of cancers.

In this chapter, we sought to develop new anti-metastatic treatment options by studying one of the physiological suppressors of metastasis, RKIP. Kinomic analysis of metastatic (BM1-VC) and non-metastatic (BM1-RKIP) tumors revealed a network of MAP kinases involving the stress-induced p38 and JNK signaling cascades in addition to ERK to be inhibited by RKIP. In vitro studies suggested that ERK inhibition alone cannot always explain downregulation of p38 and JNK activity in RKIP-expressing TNBC cells. We identified MAP3K-level kinases MLK and TAOK, which can activate p38 and JNK, as novel downstream targets of RKIP. Inhibition of MLK, TAOK, p38, and JNK by small molecule inhibitors and/or siRNAs impaired invasion in TNBC cell lines, highlighting the importance of stress kinase signaling in metastasis. Negative feedback mechanisms between p38 and JNK suggested that a single agent is not enough to inhibit the entire RKIP target kinase network. Therefore, we used high-throughput invasion assays to screen for kinase inhibitor combinations that can block invasion by partially inhibiting all three axes of the stress MAPK network. A 4-drug combination consisting of p38, JNK, MEK, and MLK inhibitiors used at sub-therapeutic doses effectively phenocopied RKIP by inhibiting MAPK network and

invasion, without affecting proliferation of TNBC cells in vitro. In xenograft and syngeneic mouse models, the 4-drug MAPKi inhibited metastasis as well as primary tumor growth without apparent overall toxicty to mice. 4-drug MAPKi also showed significant survival benefit even after cessation of the treatment. Collectively, these findings demonstrate that combinatorial treatment modalities that mimic metastasis suppressors like RKIP are vaiable therapeutic options for metastatic cancers.

3.2 Introduction

Studying RKIP is a powerful approach to unraveling intricate mechanisms that lead to the metastatic progression of cancers. RKIP's robustness in reprogramming metastatic cancer cells into a non-metastatic state in multiple solid tumor types allows for elucidating key mechanisms of metastasis. It also allows for comparisons between metastatic and non-metastatic cancers in a syngeneic background with the exception of RKIP overexpression, providing a model with less noise. More importantly, RKIP's molecular function in inhibiting kinases provides a unique opportunity to reveal signaling events that govern different steps of metastasis, and to develop effective therapeutic strategies for blocking disease progression. Understanding downstream effects of RKIP on kinase networks can guide the discovery of kinase inhibitor combinations that ultimately mimic RKIP's anti-metastatic function in tumors lacking RKIP expression.

Using kinase inhibitors as single agents has not yielded durable treatments in the clinic, as signaling networks have redundant pathways that can bypass the effect of the inhibitor. Developing effective anti-metastatic treatments will require identification of these feedback mechanisms and disabling them by combining multiple inhibitors. Similarly, RKIP has the potential to affect multiple signaling cascades, as exemplified by its inhibitory role on RAF and NFκB signaling. Therefore, it is unlikely that there is one inhibitor that will capture RKIP's function on metastatic networks. This requires studying RKIP-mediated signaling at a systems level under physiological conditions. In other words, changes in the activity

of the entire kinome must be monitored in order to gain a more complete picture of the metastatic and non-metastatic states.

RKIP's effect on the RAF-MEK-ERK cascade is well-characterized [102], and it is evident that it can interact with more than Raf-1 (see Background). However, our understanding of RKIP's function at the kinomic level is incomplete. Here, we sought to discover kinase networks altered by RKIP in the process of anti-metastatic reprogramming of TNC cells. The systems-level approach will not only allow us to uncover novel pathways targeted by RKIP, but also provide therapeutic strategies for blocking metastasis.

3.3 Results

3.3.1 RKIP regulates the activity of stress kinases in TNBC

Phospho-proteomic analysis of tumors using mass spectrometry is a commonly used method for studying the kinome of cancers [79]. This approach qiantifies phosphorylation of certain residues on kinases, but inferring the activity of kinases based on phospho-proteomic data heavily relies on prior knowledge about the correlation between the phospho-sites and the activation state of a kinase.

In order to investigate RKIP-regulated kinome, we employed an alternative method that quantifies overall activity of individual kinases in a sample. Gary L. Johnson and colleagues have developed the Multiplexed Inhibitor Bead - Mass Spectrometry (MIB-MS) method that utilizes a set of kinase inhibitors that are conjugated to magnetic beads to pull down active kinases from any sample.[25] The kinase inhibitors employed for the isolation of kinases are Type-1 inhibitors (ATP-competitive), which bind to the active conformation of kinases. Therefore, MIBs select for active kinases as a function of expression levels of a kinase as well as its conformation state. Quantitative mass spectrometry analysis of the isolated kinases allows for comparison of kinase activity across multiple samples. Johnson et al. have used this method repeatedly and successfully to elucidate adaptive changes in the kinome of

cancers as resistance mechanisms upon drug treatments [25, 92].

We employed the MIB-MS approach to compare the kinome of metastatic BM1 tumors that lack endogenous RKIP expression to non-metastatic BM1 tumors in which we re-expressed RKIP exogenously. MIB-MS analysis of tumors were performed by our collaborators Dr. Johnson and his team at the Univeristy of North Carolina. MIBs pulled down more than 300 kinases from our tumor protein lysate samples and 250 of these kinases were identified in all of the biological replicates we submitted, allowing for further analysis of differential activity. In the end, the activity of 30 kinases were significantly altered upon reintroducing RKIP into the tumors (Figure 3.1, panel A on page 32), suggesting that these kinases are important for the metastatic process.

The majority of the kinases (23 out of 30) showed a decrease in their activity, consistent with RKIP's inhibitory role (the 7 kinases with increasing activity will be discuessed later). Among these kinases was a known target was MAPK1 (ERK2), a member of the RAF-MEK-ERK cascade targeted by RKIP, which validated the power of MIB-MS approach in identifying metastatic targets. More importantly, this is the first time regulation of ERK activity by RKIP is shown to take place under physiological conditions in TNBC tumors. Previous studies have mostly focused on in vitro studies where both RKIP and putative target proteins are over-expressed at supra-phyisological levels. In vitro studies have also suggested that MAPK14 (p38α) is an indirect target of RKIP, though mechanistic understanding of this interaction is incomplete. [2]

Interestingly, the changes that RKIP induced in the TNBC kinome were not specific to a specific family of kinases. In addition to known RKIP targets MAPK1 and MAPK14, MIB-MS identified more kinases from all branches of the human kinome tree that have never been implicated as RKIP targets before (Figure 3.1, panel B on page 32), such as STE family kinases (MAP3K9, MAPK3K11, TAOK2, and MLTK), Tyrosine Kinase (TK) family (JAK3, PTK2B, HCK, BTK, AXL, and EPHA2), Tyrosine Kinase-Like (TKL) family (IRAK1), "CDK, MAPK, GSK3 and CLK" (CMGC) family (MAPK8 and MAPK9),

Calmodulin/Calcium regulated kinase (CAMK) family (STK11), "Protein Kinase A, G, C" (AGC) family (RPS6KA3, RPS6KA5, RPS6KB1, SGK3, and PRKG1), and other families including some metabolic kinases (FN3KRP, ERN1, AGK, PIKFYVE, EIF2AK4, TTK, PDXK, CHKB, and PLK4). This finding suggests that the metastatic phenotype is not controled by a single kinase family.

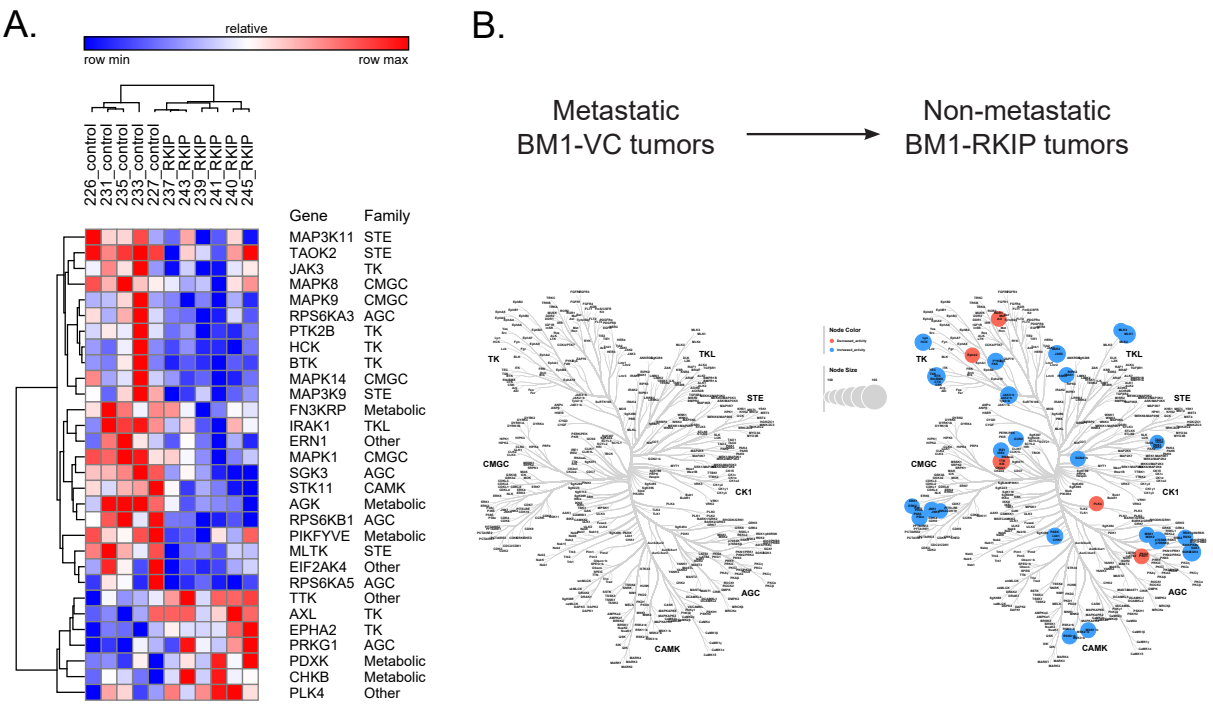

Figure 3.1: RKIP significantly regulates the activity of 30 kinases in xenograft mouse models of triple negative breast cancer (TNBC). (A) A heatmap of LFQ intensities from MIB-MS analysis for kinases the activity of which is differentially regulated between BM1-VC (control) and BM1-RKIP (RKIP) tumors. Each column represents a biological replicate (n=5 control tumors, n=6 RKIP tumors). The heatmap was scaled row-wise. Significance is determined with a two-tailed student's t-test on the LFQ values. For all the kinases depicted on the heatmap, the p-values were less than 0.05. (B) Depiction of kinases upregulated or downregulated by RKIP in the MIB-MS analysis on a kinome tree. Blue indicates downregulation of activity and red indicates upregulation of activity by RKIP with respect to the control activity levels. Size of the circles is proportional to the absolute value of the fold change of activity.

The broad range of kinases targeted by RKIP prompted us the investigate whether RKIP primarily inhibits highly active kinases in the cell. We first ranked kinases based on their activity level, determined by the label-free quantitation (LFQ) method in the metastatic

BM1-VC tumors, and identified where the significantly regulated RKIP targets fell on this activity ranking. In the top of the ranking were kinases such as MAPK1 (ERK2), EPHA2, and MAPK14 (Figure 3.2, panel A on page 34). Finding ERK to be the most active kinase is consistent with the mutational background of BM1 tumors as their parental cell line MDA-MB-231 expresses a constitutively active RAS mutant [40], which activates ERKs. RKIP inhibited not only some of the highly active kinases such as MAPK1 (ERK2) and MAPK14(p38α), but also many kinases with various levels of activity such as JAK3, SGK3, MAPK3K9 (MLK1). The effect size of regulation by RKIP on these kinases was small, ranging from 10% to 30%(corresponding to a log2 range of -0.6 to 0.6) (Figure 3.2, panel B on page 34)

Functional analysis of the 30 kinases that were significantly regulated by RKIP showed enrichment for protein phosphorylation-related gene sets, such as "phosphotransferase activity", "protein kinase activity", "protein autophosphorylation", and "protein serine / threonine / tyrosine kinase activity" (Figure 3.3, panel A on page 35). This result is expected given that the input list for this analysis was solely composed of kinases. The 23 negatively regulated kinases were enriched in "Stress-activated MAPK cascade", suggesting a role for stress pathways in TNBC metastasis (Figure 3.3, panel B).

Functional network analysis using Ingenuity® Pathway Analysis (IPA) revealed that the majority of the RKIP kinases are functionally connected (Figure 3.4, panel A on page 36). As the gene set enrichment analysis suggested, MAP kinases were at the center of the network. Community analysis of the protein-protein interaction networks generated using RKIP target kinases detected 3 major communities composed of the upstream MAP3K, the three MAPKs (ERK, JNK, p38), and the downstream RPS6Ks (Figure 3.4, panel B on page 36).

In order to validate regulation of stress MAPKs by RKIP, we used wildtype RKIP or the constitutively Raf-binding S153E mutant version in BM1 cell lines that do not express RKIP (Figure 3.5, panel A on page 37). When stress conditions were stimulated chemically using

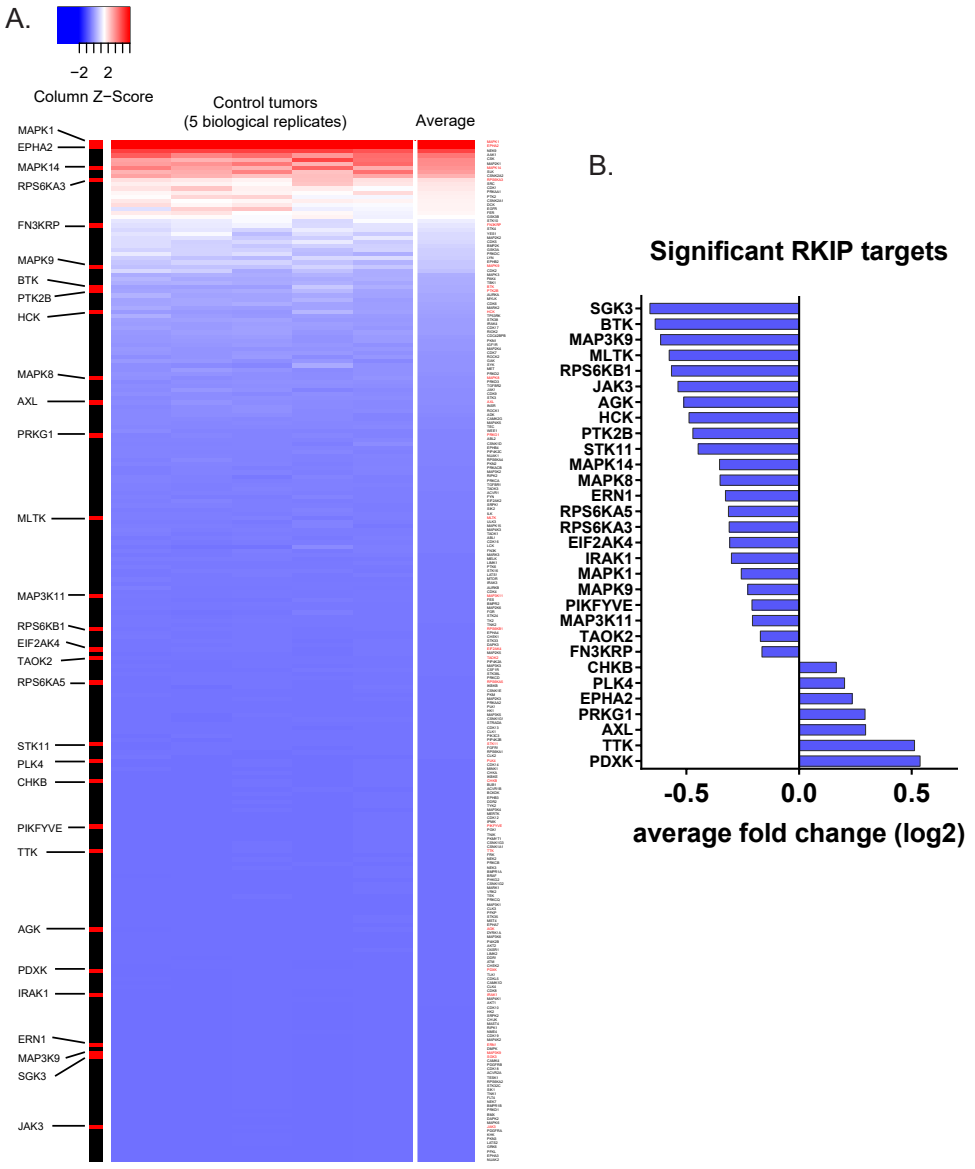

Figure 3.2: RKIP targets multiple kinases of different activity levels partially. (A) A heatmap of LFQ instensities for all 250 kinases pulled down with multiplexed inhibitor beads. Kinases were ranked based on their average LFQ intensity in the control tumor samples from high to low. The heatmap was scaled column-wise and each column represents a biological replicate (n=5 control samples). Kinases that are significantly upregulated or downregulated in their activity in the RKIP tumor samples were overlayed on the left in red. (B) Bargraph showing average fold changes in the activity of the 30 kinases regulated by RKIP in vivo. Fold changes are in log2 scale, corresponding to roughly 30% difference in either direction.

anisomycin [38], over-expression of RKIP and RKIP S153E partially inhibited induction of MAP2Ks MKK4, MKK3, and MKK6, stress MAPKs p38, JNK, and ERKs, as well as the downstream p70/p85 S6K and p90 kinase MSK1 (Figure 3.5, panel B). Downregulation

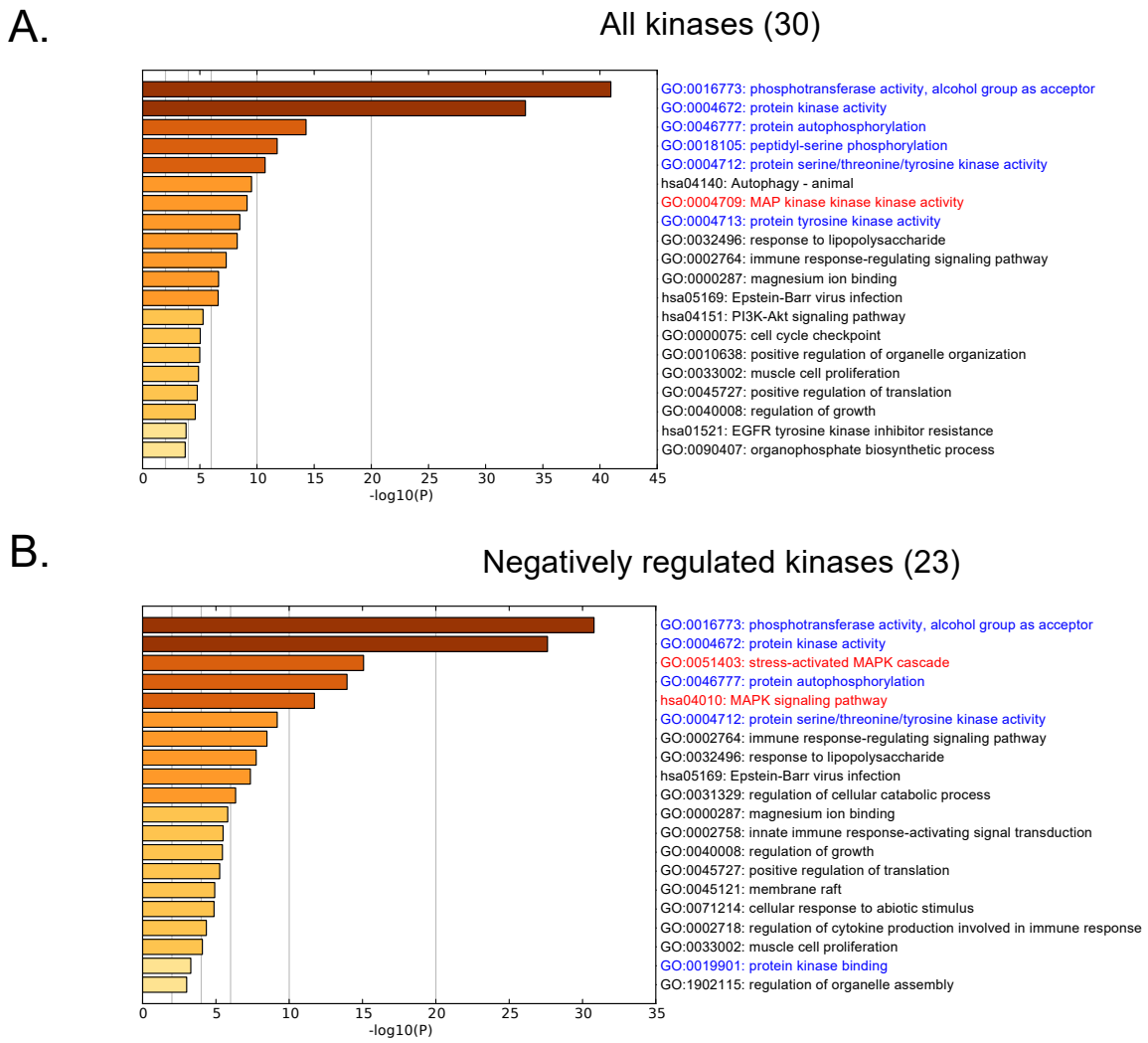

Figure 3.3: Kinases regulated by RKIP are enriched for stress-induced MAP kinases. (A) Gene set enrichment analysis by Metascape of all 30 kinases regulated by RKIP. Bargraph shows the p-values for each enriched gene set in -log10 scale. (B) Same analysis as in (A), but this time, the input kinases set was the 23 kinases that were downreguated by RKIP.

of stress kinase activity was also apparent when the cells were induced with serum as well (Figure 3.5, panel C), though serum is a much weaker inducer of p38 and JNK compared to anisomycin. Inhibition of stress kinase activity by RKIP was not limited to the BM1 cell line. Another human TNBC cell line MB436 shows similar results under anisomycin induction (Figure 3.6, panel A on page 38).

We also investigated RKIP signaling in mouse TNBC cell lines LMB and M6C. In both cell lines RKIP and RKIP S153E impaired p38 and JNK activation upon anisomycin or

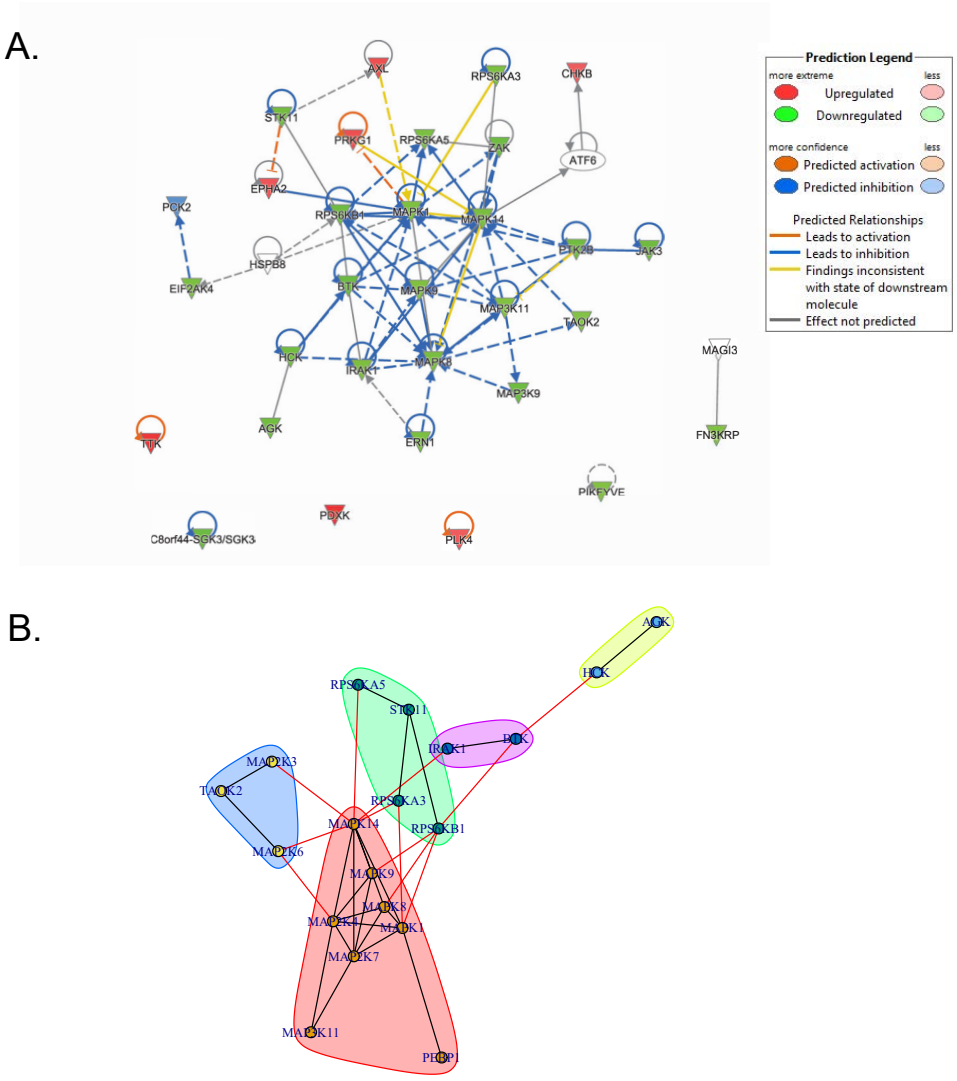

Figure 3.4: Network analysis of MIB kinases reveal a highly connected stress MAPK network regulated by RKIP. (A) Ingenuity® Pathway Analysis (IPA) on the 30 kinases regulated by RKIP. Each triangle (node) represents a kinase and each arrow (edge) represents a functional relationship (activation or inhibition). Red nodes indicate upregulation of kinase activity and green nodes indicate downregulation of kinase activity by RKIP in the input data set. Coloring of the edges represent the IPA prediction about the state of the interaction - red edges predict activation, blue edges predict inhibition. A complete color key is included in the top right corner in the Prediction Legend. (B) Direct protein-protein interaction network of the 30 kinases with community analysis. Nodes represent kianses and edges represent direct interactions. Black edges indicate within-community interactions, whereas red edges indicate inter-community interactions. Kinases that did not have direct interactions are not shown on the network.

serum treatment, though in some cases RKIP S153E was more potent (Figure 3.6, panel B for LMB and panel C for M6C)

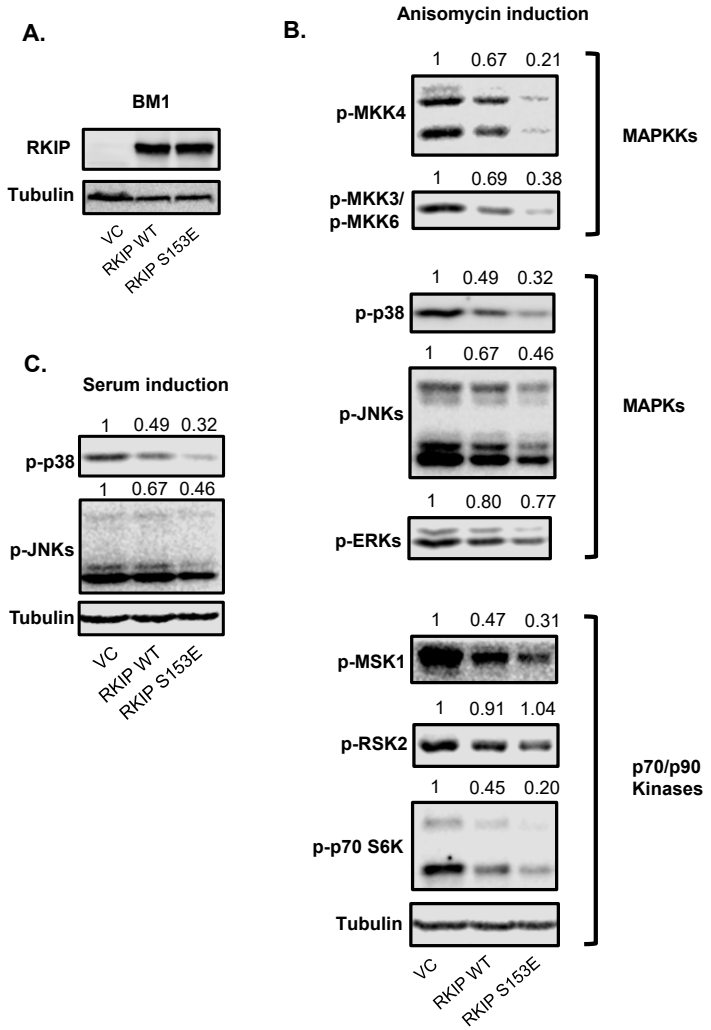

Figure 3.5: Inhibition of stress MAPKs by RKIP in the human TNBC cell line BM1. (A) Western blot showing the exogenous expression of wild-type RKIP or constutively Raf-binding S153E mutant RKIP in the BM1 cell line. (B) Inhibition of MAPKKs, MAPKs and downstream p70/p90 kinases by wild-type and mutant RKIP overexpression. BM1 cells were starved in serum-free mediate overnight and induced with anisomycin (25ng/ml) for 30 minutes before lysis. For each kinase, the activity was monitored by the phosphorylated state of the kinase which corresponds to activation status of the kinase. For a detailed list of the phopho-sites queried for this analysis, please refer to the Materials and Methods section. Band intensities were measured by densitometry, normalized to the intensity of Tubulin for that band on the same gel, and shown above the respective band. (C) Inhibition of stress kinases p38 and JNK by RKIP under serum conditions. BM1 cells were starved overnight, and induced with 10% serum for 30 minutes before lysis.

The fact that RKIP inhibits stress kinases suggests that p38 and JNK signaling are important for metastasis. Chemical inhibition of p38 and JNK activity with small molecule

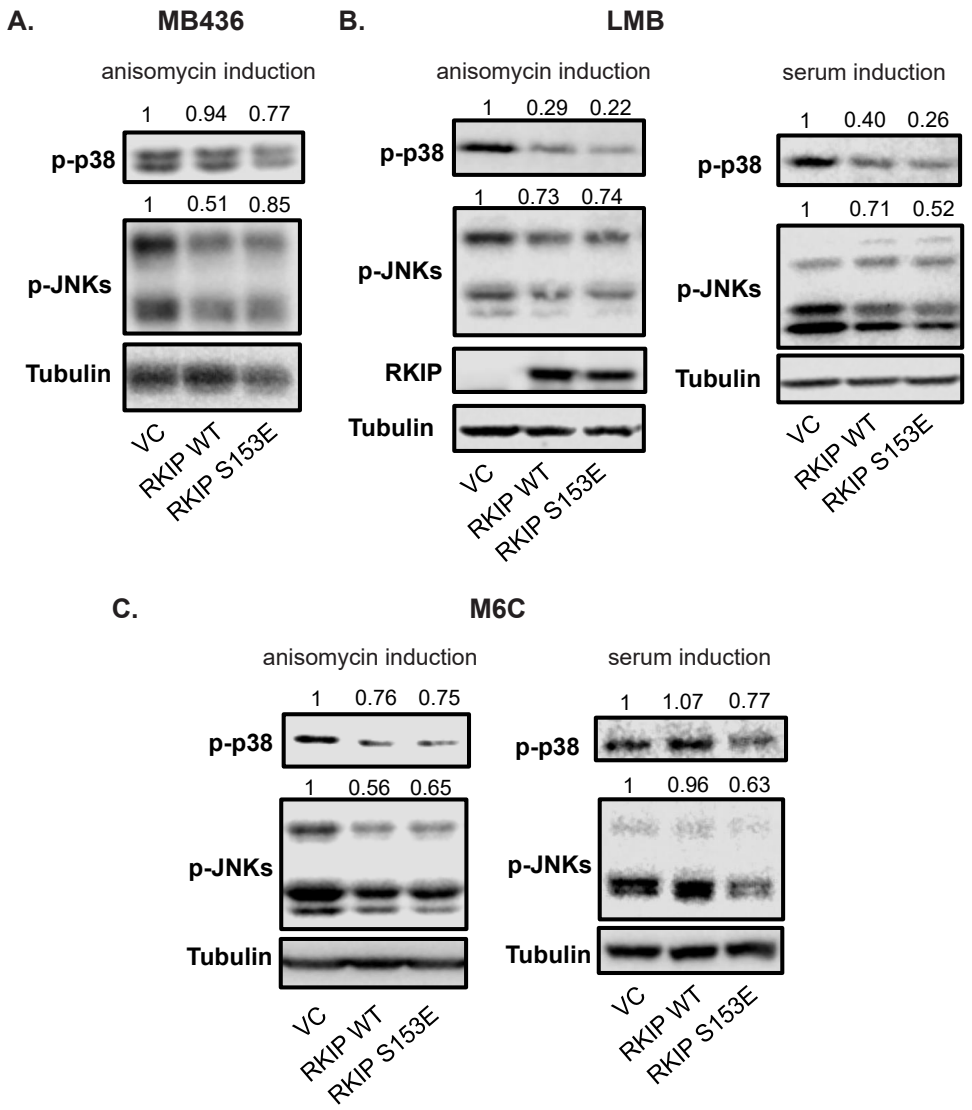

Figure 3.6: Regulation of stress MAPKs p38 and JNK by RKIP in other TNBC cell lines. (A) MB436 (human), (B) LMB (mouse), and (C) M6C (mouse) cells were starved overnight and induced by anisomycin (25ng/ml) or by serum (10%) for 30 minutes before lysis.

inhibitors specifically targeting these kinases mimicked RKIP's function by inhibiting invasive and migratory capability of BM1 cell line in a dose-dependent manner (Figure 3.7).

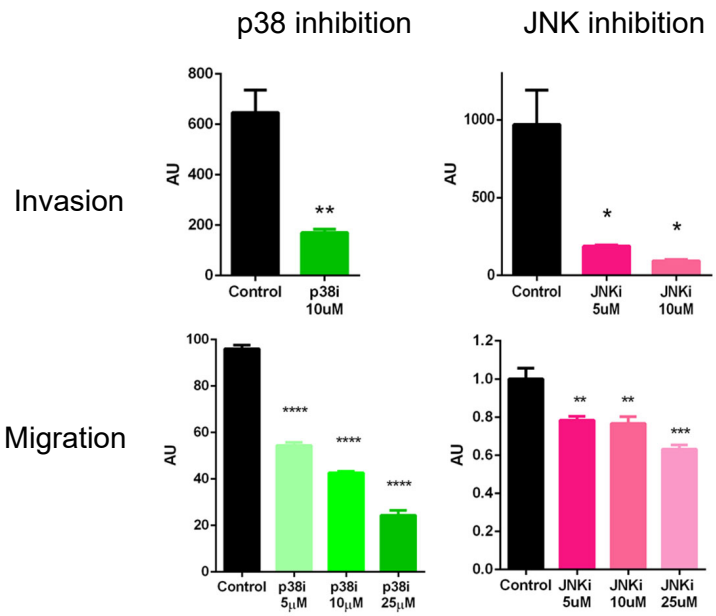

Figure 3.7: p38 and JNK activity is important for invasion and migration of BM1 cells. BM1 cells were treated with the p38 inhibitor SB203580 or the JNK inhibitor SP600125 at the indicated doses during the experiments. Plot shows mean ± s.e.m. (n=3 technical replicates per treatment group). Statistical signficance was determined by a two-tailed t-test with for each dose with respect to the control treatment.(p-values: * $p < 0.05$, ** $p < 0.01$, *** $p < 0.001$, **** $p < 0.0001$)

3.3.2 RKIP can regulate stress kinases independently of the RAF signaling pathway

Other studies have previously shown that there is cross-talk between different members of the MAPK family kinases [47]. RKIP is primarily known to bind Raf and inhibit downstream MEK and ERK activation. Since our MIB-MS data suggested RKIP can also downregulate stress MAPKs p38 and JNK as well, we wanted to investigate if this inhibition was downstream of the RAF-MEK-ERK inhibition. When we mimicked RKIP's function using a specific MEK inhibitior (Trametinib) which blocks MEK and ERK activation, JNK signaling was also inhibited in a dose-dependent manner in 3 out of 4 cell lines tested (Figure 3.8 on page 41). This suggests that the JNK signaling can be downstream of the ERK signaling when the cancer cells are induced by anisomycin. In contrast, there was no dose-dependent

pattern in the changes observed in p38 activity. At lower doses of MEKi, phopsho-p38 seems to decrease partially, but as the dose gets higher, there is a re-induction of p38. This effect was observed in BM1, LMB, and M6C cells, but not MB436 cells (Figure 3.8, panel A, C, and D). In MB436 cells, MEK inhibition under anisomycin induction caused gradual increase in the phosphorylation of p38. (Figure 3.8, panel B)

When the stress signaling is induced by serum, the response to MEK inhibition is different. There is no dose-dependent effect on p38 activity upon MEK inhibition under serum conditions, as it flactuates across different doses of MEK. JNK activity, on the other hand, tends to increase at higher doses of MEKi at least in MB436, and M6C cell lines. This phenotype might be isoform-specific as the quantification of the overall JNK signal in the western blots do not always reflect the patters observed in some bands (e.g. higher vs. lower molecular weight JNK bands).

These findings suggests that the influence of Raf-Mek-Erk cascade inhibition on p38 and JNK signaling is dependent on cell type as well as the type of induction. Even though the stress response to MEK inhibition is different under different conditions, one thing is clear: inhibition of ERK signaling is not enough to explain RKIP's effect on p38 and JNK. RKIP can block p38 and JNK activation under both anisomycin and serum, which is not recapitulated by using MEK inhibitor. This suggest that there are other mechanisms by which RKIP inhibits stress kinases, which will be topic of the next section.

3.3.3 RKIP inhibits the activity of upstream stress kinases TAOKs and MLKs

Raf, the well characterized target of RKIP, is a MAP3K level kinase that primarily activates MEK and ERK. Since inhibition of MEK activity cannot always account for the inhibition of p38 and JNK signaling, we looked for other upstream kinases. Our initial MIB analysis already identified other MAP3K level kinases which are known to activate p38 and JNK. Among these are the thousand-and-one kinases (TAOKs) and the mixed lineage Kinases

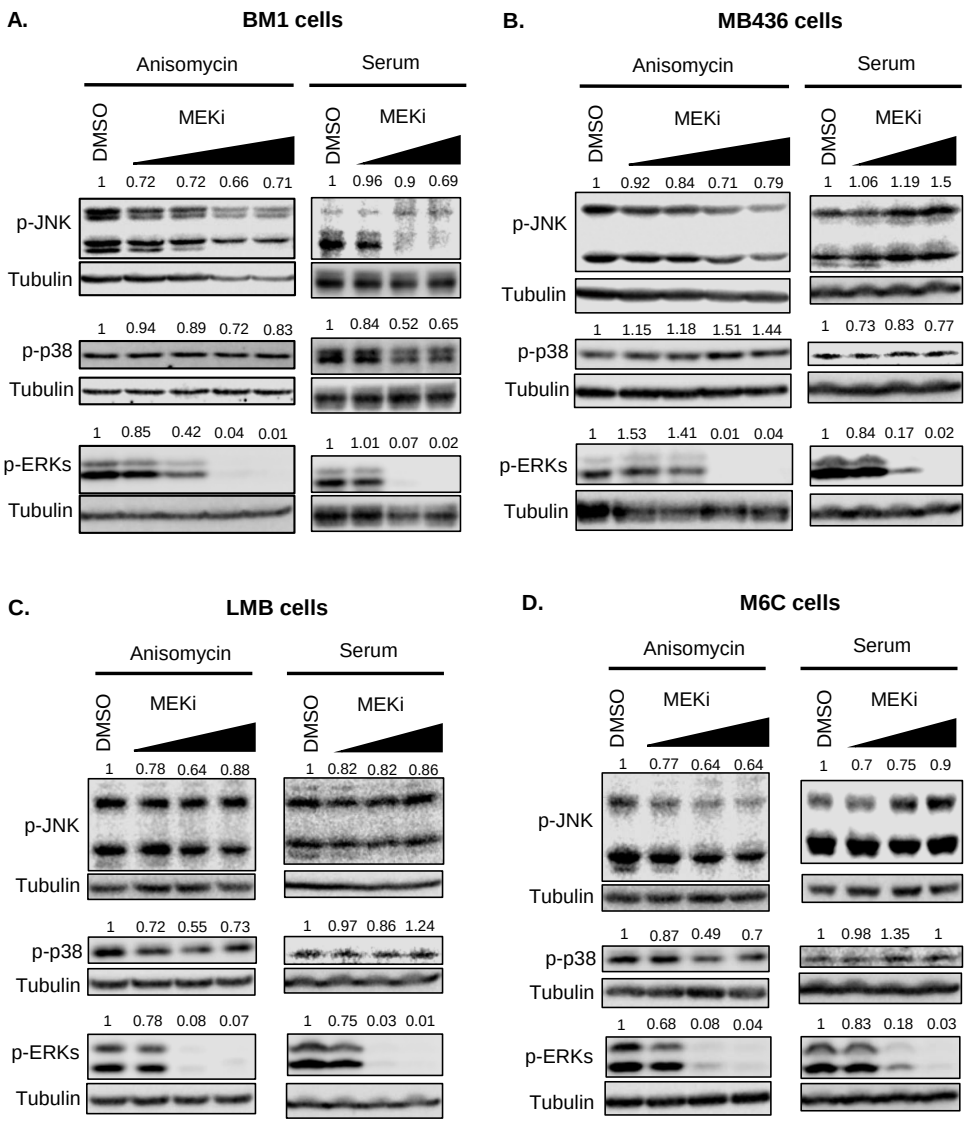

Figure 3.8: Reduction in ERK activity cannot account for RKIP's inhibitory function on p38 and JNK activity.Western blots demonstrating activity of JNK, p38, and ERK kinases in BM1(A), MB436(B), LMB(C), and M6C(D) cells upon overnight starvation, pre-treatment with MEK inhibitor Trametinib at increasing doses (0.1,1,10,100nM for BM1 and MB436 cells. 1,10,100nM for LMB and M6C cells) for 30 minutes, and induction with either anisomycin (25ng/ml, left panels) or 10% serum (right panels) in the presence of the inhibitor for 30 minutes.

(MLKs). MIB results showed that RKIP inhibits the activity of TAOK2, MLK1, MLK3, and MLTK (also known as ZAK). We hypothesized that RKIP regulates stress kinases p38 and JNK via inhibiting upstream TAOKs and MLKs.

We focused on TAO kinases and MLK3 because there were anti-phospho antibodies

available to assess the activity of these kinases via Western blots. Validating the MIB results from tumors, RKIP inhibited activity of TAOK1, TAOK2, and TAOK3, as well as MLK3 in vitro when BM1 and MB436 cells were induced with anisomycin (Figure 3.9 on page 42).

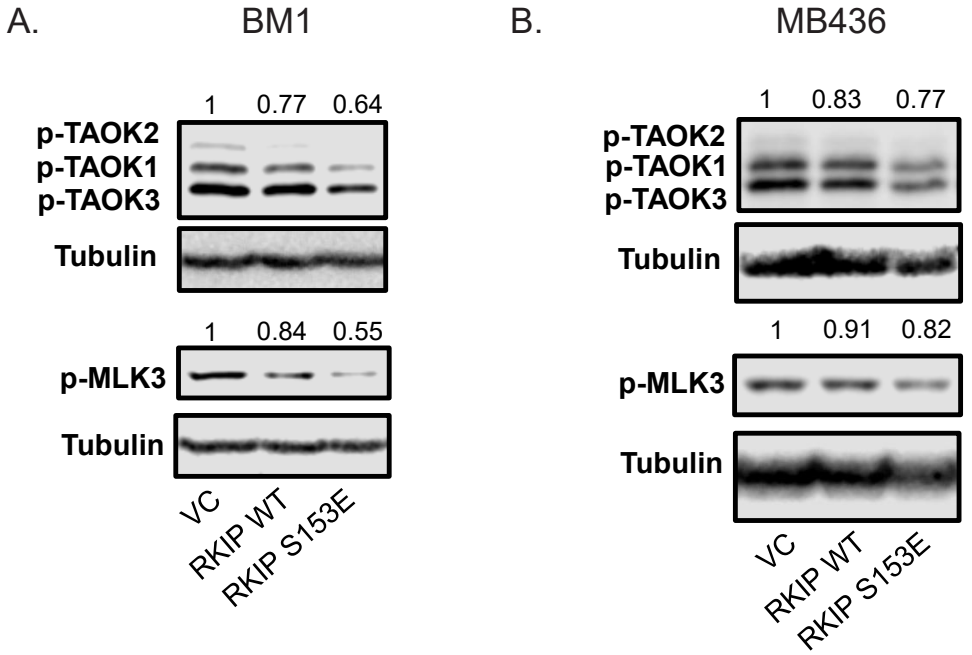

Figure 3.9: RKIP inhibits the activity of upstream MAP3K level TAO kinases and MLKs. BM1(A) and MB436(B) cells were starved overnight, and induced with anisomycin (25ng/ml) for 30 minuted.

Even though RKIP downregulates the activity of all three TAO kinases in vitro, only TAOK2 was significantly regulated in vivo according to the MIB analysis of BM1 tumors. These results were recapitulated in syngeneic M6C tumors, where Western blot analysis of phosphorylated TAOKs showed a significant reduction by RKIP only in TAOK2 activity (Figure 3.10 on page 43). These results sugges that RKIP has the ability to regulate all three TAOKs, but in vivo TAOK2 is its primary target.

Next, we wanted to test if TAOKs and MLKs are important in stress kinase signaling, invasion, and proliferation in our cell lines in vitro. First, we inhibited expression of TAOKs using siRNA technology targeting each TAOK individually. Since RKIP seems to downreg-

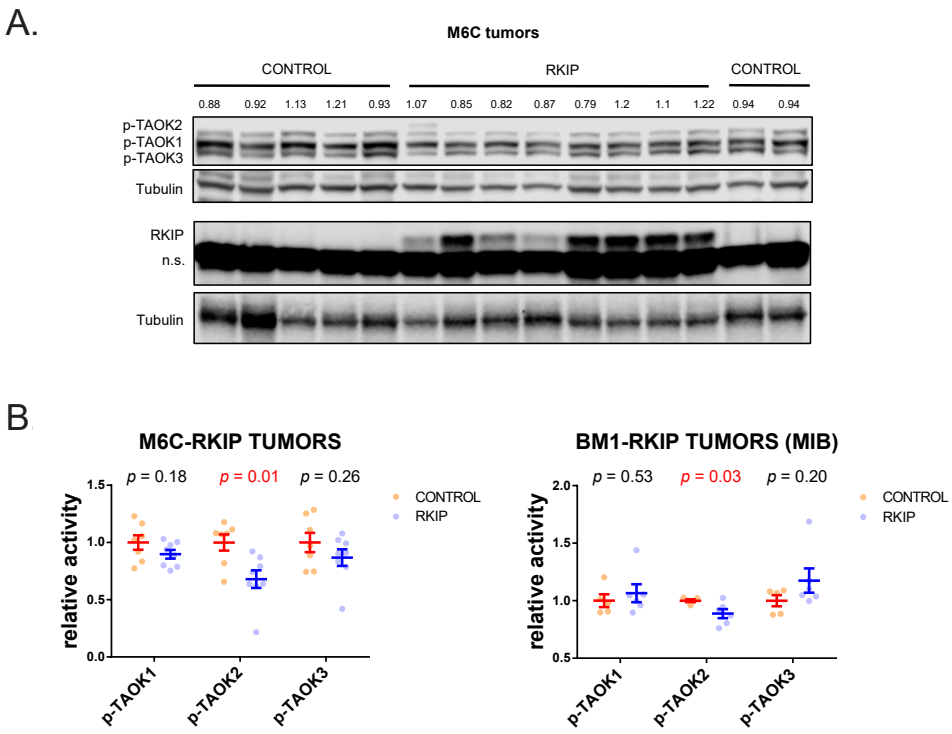

Figure 3.10: RKIP targets TAOK2 in vivo. (A) M6C cell with or without exogenous RKIP overexpression were injected orthotopically into REAR mice, and the tumors were isolated 4 weeks later when they reached roughly 1.5cm diameter. Western blot shows the activity of TAO kinases 1,2, and 3 and the RKIP overexpression in the protein lysates collected from these tumors (n=7 Control tumors, n=8 RKIP tumors. n.s - non-specific antibody binding. (B) Densitometery quantification of the western signal for each TAO kinase in Control and RKIP M6C tumors (left panel). Normalized LFQ intensity for TAO kinases 1, 2, and 3 in the MIB-MS data, originally depicted as a heatmap in Figure 3.1, panel A, from BM1 tumors with or without exogenous RKIP expression (right panel). Each dot on the graphs represents a biological replicate and the data are shown as mean ± s.e.m. Exact p-values are determined by a two-tailed t-test.

ulate activity of all three TAOKs in vitro, we also made a cocktail of all three si-TAOK constructs (si-Combo). We confirmed the knock down of TAOKs by quantitative RT-PCR, which suggested that the siRNA constructs used for this study were not completely specific to individual TAOKs (Figure 3.10, panel A on page 43). Since we are only looking for an effect on stress kinase activity upon an overall downregulation of TAO kinases just in the case of RKIP, the non-specificity of the si-TAOKs is not of concern.

When we knocked down TAOK expression in BM1 cells both p38 and JNK activation by

anisomycin was inhibited by si-TAOK1, si-TAOK3, and si-Combo (Figure 3.10, panel B). TAOK2 knockdown suprisingly did not have any obvious effect on the stress kinase signaling, potentially due to the fact that it seems to be the least active TAOK among the three TAOKs (faintest band on the p-TAOK Western blots). Under serum conditions, however, knockdown of TAOKs resulted in induction of p38 activity, while si-TAOK1 moderately downregulated JNK (Figure 3.10, panel C). The results were almost opposite in the MB436 cells, where p38 and JNK activity was inhibited by si-TAOK1, si-TAOK2, and si-TAOK3 in serum, but not in anisomycin (Figure 3.10, panels D and E). These results demonstrate that, though TAO kinases are capable of regulating both p38 and JNK activity, their function heavily depends on the cell type and the type of induction.

MLKs primarily activate the JNK pathway [80]. When we inhibited MLK activity with URMC-099, a small molecule inhibitor that targets MLKs 1/2/3 and LRRK2, we observed less JNK activation across all 4 cell lines tested under both anisomycin and serum conditions (Figure 3.11 on page 43). The only exception to this observation was M6C cells under anisomycin induction. In these conditions the MLK inhibitor induced more phospho-JNK (Figure 3.11, panel D), suggesting that negative feedback mechanisms that override the MLK inhibition exist in M6C cells. In human cell lines BM1 and MB436, but not in mouse cell lines, high doses of MLKi also blocked p38 activation when the cells were induced by anisomycin (Figure 3.11, panel A and B in comparison with C and D).

Inhibition of TAO and MLK kinases phenocopy RKIP's role on invasion. TAOK blockade by siRNAs and MLK inhbition by URMC-099 both result in diminished invasiveness in BM1 and MB436 cells in vitro. This observation is consistent with the previous findings on p38 and JNK's role in invasion, and argues for TAOK and MLK involvement in stress-mediated invasion.

Overall, these findings suggest that TAOKs and MLKs are capable of regulating both p38 and JNK in a context-dependent manner. But the results also highlight an important point about these in vitro studies, that there can be feedback mechanisms which alter the

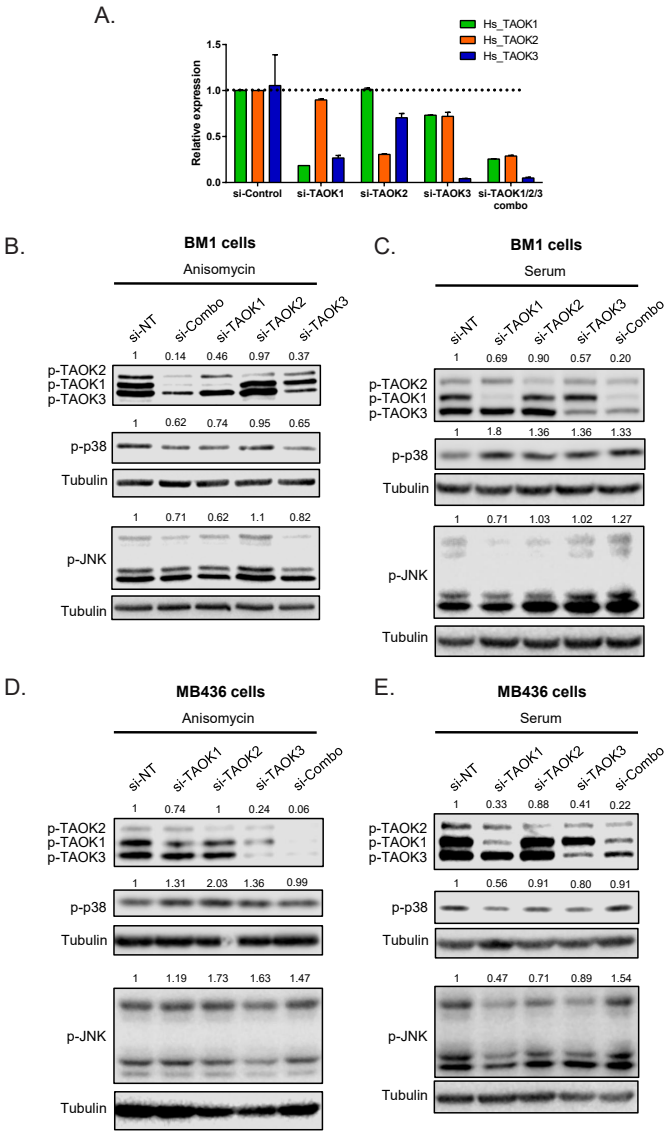

Figure 3.11: TAO kinases regulate p38 and JNK activity under certain circumstances in vitro. (A)Quantitative RT-PCR analysis of human TAOK1, TAOK2, and TAOK3 tanscripts in BM1 cells treated with si-RNAs againt the TAOKs. Bargraph shows the normalized expression of each TAOK as mean ± s.e.m of at least n=2 technical replicates. Expression values were calibrated to the expression for each TAOK in the si-Control sample. BM1 cells (B-C) and MB436 cells (D-E) were transduced with siRNAs targeting TAO kinases for 24 hours. Then the cells were starved overnight and induced with anisomycin (25ng/ml) (B and D) or 10% serum (C and E) for 30 minutes.

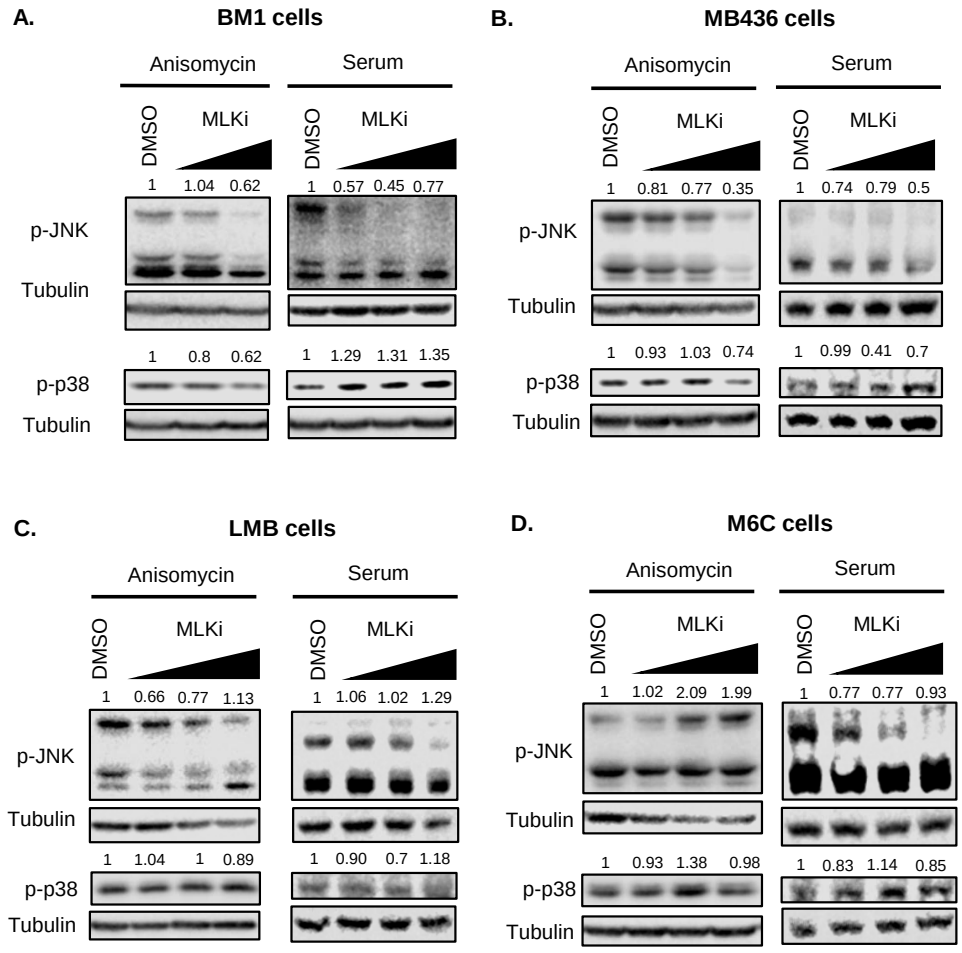

Figure 3.12: MLK inhibition blocks JNK activation. Western blots demonstrating activity of JNK and p38 kinases in BM1(A), MB436(B), LMB(C), and M6C(D) cells upon overnight starvation, pre-treatment with MLK inhibitor URMC-099 at increasing doses (50nM, 200nM, 1μM) for 30 minutes, and induction with either anisomycin (25ng/ml, left panels) or 10% serum (right panels) in the presence of the inhibitor for 30 minutes.

output of a signaling event and it is difficult to predict the behaviour of a network without identifying these hidden bypass mechanisms.

3.3.4 Negative feedback loops between p38 and JNK signaling manifest under certain conditions

RKIP effectively inhibits all three axes of the MAPK network. Targeting one axis may prove ineffective because the MAPK network is tightly regulated through feedback mechanisms.

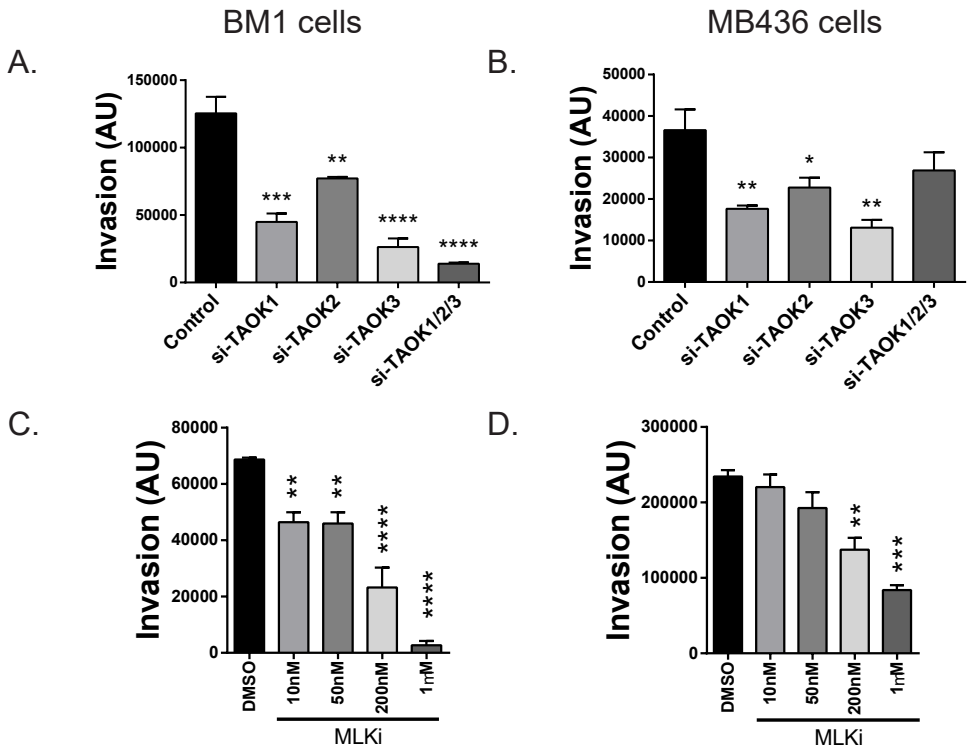

Figure 3.13: TAOK and MLK inhibition diminishes invasiveness of human TNBC cell lines. BM1 (A) and M436 (B) cells were transduced with the indicated si-RNA contructs for 48 hours and plated for Boyden chamber invasion assay. Live cells in the bottom well were quantified with Calcein AM staining as a read-out of invaded cells after 24 hours. BM1 (C) and MB436 (D) cells were plated for Boyden chamber invasion assay, with the indicated doses of the MLKi inhibitor URMC-099. Invaded cells were quantified 24 hours later. Data are plotted as mean ± s.e.m and significance was determined by two-tailed t-test with respect to the DMSO control samples. (A) and (B) are representatives of two independent experiments. (p-values: * $p < 0.05$, ** $p < 0.01$, *** $p < 0.001$, **** $p < 0.0001$)

Understanding these feedback mechanisms within TNBC is crucial for developing effective combinatorial therapies. In order to investigate the types of feedbacks embedded within the stress kinase networks, we used small molecule inhibitors that are specific to the p38 and JNK kinases.

Under serum induction, we observed the presence of negative feedback between the p38 and JNK pathways in BM1 cells (Figure 3.14, panel A on page 48). p38 inhibition resulted in more phosphorylated JNK, and JNK inhibition induced more phospho-p38 in a dose dependent manner in BM1 cells. Interestingly, these feedback loops were different under anisomycin-induced stress conditions. p38i-induced JNK activation was specific to serum

conditions and was not observed in anisomycin induced cells (Figure 3.14, panel B). JNK inhibtor increased p38 activity regardless of inducer. MB436, M6C, and LMB cells showed the same negative relationship between p38 and JNK activity as well, when the cells were induced with serum (Figure 3.15, on page 49). JNK activation upon p38 inhibition was mediated by MLKs becuase JNK was not induced when BM1 cells were co-treated with p38i and MLKi (Figure 3.16, panel A on page 50). Combined treatment with JNKi and MLKi further increased the intensity of p38 activation with respect to JNKi alone (Figure 3.16, panel B), suggesting that MLK mediates p38-to-JNK negative feedback but not JNK-to-p38.

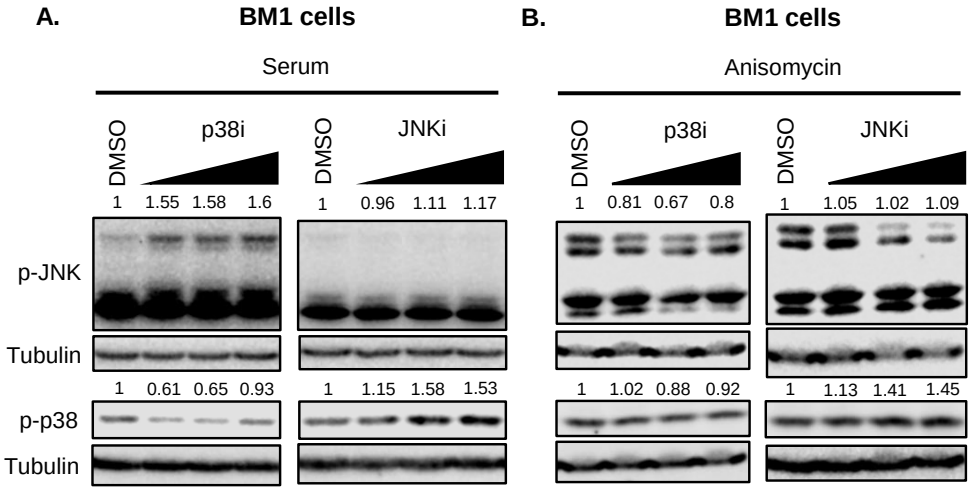

Figure 3.14: Negative feedback between p38 and JNK in BM1 cells. Western blots demonstrating activity of JNK, and p38 kinases in BM1 cells upon overnight starvation, pretreatment with p38 inhibitor SB203580 (left panels) and JNK inhibitor SP600125 (right panels) at increasing doses (1, 10, 25 μM) for 30 minutes, and induction with either 10% serum (A) or anisomycin (25ng/ml) (B) in the presence of the inhibitors for 30 minutes.

3.3.5 A combination of four MAPK inhibitors mimic RKIP's effect on stress signaling in vitro

The experimentally-validated RKIP stress kinase network with the feedback mechanisms suggested that inhibiting an individual MAPK axis (or one node on the network) would be ineffective in inhibiting the entire network (Figure 3.17, on page 51) because the feedback loops differ with cell type and stimulus. It was clear that we needed to combine multiple

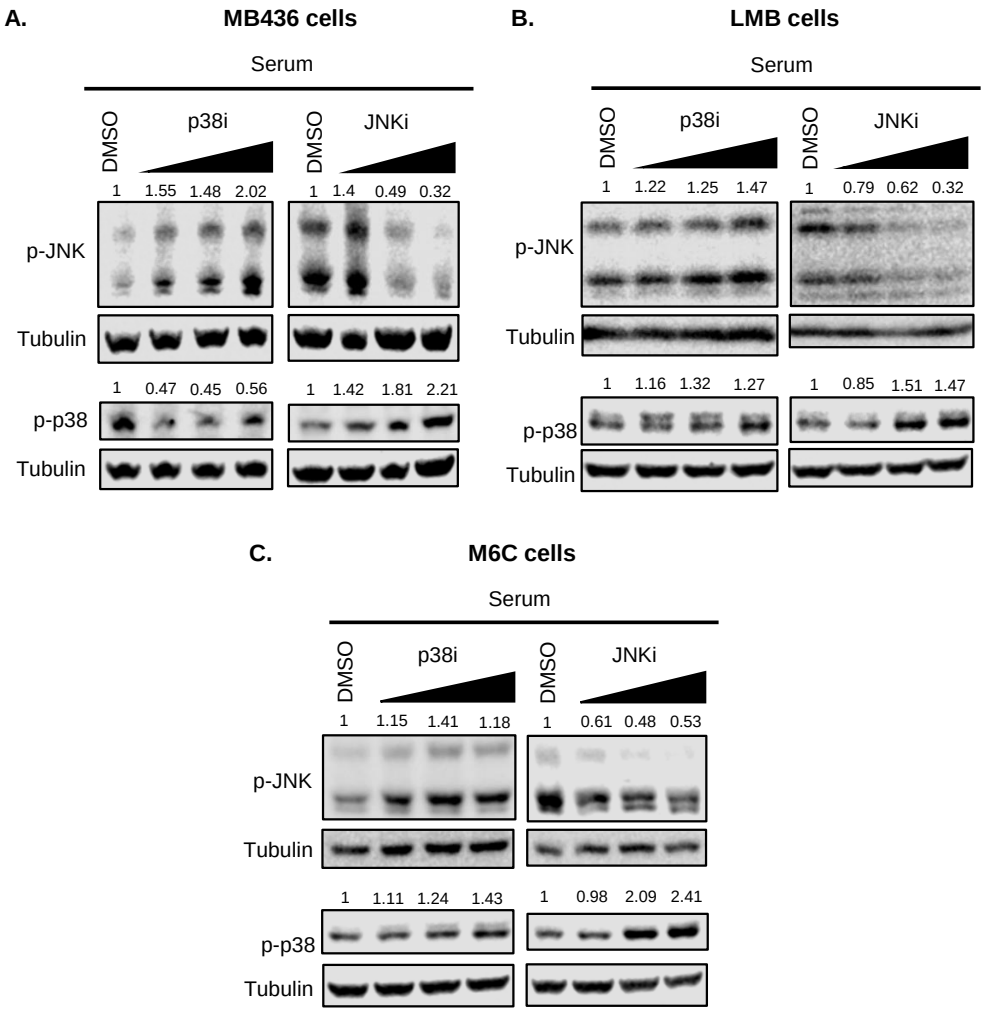

Figure 3.15: Negative feedback between p38 and JNK in MB436, LMB, and M6C cells. Western blots demonstrating activity of JNK, and p38 kinases in MB436 (A), LMB (B), and M6C (C) cells upon overnight starvation, pre-treatment with p38 inhibitor SB203580 (left panels) and JNK inhibitor SP600125 (right panels) at increasing doses (1, 10, 25 μM) for 30 minutes, and induction with either 10% serum in the presence of the inhibitors for 30 minutes.

MAPK inhibitors to mimic RKIP's effect on the core network. We reasoned that, if we screen for combinations of MAPK inhibitors that inhibit invasion of TNBC cells better than the individual drugs alone, those combinations would be more likely to target all three axes of the MAPK network. Furthermore, we wanted to mimic RKIP by using sub-threshold doses.

Since we are aiming to mimic RKIP's funtion, we strategized to start with a dose-response analysis of individual MAPK inhibitors to identify doses at which these inhibitors inhibited

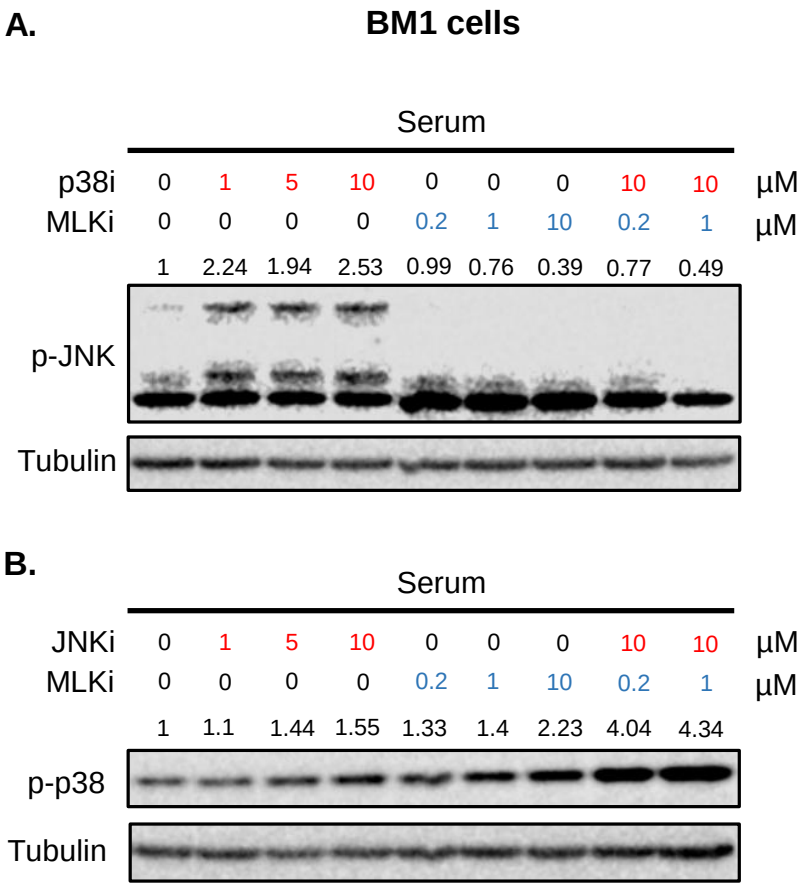

Figure 3.16: JNK activation upon p38 inhibition is mediated by MLK in BM1 cells. (A) Western blot showing JNK activity when BM1 cells were starved overnight, pre-treated with p38i alone, MLKi alone, or p38i and MLKi together at the indicated doses, and induced with 10% serum in the presence of the inhibitors. (B) Western blot showing p38 activity when BM1 cells were starved overnight, pre-treated with JNKi alone, MLKi alone, or JNKi and MLKi together at the indicated doses, and induced with 10% serum in the presence of the inhibitors.

invasion without affecting growth and proliferation of cancer cells. For this analysis, we used SB203580 (p38i), SP600125 (JNKi), Trametinib (MEKi), and URMC-099 (MLKi) (Figure 3.18, on page 52).

In 2016, Goldsmith and colleagues published a series of scaffold molecules that act as TAOK2 inhibitors [77]. In collaboration with Goldsmith's team, we have tried two of these molecules to see if they inhibited downstream stress kinases. Since TAOK2 is upstream of p38, we were primarily looking for blockade of p38 activity with these inhibitors. Out of the

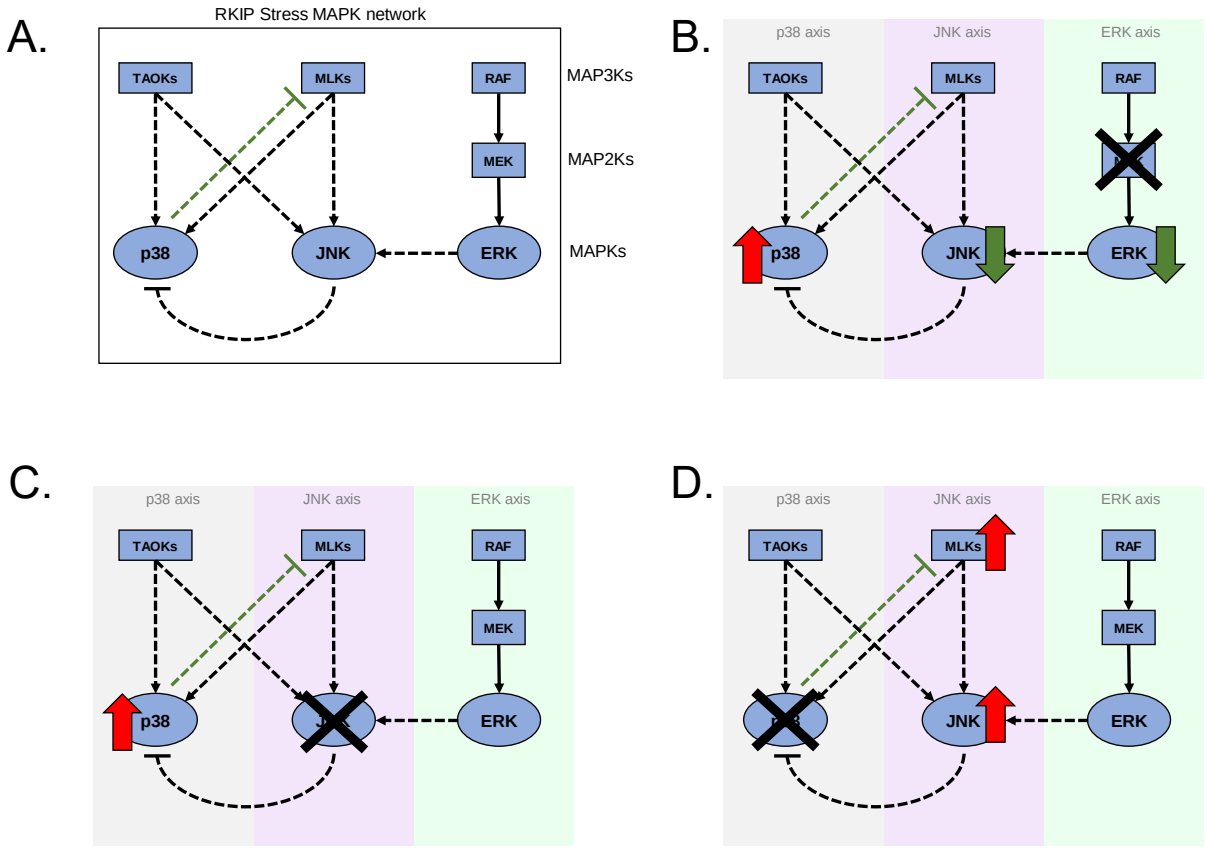

Figure 3.17: Diagram showing the experimentally-validated RKIP stress MAPK network and different scenarios of single agent targeting. Solid lines represent direct interactions, whereas dashed lines represent direct or indirect interactions. Black lines are interactions observed under anisomycin induction, and green lines are specific to serum induction. (A) JNK is downstream of MEK signaling, but p38 is not. Both TAOKs and MLKs can regulate JNK and p38 in a context-dependent manner. JNK inhibition induces p38 activation in anisomycin and serum. p38 inhibition induces JNK activation only under serum induction, which is mediated through MLK. (B) In the case of MEK inactivation, ERK and JNK activity is predicted to decrease but this can induce p38 activation due to the negative relationship between JNK and p38. (C) In the case of JNK inhibition, p38 activity will increase and ERK may stay the same. (D) In the case of p38 inhibition JNK and possibly MLK will become activated and ERK may stay the same. None of these single target scenarios predict downregulation of all three MAPK axes.

inhibitors we received, SW172006 (shortened as SW-006) is much more specific to TAOK2 than SW034538 (shortened as SW-538) (for specificity screen results, refer to the original publication [77]). Dose-response experiments under serum conditions showed that SW-006 blocks p38 induction partially even at doses as high as 100μM (Figure 3.19, on page 53).

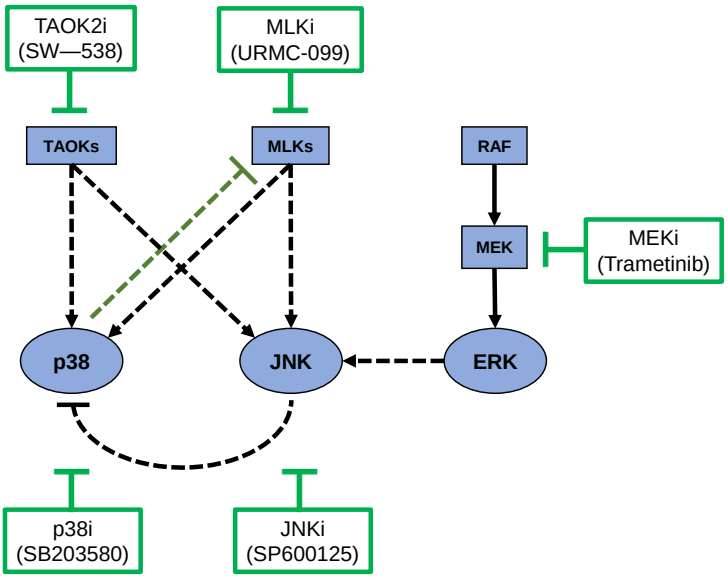

Figure 3.18: Small molecule inhibitors used for the anti-invasive combinatorial drug screen

SW-538, on the other hand, inhibited p70/85 S6K activity but slightly boosted p38 activation in a dose-dependent manner, probably due to its effect on other kinases. Interestingly, SW-006 partially impaired p38 activation due to JNKi treatment (Figure 3.20, on page 54), suggesting that TAOK2 might play a role in negative feedback loop between JNK and p38. In a chemotactic invasion assay, both SW-006 and SW-538 blocked invasion of BM1 cells (Figure 3.21, panels A and B on page 55), but they were also toxic to the cells at the indicated doses (Figure 3.21, panels A and C).

We were interested in investigating if the TAOK2 inhibitor SW-538 would have a combinatorial effect with any of these MAPK inhibitors because of its target profile [77]. Therefore, we included SW-538 in this phenotypic analysis as well (Figure 3.18, on page 52). In order to test proliferation and invasion properties of tumor cells under exposure to different doses of these inhibitors, we employed a high-throughput chemotactic invasion assay using nuclear-labeled BM1 cells. This assay is similar to Boyden chamber chemotaxis assays in that it has a porous membrane that separates the upper and lower chambers in order to create a chemotactic gradient, but it is set up in the 96-well format to allow for high-throughput testing. More importantly, live cell imaging component of the assays allows for monitoring

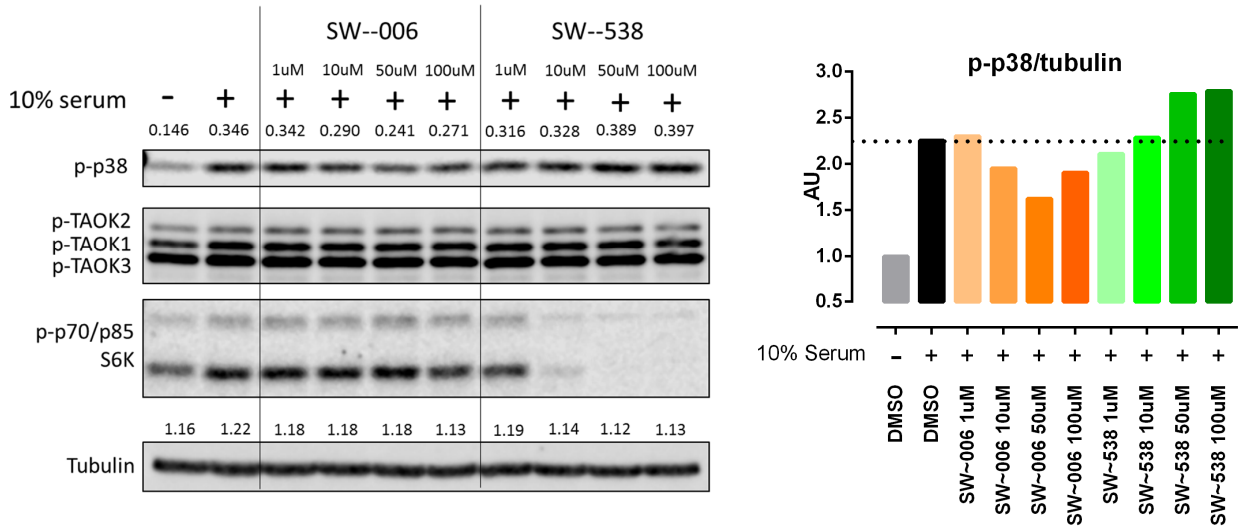

Figure 3.19: The effect of small molecule inhibitors of TAOK2 on p38 signaling under serum conditions. (Left panel) Western blot showing p38, TAOK1/2/3, and p70 S6K activity when BM1 cells were starved overnight, pre-treated with TAOK2 inhibitiors SW-006 and SW538 at the indicated doses, and induced with 10% serum in the presence of the inhibitors. Band intensities were measured by densitometry, normalized to the intensity of Tubulin for that band on the same gel, and shown above the respective band. (Right panel) Bargraph showing the phopsho-p38 signal on the Western blot in (A), normalized to Tubulin signal, and calibrated to the non-induced signal (First lane).

over time overall number of cells within each well (proliferation) as well as the percentage of cells that make it to the bottom chamber (invasion).

While determining the doses to be tested for this experiment, we made sure to go at least one dose higher and one dose lower than the doses at which these drugs are commonly used for in vitro studies in the literature. This meant a range of 1-20μM for SB203580, 1-20μM for SP600125, 1nM-1μM for Trametinib, and 10nM-10μM for URMC-099. Since the TAOK2 inhibitor SW-538 is a recently developed drug, there are no standard concentrations. Based on our signaling studies from previous sections, we decided that a range of 0.1-25μM would be appropriate.

Our initial analysis showed that all of these inhibitors blocked invasion of nuclear-labeled BM1 cells in a dose-dependent manner (Figure 3.22, on page 56). p38 inhibitor did not affect proliferation within the dose range tested. JNK and TAOK2 inhibitors slowed growth

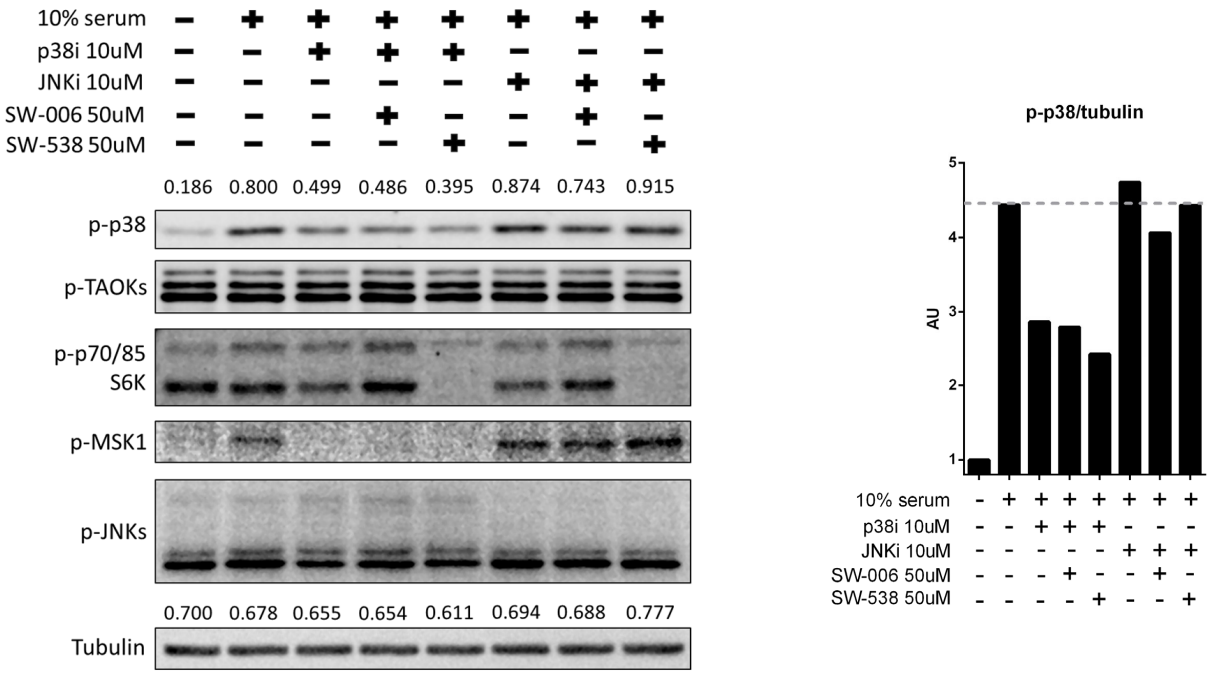

Figure 3.20: TAOK2 might play a role in JNKi-induced p38 overactivation. (Left panel) Western blot showing p38, TAOK1/2/3, and p70 S6K, MSK1, and JNK activity when BM1 cells were starved overnight, pre-treated with the indicated combinations and concentrations of p38i, JNKi, and the TAOK2 inhibitiors SW-006 and SW538, and induced with 10% serum for 30 minutes in the presence of these inhibitors. Band intensities were measured by densitometry, normalized to the intensity of Tubulin for that band on the same gel, and shown above the respective band. (Right panel) Bargraph showing the phopsho-p38 signal on the Western blot in (A), normalized to Tubulin signal, and calibrated to the non-induced signal (First lane).

and/or induced cell death at 10μM or higher. A similar phenotype was observed for the MEK inhibitor for 100nM and 1μM doses. MLK inhibitor was toxic to the cells at 10μM, but did not affect growth at the other doses tested. For the combination screen, we chose 1μM for p38i, 1μM for JNKi, 1/10nM for MEKi, 50nM for MLKi, and 0.1/1μM for TAOK2i.

Out of all the combinations tested, only 2 inhibitors showed a significant combinatorial effect on blocking invasion: (1) p38i + JNKi, (2) MEKi + MLKi (Figure 3.23, on page 57). These two dual combinations inhibited chemotactic invasion of cells without affecting overall proliferation. In terms of stress MAPK signaling, however, the dual combinations failed to inhibit all three axes of the MAPK network. In BM1 cells, p38i + JNKi was effective in inhibiting p38 and JNK phosphorylation, but inhibition of ERK activity was minimal

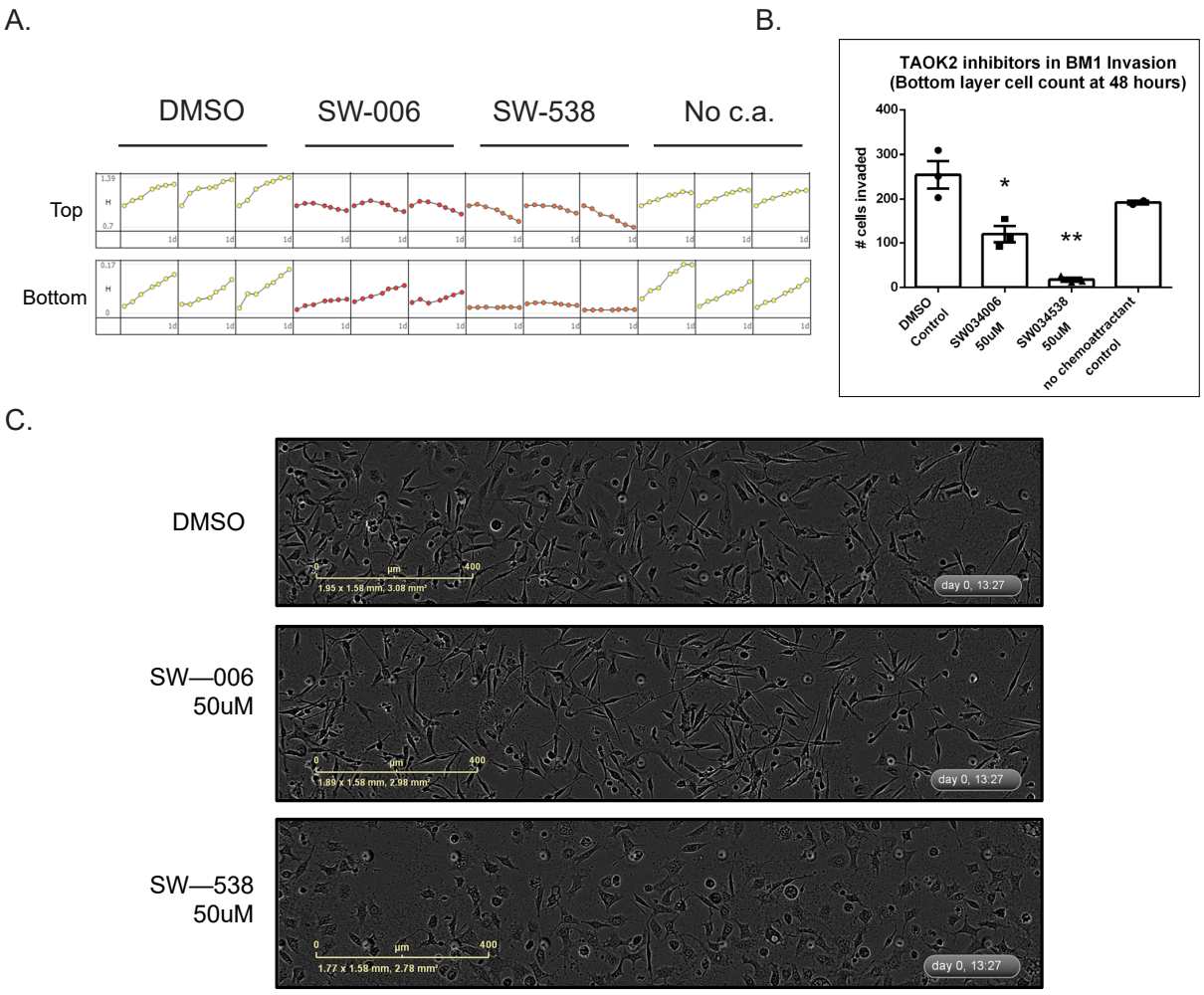

Figure 3.21: TAOK2 inhibitors block invasion of BM1 cells, but are also toxic to cells. (A) Percent confluence of nuclear-labeled BM1 cells on the top and bottom layers of the pourous membrane. Confluence was measured every 4 hours over the period of 30 hours. Top layer's growth media was added the indicated inhibitiors or DMSO as control. All wells had EGF (200ng/ml) as the chemoattractant in the bottom layer except for the wells labeled "No c.a." standing for no chemoattractant. Data were collected from n=3 technical replicates. (B) Barplot showing number of invaded cells in the bottom layer at the end of 48 hours. (C) Representative phase-contrast images of the BM1 cells from (A) under TAOK2i treatment.

(Figure 3.24, panel A on page 58). MEKi + MLKi combination was effective in blocking ERK and JNK activity, but p38 signaling remained active. Since the two dual combinations demonstrated opposite but complementary effects on p38 and ERK signaling, we reasoned that combining them could result in downregulation of the entire network. Combination of all four MAPK inhibitors (p38i + JNKi + MEKi+ MLKi) mimicked RKIP signaling

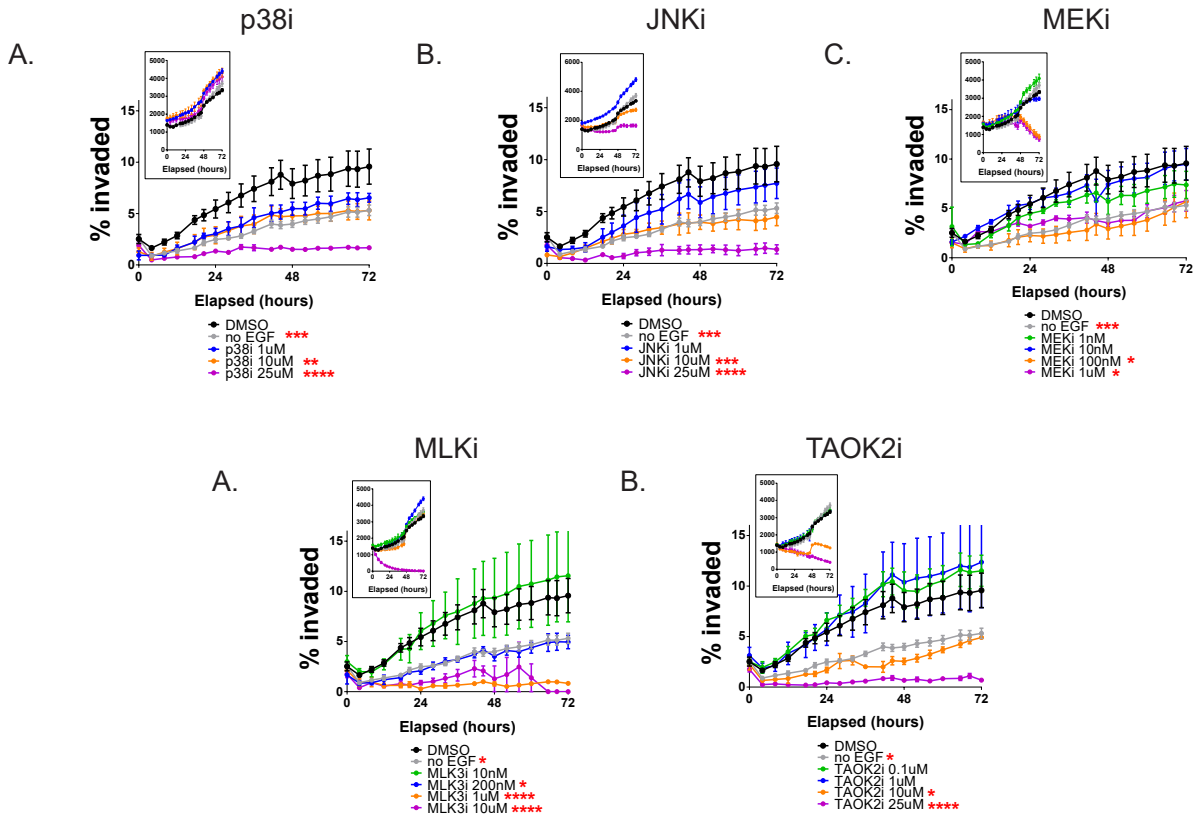

Figure 3.22: Dose response for invasion and proliferation with individual MAPK inhibitors. Inset shows proliferation measured as the total number of cells in the bottom and top layers. Invasion is measured as percentage of cells that made it to the bottom layer over total number of cells in the presence of p38i (A), JNKI (B), MEKi (C), MLKi (D), and TAOK2i (E) at the indicated doses. Data are plotted as mean ± s.e.m. for each time point and the p-values are calculated based on invasion data at the 72-hour time point using 2-way ANOVA with multiple comparison. (p-values: * $p < 0.05$, ** $p < 0.01$, *** $p < 0.001$, **** $p < 0.0001$)

by partially blocking signaling through all three axes of the RKIP stress MAPK network. Similar results were observed in MB436 cell lines as well (Figure 3.24, panel B). In the mouse cell line LMB, MEKi + MLKi dual combination was just as effective as the 4-drug MAPKi combination (Figure 3.24, panel C). However, in the end, the 4-drug combination was the only treatment that was able to mimic RKIP signaling across all three cell lines.

Moreover, the 4-drug MAPKi demonstrated a combinatorial phenotypic advantage over the dual treatments. Consistent with the observations regarding the signaling networks, the 4-drug MAPKi was more effective in blocking chemotactic invasion of nuclear-labeled BM1

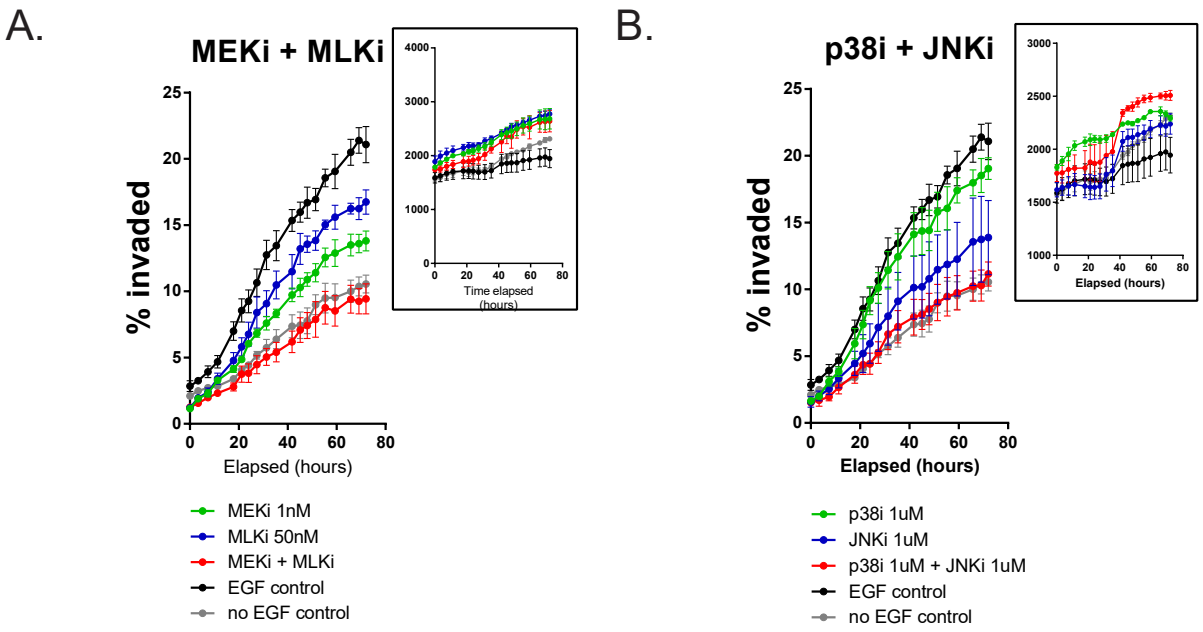

Figure 3.23: Dual MAPKi combinations. Chemotactic invasion assay results showing combinatorial effect of MEKi and MLKi (A), and p38i and JNKi (B). Inset shows proliferation measured as the total number of cells in the bottom and top layers over time. Data are plotted as mean ± s.e.m. of n=3 technical replicates, and the graphs are representative of n=2 indepdendent experiments.

cells than the p38i + JNKi and MEKi + MLKi combinations, without causing major change in the proliferative rate of the cells (Figure 3.25, on page 59). We validated the anti-invasive role of the 4-drug combination in regular Boyden chamber assays and 3D growth assays across multiple breast cancer cell lines (Figure 3.26, on page 60). In LMB cells, the doses used for the initial BM1 studies were growth-inhibitory, so for this cell line we decreased the doses of each drug proportionally. Nevertheless, in all of the cell lines tested, the 4-drug combination blocked chemotactic invasion of cancer cells at doses where the 3D growth properties of the cells remain uneffected. All of these results suggest that the 4-drug MAPKi combination mimics RKIP phenotype in vitro.

From a therapeutic standpoint, an anti-metastatic treatment that combines four different small molecule inhibitors may raise drug-related toxicity issues. To address this issue in vitro, we treated immortalized normal mammary epithelium cell lines MCF10A and 184A1 with

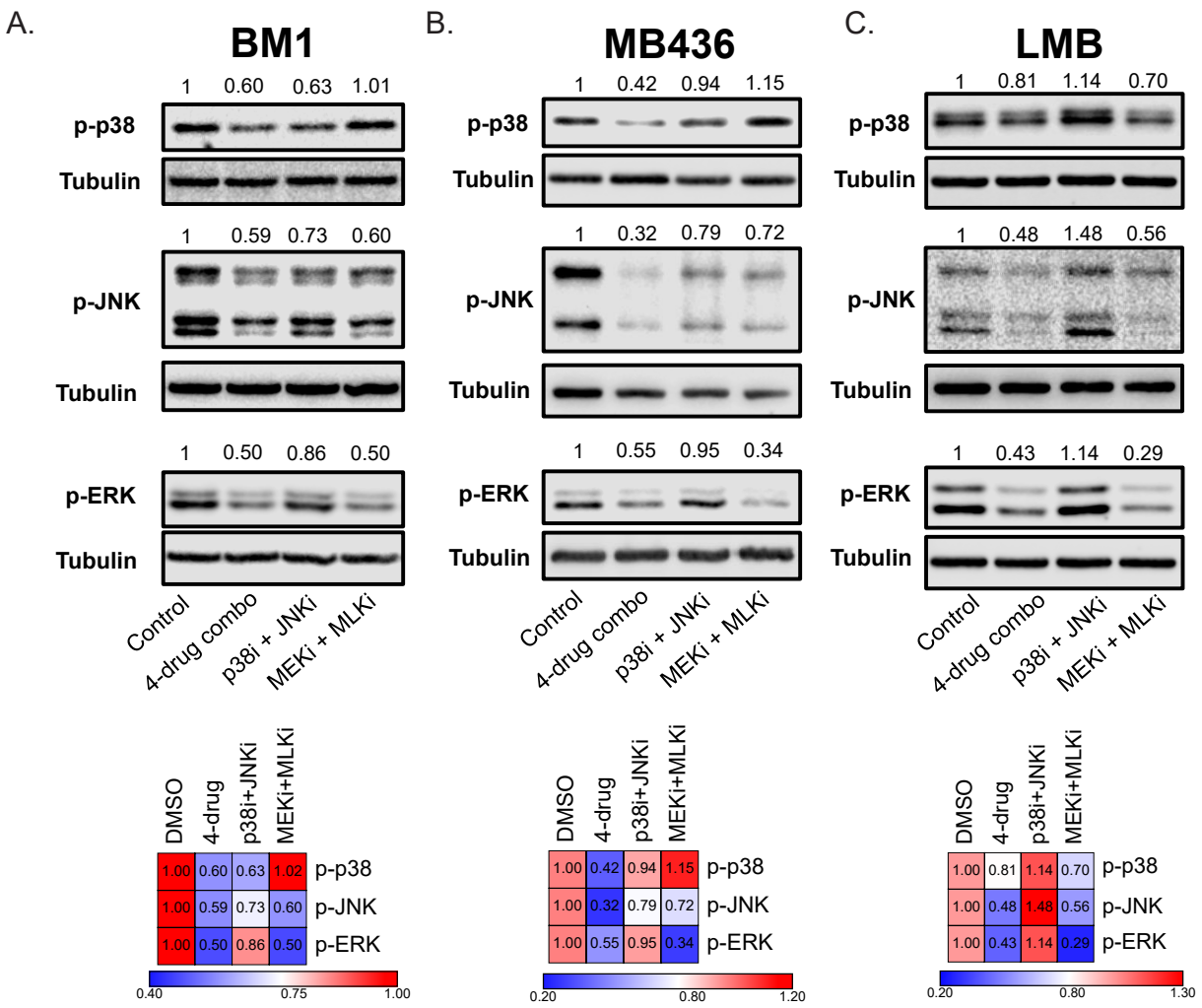

Figure 3.24: 2-drug vs. 4-drug MAPKi combination effect on MAPK stress kinase signaling. Western blot showing p38, JNK, and ERK activity when BM1 (A), MB436 (B), and LMB (C) cells were starved overnight, pre-treated with the MEKi(1nM)+MLKi(50nM) combination, the p38i(1µM)+JNKi(1µM) combination, or all four inhibitors, and induced with anisomycin (25ng/ml) for 30 minutes in the presence of these inhibitors. Band intensities were measured by densitometry, normalized to the intensity of Tubulin for that band on the same gel, and shown above the respective bands as well as the heatmaps below each Western blot.

the 4-drug MAPKi. At the doses used on BM1 cells, the MAPKi combination did not affect overall proliferation of these two cell lines in 2D cultures (red curve vs. black curve) (Figure 3.27, A and B left panels on page 61). Under 3D conditions there was a small decrease in the proliferative rate when the cells were treated with the 4-drug combination, MEKi + MLKi combination, or MEKi alone (Figure 3.27, A and B right panels). Overall, these

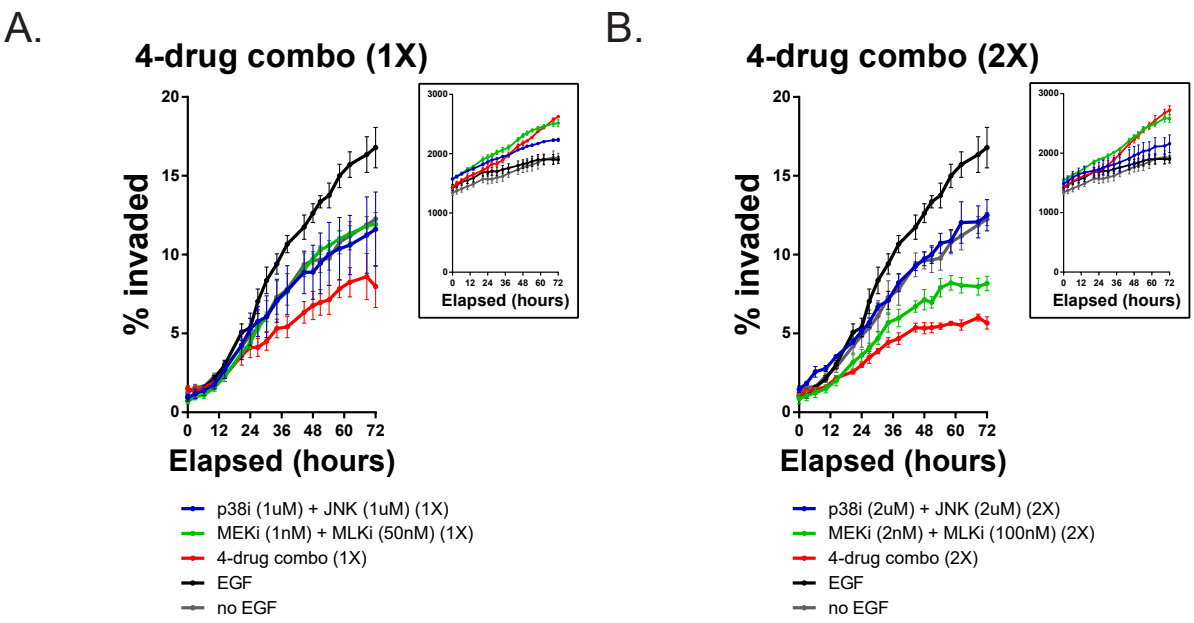

Figure 3.25: Chemotactic invasion assay results showing the effect of 2-drug vs. 4-drug MAPKi combination on invasion when the inhibitors are combined at 1X concentrations (A) or 2X concentrations (B). Inset shows proliferation measured as the total number of cells in the bottom and top layers over time. Data are plotted as mean ± s.e.m. of n=3 technical replicates.

results suggest that the 4-drug combination is not toxic to normal cells.

3.3.6 The effect of combination treatment is not always additive of individual inhibitors

Since we decided to combine two dual combinations based on their complementary effect on MAPK network, we also wondered if adding a third inhibitor to a dual combination would also work just as well. In terms of anti-invasion phenotype, adding a third inhibitor to the p38i + JNKi and MEKi + MLKi combinations did not improve the efficacy of the dual combination (Figure 3.28, on page 62). Surprisingly, in some cases, addition of a third inhibitor that targets another member of the MAPK network counteracted the anti-invasive function of the dual treatment (Figure 3.28, C and D). In terms of signaling, it is possible to achieve downregulation of all three axes with three inhibitors, especially in anisomycin

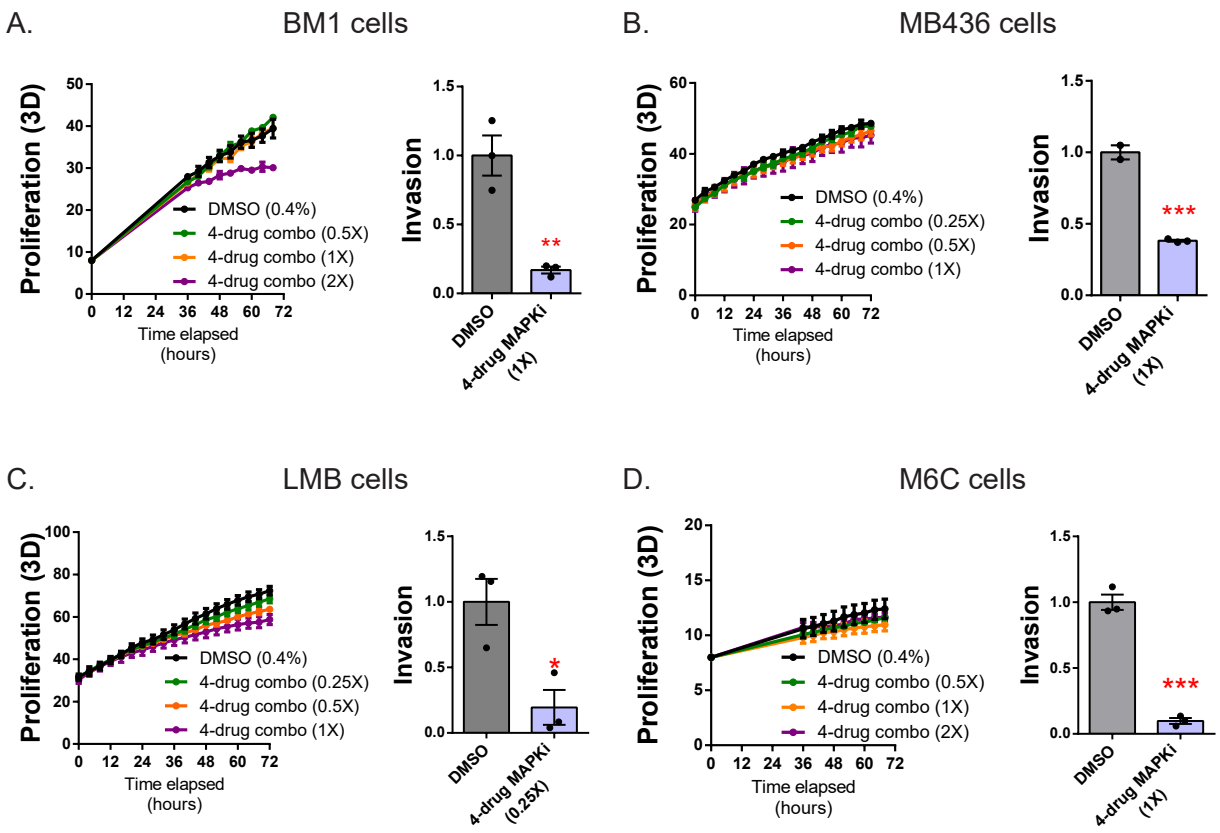

Figure 3.26: 4-drug MAPKi combination blocks invasion without affecting proliferation in TNBC cell lines under 3D conditions. Time course plots (left panels) show growth curves of BM1 (A), MB436 (B), LMB (C), and M6C (D) cells in 2mg/ml basement membrane extract over the course of 72 hours. Bargraphs (right panels) show regular Boyden chamber assay results demontrating inhibition of invasion with the 4-drug MAPKi combination at the indicated doses. All the experimental data depicted here are plotted as mean ± s.e.m. of n=3 technical replicates. P-values were calculated by two-tailed t-test. (p-values: * $p < 0.05$, ** $p < 0.01$, *** $p < 0.001$, **** $p < 0.0001$)

induced cases (Figure 3.29, panel B on page 63). Invasion assays, however, include serum as the chemoattractant. Under serum conditions, 4-drug treatment still outperforms 3-drug and 2-drug combinations (Figure 3.29, panel A) in blocking MAPK induction. Importantly, the 4-drug combination not only works better than dual or triple treatments in most cases, it is also more robust in its function as it can work in multiple cell lines under different conditions (heatmaps in Figure 3.29). These findings suggest that the efficacy of each combination depends on the type of induction and other combinations might work comparably to the 4-drug combination under tumor stress conditions.

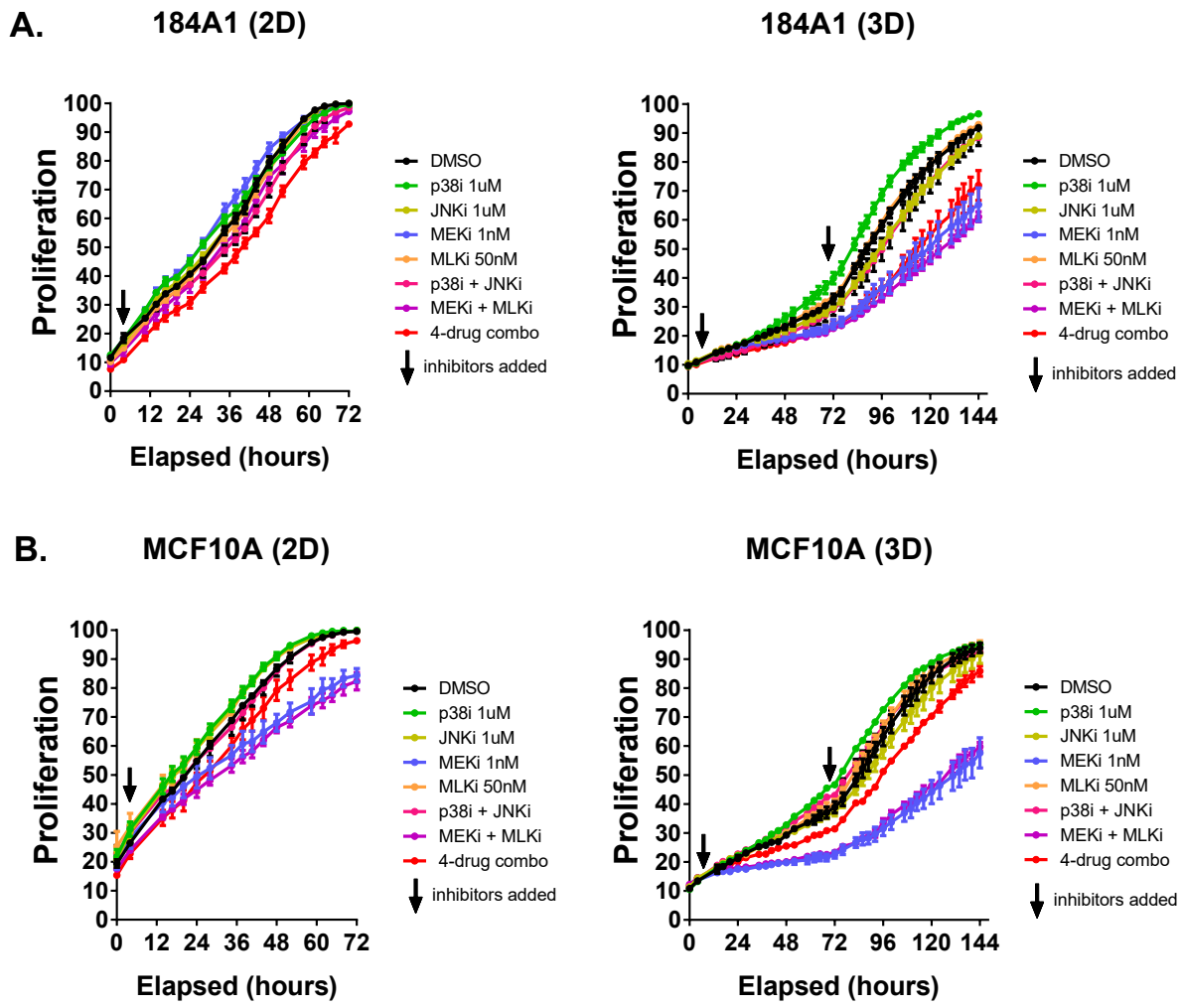

Figure 3.27: 4-drug MAPKi combination does not affect normal mammary epithelial cell line proliferation. Immortalized normal mammary epithelium cell lines 184A1 (A), and MCF10A (B) were grown in 2D (left panels) or 3D (right panels) condition over the course of 72 hours in the presence of indicated inhibitor combinations and dosages. Proliferation is measured as percent confluence and plotted as mean ± s.e.m. of n=3 technical replicates.

Another important feature of the 4-drug MAPKi combination is that each of the four drugs are used at sub-therapeutic doses. SB203580 and SP600126 are usually used at 10μM in phenotypic studies. Trametinib is used at around 10nM and URMC-099 is used at 200nM. In our MAPKi combination treatment, they are used at 1μM, 1μM, 1nM, and 50nM, respectively, all of which is about an order of magnitude below the literature dosages for each drug. At these doses, these inhibitors partially inhibit the RKIP-signaling network without

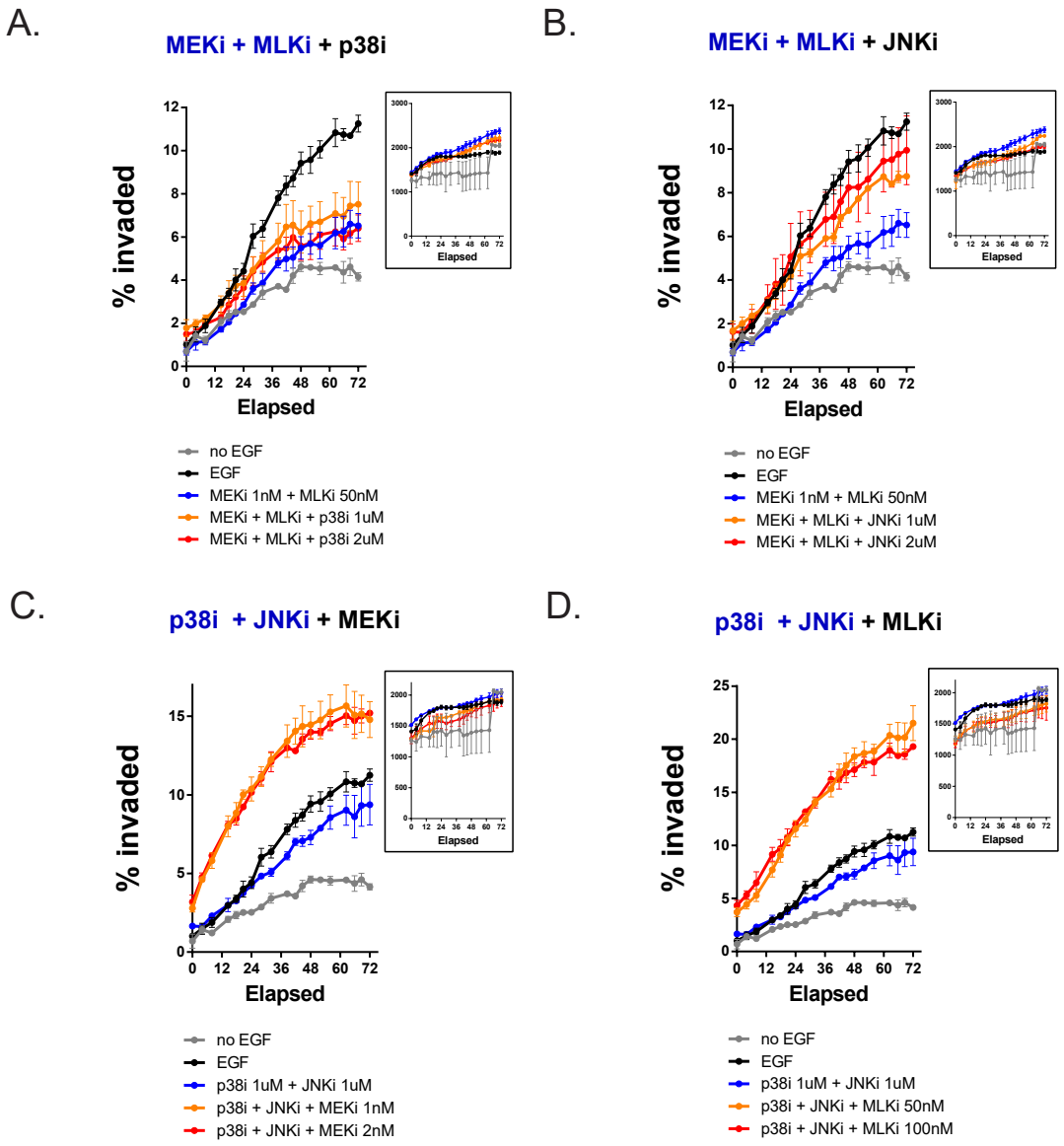

Figure 3.28: Adding a third MAPK inhibitor to the dual combinations do not always improve anti-invasive efficacy. Chemotactic invasion assay results showing the anti-invasive effect of adding p38i (A) or JNKi (B) to the MEKi+MLKi combination, and adding MEKi (C) or MLKi (D) to the p38i+JNKi combination at 1X concentrations. Inset shows proliferation measured as the total number of cells in the bottom and top layers over time. Data are plotted as mean ± s.e.m. of n=3 technical replicates.

causing toxicity or substential growth arrest. All of these data highlight the fact that the MAPKi combination successfully phenocopies RKIP in vitro.

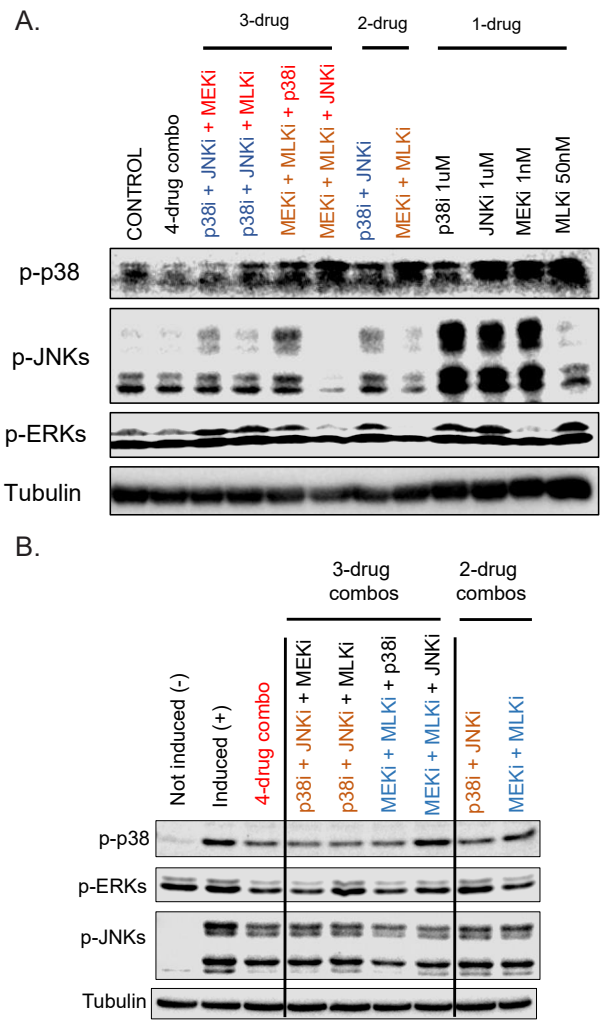

Figure 3.29: 4-drug MAPKi is more effective in inhibiting RKIP stress MAPK network than 3-drug or 2-drug combinations. Western blot showing p38, JNK, and ERK activity when BM1cells are starved overnight, pre-treated with the indicated 2-/3-/4-drug combination at 1X doses, and induced with 10% serum (A) or 25ng/ml anisomycin (B) for 30 minutes in the presence of these inhibitor combinations.

3.3.7 Combination of the MAPK inhibitors at sub-therapeutic doses block tumor growth and metastasis in syngeneic and xenograft models of TNBC

Translating the 4-drug MAPKi combination into an in vivo treatment module is challenging for multiple reasons. First, in vitro dosages that we optimized for the phenotypic studies will not be the same in vivo, as each of these inhibitors will have different pharmacokinetic

and pharmacodynamic properties in mice. Delivery efficacy and cellular uptake rates also differ in vitro vs. in vivo. Second, in vivo conditions have a lot of extracellular components that effect the efficacy of the treatment. We did not perform any in vitro studies to predict how the stromal components (e.g. fibroblasts, endothelial cells) or the immune component (innate and adaptive) interact with our RKIP-mimicking combination treatment. These are important considerations, especially when kinase inhibitors are being used for treatment, as most of these inhibitors target pathways that are fundamental to the functioning of healthy tissue as well.

Due to these concerns, we decided to follow a similar dose selection approach to what we used in vitro. We decided to perform a dose response study with each individual drug to determine a dose lower than the IC50 value for the primary tumor growth phenotype. We also chose to carry out these initial experiments in a syngeneic model using LMB cells and C57Bl/6 mice so that the phenotypic observations we make are in the presence of an intact immune system and a physiological stroma.

As we were determining the dose range for each drug, we capped the highest dose at the standard dose used in the literature for phenotypic studies. Since most of the studies using these inhibitors look for effects on tumor growth, we presumed that at these literature-based doses, we are likely to start seeing effects on primary growth. Therefore, we selected 10mg/kg/day as the cap for SB203580, SP600125, and URMC-099. Trametinib is used at 2-5mg/kg/day dose as it is more potent than the other inhibitors. So we capped it at 5mg/kg/day.

To our suprise SB203580, SP600125, or URMC-099 had no effect on LMB tumor growth at 10mg/kg/day (Figure 3.30, on page 65). Trametinib showed a dose response with an IC50 value around 2.5mg/kg/day. Instead of doing a separate dose response experiment for the metastasis phenotype, we used macrophage infiltration within the primary tumor as a proxy for the metastatic potential of the tumors. This is because we have previously shown that RKIP inhibits tumor-associated macrophage infiltration and there is a strong correlation

between macrophage content of a tumor and the metastatic potential [30]. Quantification of F4/80 staining of the primary tumors showed a slight dose-dependent decrease with MEKi (Figure 3.31, on page 66).

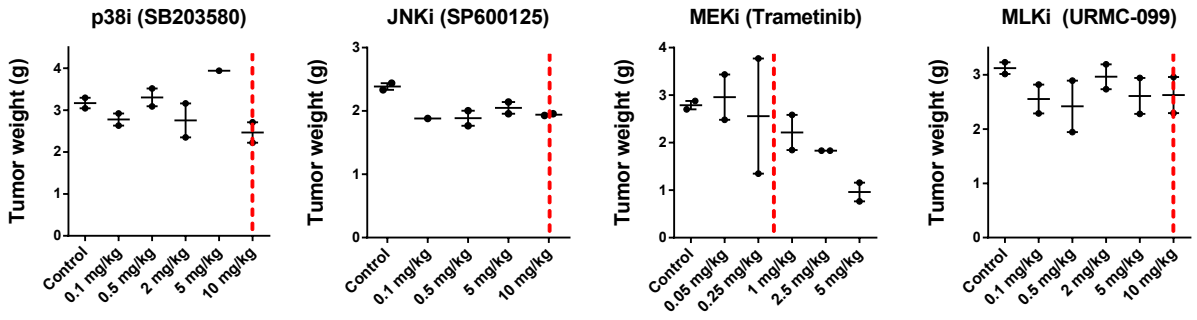

Figure 3.30: Dose-respone plots with individual MAPK inhibitors in syngeneic LMB tumors. Tumor weights were measured at the end of a 3-week treatment period with the four inhibitors at the indicated concentrations. Each dot represents a biological replicate. Red dashed lines indicate the concentrations at which each inhibitor is used in the 4-drug combination (10mg/kg/day for p38i, JNKi, and MLKi, and 0.5mg/kg/day for MEKi).

Based on these initial dose response studies, we chose 10mg/kg/day for p38i, JNKi, and MLKi, and 0.5mg/kg/day for MEKi as the doses to be used in the 4-drug MAPKi combination in vivo. To test the effect of the 4-drug MAPKi on metastasis in vivo, we injected pre-programmed LMB cells into the teil vein of C57Bl/6 mice and continued to treat the mice with the MAPKi combination for 3 weeks at 1X or 0.5X concentrations (for details, see Metarials and Methods and Figure 3.32, panel A on page 68). Treating the mice with the MAPKi combination significantly reduced the number of surface metastatic nodules in the lungs in a dose-dependent manner (Figure 3.32, panel B and C). When we tested the effect of the combination on primary tumor growth, we observed a partial inhibition of growth over the course of the treatment (Figure 3.32, panel D). To test whether the effect of MAPKi was on extravasation or colonization of the tumor cells, we injected pre-treated LMB cells into the teil vein of the mice, but then treated the mice with for only 48 hours (two injections only, one on day 0 and one on day 1) during which the tumor cells are primarily extravasating. Then the metastases were allowed to colonize without exposure to the MAPKi

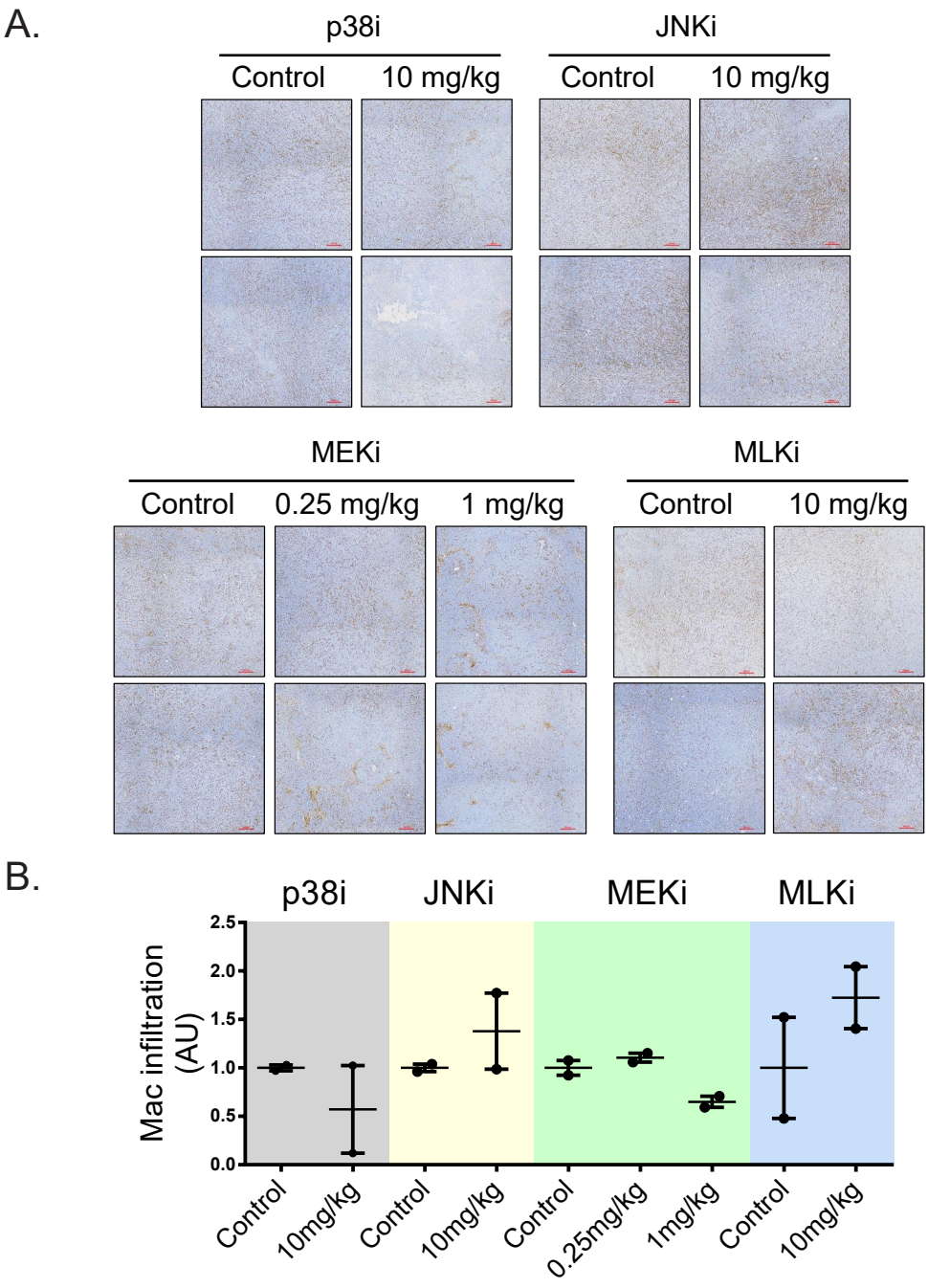

Figure 3.31: Macrophage infiltration into the primary LMB tumors under individual MAPK inhibitor treatment. (A) Macrophage infiltration was measured by F4/80 immunohistochemical staining on formalin fixed, paraffin-embedded tissue sections from tumors treated with the indiviual MAPK inhibitors. Each square panel represents a field from a biological replicate. (B) Quantification of the F4/80 staining. Data are shown as the mean ± s.e.m. of 5 randomly chosen fields on each biological replicate sample.

combination for the rest of the experiment. Even when we use the MAPKi treatment for only 2 days, there was a significant decrease in the metastatic tumors at the end of the study (Figure 3.32, panel E), suggesting that at least some of the effect of MAPKi can be attributed to impaired extravasation. Moreover, we observed a trend towards decreased macrophage infiltration in tumors treated with the MAPKi combination, but due to small samples sizes, the difference did not reach signficance (Figure 3.33, on page 69). All of these data combined argue that the 4-drug MAPKi combination at these in vivo doses not only has anti-metastatic function, but also a growth-inhibitory function.

It is important to note that the 4-drug MAPKi combination did not induce overall toxicity in mice as indicated by the lack of any weight loss (Figure 3.32, panel F), skin problems, or sign of pain.

Similar but even more robust results were obtained with a xenograft model using bone-tropic, luciferase-expressing BM1 cells in athymic nude mice. MAPKi inhibited metastatic burden in the bones after a 3-week treatment course (Figure 3.34, panel A through C on page 70), and blocked primary tumor growth at the same time (Figure 3.34, panel D). With these xenograft studies, we also wanted to test if the treatment had long-term effects. After cessation of the treatment, primary tumors grew back (faster in the 0.5X treatment group than in the 1X treatment group) (Figure 3.34, panel D). In the metastasis experiments, the mice started reaching the study end point weeks after treatment cessation, suggesting that the lung metastases were coming back. Nevertheless, the treatment significantly delayed reaching the end point and improved overall survival in these mice (Figure 3.34, panel E).Like the syngenic studies, we did not observe any weight loss in mice due to treatment (Figure 3.34, panel F). These findings argue that our 4-drug MAPKi treatment's effects are temporary, but it can be a powerful chronic treatment module that slows down further spreading of the cancer.

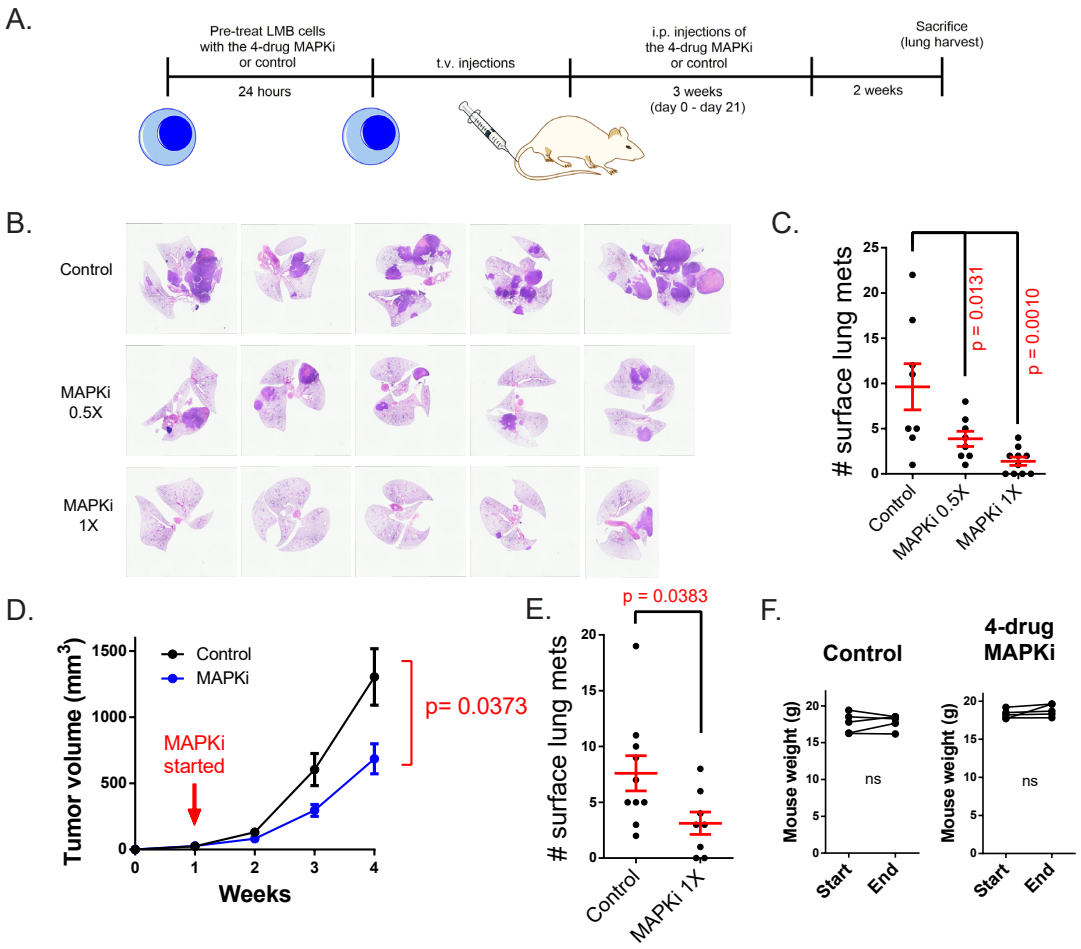

Figure 3.32: Effect of 4-drug MAPKi treatment on LMB metastasis and primary tumor growth. (A) Diagram showing experimental timeline for the metastasis assay. (B) H&E staining on the tissue sections of the lungs of mice treated with either the vehicle control or the 4-drug MAPKi at 0.5X and 1X. (C) Quantification of the overt metastases on the lung surface after 3-weeks of treatment. Each dot represents a biological replicate (D) Growth curves for the primary tumors. LMB cells were injected orthotopically, and when the tumors reached 50-100mm^3 volume, mice were treated with control or the 4-drug MAPKi (1X) for three weeks. Tumor size was measured with a caliper. The p-value is calculated using 2-way ANOVA. (E) Quantification of the overt metastases on the lung surface at week 5 post-inoculation when the mice recieved treatment only on days 0 and 1. Each dot represents a biological replicate. For C through E, data are plotted as mean ± s.e.m. (F) Overall body weight of control- or MAPKi-treated mice, at the start and end of the study. Exact p-values are calculated using a two-tailed t-test. ns - not significant

3.4 Discussion

In this study, we have demonstrated the utility of understanding the function of phyiological suppressors of the metastatic process in developing effective therapies against metastatic

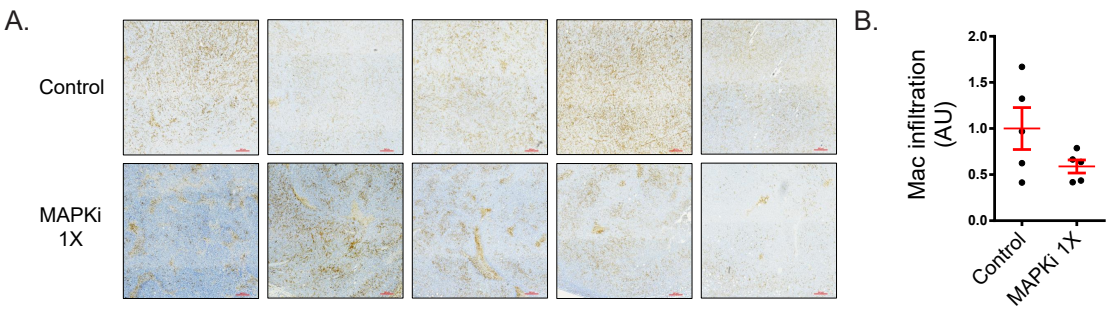

Figure 3.33: Macrophage infiltration into the primary LMB tumors treated with control or the MAPKi combination (1X). (A) Formalin-fixed paraffin-embedded tumor sections were stained for F4/80. Each experimental group had 5 biological replicate, and each square panel represents a field from a biological replicate sample. (B) Quantification of the F4/80 staining. Significant differences between the groups were tested by a two-tailed t-test.

disease, especially in cases where reintroducing the suppressor itself within the diseased tissue is technically challenging. Our approach towards elucidating the mechanisms of RKIP not only idetified novel signaling networks and target genes regulated by RKIP, but also revealed novel treatment modalities that are different than current clinical practices. Namely, we investigated the efficacy of combination therapies that are comprised of more than 2 small molecule inhibitors, each used at their sub-therapeutic doses. This was to mimic RKIP's molecular function in partially inhibiting the activity of multiple kinases in order to reprogram a metastatic cell into a non-metastatic one. Our findings demonstrate that by partially inhibiting all three MAPKs (ERK, p38, and JNK) using kinase inhibitors at low doses, we can revert metastatic phenotype without causing toxicity in vitro and in vivo.

For identification of the kinomic changes, we employed MIB-MS method carried out by Dr. Gary Johnson's team, which utilizes magnetic inhibitor beads. This method is superior to other phospho-proteomic approaches because it does not require prior knowledge about the functional annotation for the phosphorylated sites identified. Instead, it pulls down kinases that are in their active confirmation because the type-I inhibitors used for the pull-down are bound to the ATP-binding pocket of the kinases. This allows for quantification of overall activity for a kinase. However, the MIB-MS method does not provide information on the quantity of the inactive species or the total protein expression for a

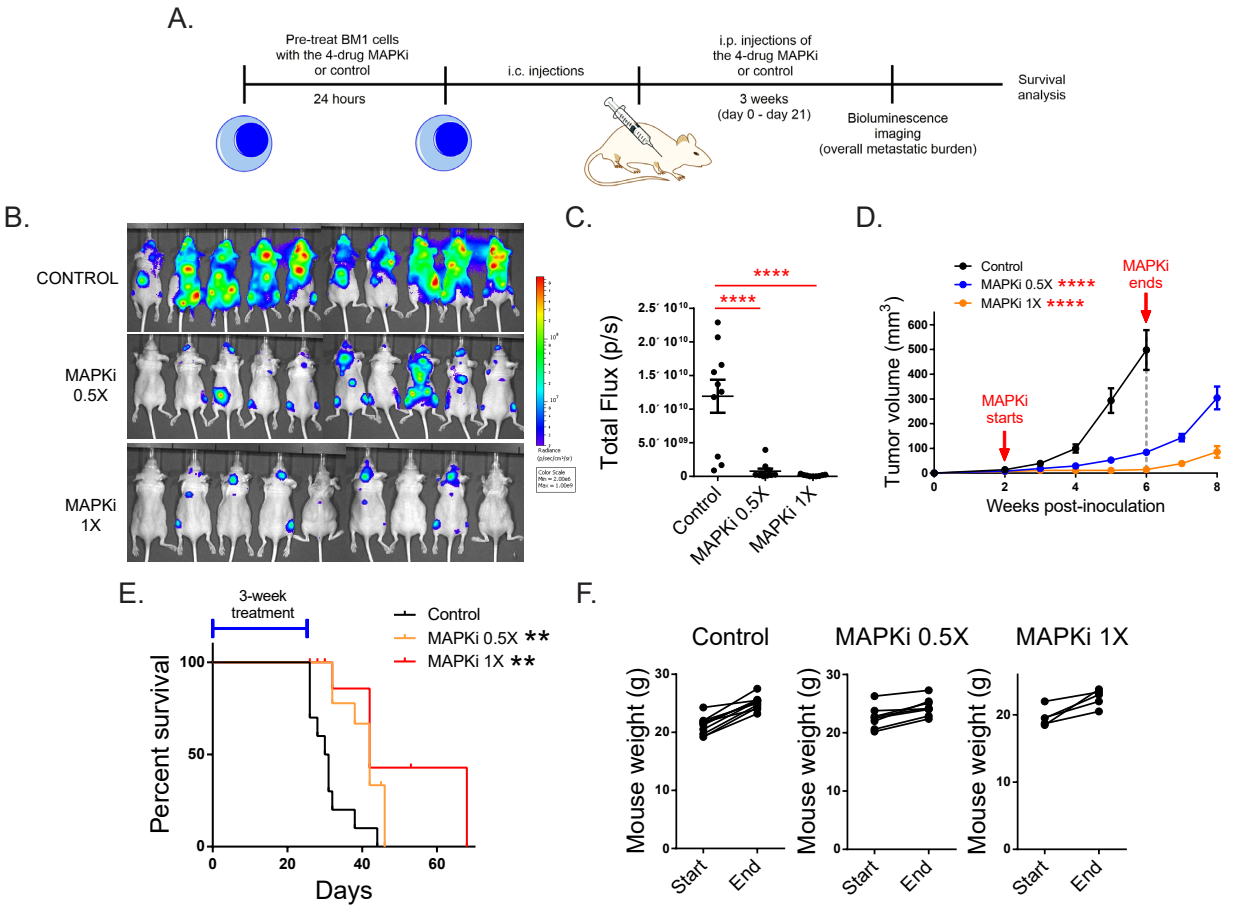

Figure 3.34: Effect of 4-drug MAPKi treatment on BM1 metastasis and primary tumor growth, and survival. (A) Diagram showing experimental timeline for the metastasis assay. (B) Bioluminescence imaging of the mice treated with Control, MAPKi 0.5X, MAPKi 1X at the end of the 3-week treatment (C) Quantification of the metastatic tumor burden in mice, measured by the total flux of the bioluminescence signal. Each dot on the plot represents a biological replicate. Significance was tested with a two-tailed t-test. (D) Growth curves for the primary tumors. BM1 cells were injected orthotopically into athymic nuce mice, and when the tumors reached 50-100mm^3 volume (roughly 2 weeks), mice were treated with control or the 4-drug MAPKi (at 1X and 0.5X) for two weeks. Then the treatment stopped and tumors were allowed to grow. Tumor size was measured with a caliper. Significance was tested using 2-way ANOVA with multiple comparisons on data points collected up to 6-weeks post-inoculation (treatment end date). (E) Kaplan-Meier curve showing survival of mice from (A) after treatment cessation. Log-rank test was used to test significance. (F) Overall body weight of control- or MAPKi-treated mice, at the start and end of the study. (p-values: * $p < 0.05$, ** $p < 0.01$, *** $p < 0.001$, **** $p < 0.0001$)

kinase. The MIB-MS method is not commercially available as the Johnson lab performs all their analyses in-house. However, alternative kinomic profiling can be carried out using commercially available high-throughput kinase activity arrays like PamGene's PamChip ar-

rays (https://www.pamgene.com/en/pamchip.htm) or Eurofins' scanMAX and KINOMEscan (https://www.eurofinsdiscoveryservices.com) .

The coverage of the MIB pull-down depends on the affinity of the inhibitor beads towards all the kinases in a cell. Dr. Johnson's team report the kinome coverage for this assay to be >85% [91] after optimization of the kinase inhibitors used. From the BM1 tumors, we were able to isolate 250 different kinase species that were expressed in all of the samples, which corresponds to roughly 50% of the entire known kinome. This can be explained by the unexpressed portion of the kinome in BM1 tumors, or the presence of many low abundance kinases that the MIBs cannot pull down. Potential for false negatives in our analysis suggests that there can be more putative RKIP targets than identified here.

Our MIB analysis of RKIP-expressing tumors revealed that, in order to reprogram metastatic cells into a non-metastatic state like RKIP does, one needs to target multiple kinases with varying activity levels and target them partially. This tratment strategy is very different than most existing treatment modalities towards metastatic disease. Other groups have conducted similar mass spectrometry-based approaches to identify most active and targetable kinases in cancers in order to kill cancer cells [69]. This approach assumes that tumors are dependent on these highly active (and most of the time mutated) kinases to proliferate. Therefore, there is good incentive to use highest doses that a patient's body can handle to eradicate tumor cells. Though this might prove effective against slowing tumor growth, it may not be as effective in blocking phenotypic shift towards metastatic state. In fact, in a lot of cases, aggressive treatment can cause more metastatic disease. Our analysis of the RKIP-regulated kinome argues that in order to slow down metastatic progression of cancers, an effective strategy would be to use combinations of multiple targeted agents at low doses.

The results of our drug combination screen suggested that a combination of four MAPK inhibitors (p38 inhibitor SB203580, JNK inhibitor SP600125, MEK inhibitor Trametinib, and MLK inhibitor URMC-099) used at sub-therapeutic doses (1uM for SB203580 and SP600125,

1nM for Trametinib, and 50nM for URMC-099) effectively phenocopies RKIP in vitro. This combination partially inhibits activity of ERK, p38, and JNK axes of the RKIP network in stress conditions and subsequently inhibits invasion capability of TNBC cell lines. We chose these inhibitors to include in our initial drug screen either because there is a large body of literature characterizing these drugs or because these drugs are being tested for use in patients in clinical trials. However, the particular pairing of these specific inhibitors is by no means the only one that can mimic RKIP. In fact, we predict that any combination of drugs that can target p38, JNK, and ERK together should mimic RKIP function to a certain capacity. This also highlights the fact that a particular combination does not have to contain more than 2 inhibitors to block an entire network. It is possible to use dual-specificity kinases, or multi-target kinases in the screen to broaden the effect of a kinase on the network and maybe reduce the number of inhibitors used. The reason this study yielded a 4-drug combination is because the inhibitors we chose are considered to be very specific towards one MAPK target (except for URMC-099, which targets multiple MLKs as well as DLK and LRRK2), and, therefore, inhibiting all three MAPK axes required more than one inhibitor.

Another reason for using multiple kinase inhibitors is the presence of negative feedback mechanisms embedded within signaling networks. Especially, in the MAPK network, interactions between different MAPKs are ample and involve other upstream or downstream MAPKs that connect different cascade within the network. The cross-talk between p38, JNK, and ERK makes the metastatic MAPK network more robust as such that inhibition of one of these kinases result in induction of another. For example, treating TNBC cell lines with the p38 inhibitor SB203580 results in over-activation of JNK, and this effect is mediated by the upstream MLKs. Including an MLK inhibitor in our cocktail of drugs allow for uni-directional uncoupling of these two cascades. We have also shown preliminary evidence that indicate involvement of TAO kinases in the JNK inhibitor-induced p38 activation. If TAOKs are truely activating p38 in response to JNK inhibition, then a TAOKi + MLKi

combination would not only block p38 and JNK activation in stress, but it would also dismantle the negative relationship between these two MAPK cascades which can potentially be a resistance mechanism. In this case, combining TAOKi, MLKi, and MEKi might have the similar effect of overall network inhibition to the 4-drug MAPKi or RKIP. Understanding the feedback mechanisms and the cross-talk between different cascades of a network allows for hypothesis generation regarding combination treatments.

An interesting finding of our study is that adding multiple inhibitors together does not always have the combined effect of the individual inhibitors. This can also be attributed to the negative cross-talk between targeted cascades, where adding another inhibitor to the mix can counteract the efficacy of the overall treatment while increasing the toxicity. Therefore, if multiple drugs are being combined at once, each combination should be considered as a separate meta-treatment without assuming additive effect.

The 4-drug MAPKi cocktail effectively mimiced RKIP's function in vitro by blocking invasion of tumor cells without affecting their growth or overall proliferation. When we tried a similar approach in mouse models of TNBC, however, MAPKi decreased primary tumor growth as well. This could be because of different pharmacokinetic and pharmacodynamic properties of each drug, or the presence of tumor microenvrionment contributing to the overall drug efficacy, which collectively render in vivo optimization non-trivial. Nevertheless, our in vivo studies suggest that the MAPKi combination has the potential to function as both a metastasis suppressor and a tumor suppressor depending on the context.

Our research supports the idea that stress signaling is important for metastatic progression of cancers. Previous work demonstrated that cellular stress (e.g. oncogenic stress, protein misfolding) and microenvironmental stress (e.g. hypoxia, nutrient deprivation, and tissue tension/stiffness) can induce EMT phenotype in cancer cells, increasing the metastatic rate of tumors. For example, p38 and JNK can stabilize TWIST1 to promote breast cancer invasion [42]. p38 activity correlates positively with SNAIL expression in ovarian cancers [39]. JNK inhibition can revert EMT phenotype induced by HER2/AKT signaling in gas-

tric cancers [17]. In our TNBC model systems, RKIP does not regulate EMT markers, nor it correlates with EMT genes in the TCGA breast cancer patient data [103], yet it blocks metastatic progression by inhibiting stress kinase signaling. This suggests that stress kinase signaling is important in later stages of metastasis as well, and a good therapeutic target for metastasis.

The results of this study are also important because it significantly expands our knowledge of how RKIP functions as a metastasis suppressor. This is the first study that investigates RKIP's effect on the kinome of tumor cells at the systems level. Moreover, here we study RKIP's function on metastatic signaling in vivo, which is different than majority of the previous work that has been done under non-physiological conditions. Using the MIB-MS method, we not only validated regulation of known RKIP targets such as ERK in tumors, but also identified other kinases that are regulated by RKIP indepdently of the RAF signaling. In particular, stress MAPKs JNK, MLKs, and TAOKs have never been implicated as a part of the RKIP-network before. To our best knowledge, there is only one study that implicates p38 as an indirect RKIP target [2]. In this study, the authors show that when RKIP is depleted, p38 kinase becomes activated indirectly due to increased reactive oxygen species (ROS) in tumor cells. Our work identifies an alternative route to p38 inhibition by RKIP which involves the upstream MAP3Ks TAOKs and MLKs. Whether RKIP directly binds to these MAP3Ks, or it has other binding partners that converge to the stress MAPK network remains to be explored.

CHAPTER 4

AN INTEGRATED APPROACH FOR IDENTIFICATION OF RKIP TARGET GENES

4.1 Abstract

RKIP is a metastasis suppressor that inhibits a network of stress-induced MAP kinases in triple negative breast cancers. We have demonstrated that a combination of p38, JNK, MEK, and ERK inhibitors can mimic RKIP's function in vitro when each inhibitor is used at sub-therapeutic doses. Downstream metastatic gene targets of this stress MAPK network, however, are not known. In this chapter, we described a computational approach to identify clinically-relevant gene targets of the RKIP-network by overlapping experimentally-derived and patient-derived high-throughput data. Integrated analysis of genes downregulated by RKIP in xenografted tumors and genes that negatively correlate with RKIP in TCGA breast cancer data set, we identified a set of putative RKIP targets involved in cell-matrix adhesion, invasion, and motility. In vitro studies showed that both RKIP and the 4-drug MAPKi blocked induction of metastatic gene expression under stress conditions. We identifid RKIP's translational target BACH1 to be one of the transcription factors that regulate the expression of the adhesion/motility genes.We observed consistent negative correlations between RKIP and these metastatic genes across multiple solid tumor types in the TCGA data, suggesting that RKIP's effect on stress-induced metastatic gene networks is beyond just TNBC. Finally, we identified at least four other metastasis suppressors that also negatively correlate with motility-related gene sets in breast cancers, suggesting that this is a hallmark of metastasis suppressors. Collectively, our findings shed light on the mechanisms by which RKIP blocks metastatic phenotype induced by cellular stress and identify potential markers that can be used to develop predictive and prognostic markers for metastatic potential in cancers.

4.2 Introduction

Elucidating metastatic genes regulated by RKIP can reveal new therapeutic strategies as well as unravel mechanisms of metastasis. Previous work from the Rosner laboratory mapped out a metastatic regulatory network dowsntream of the RAF-MEK-ERK cascade (reviewed in detail by Yesilkanal and Rosner [102]. Transcriptional activation of LIN28, a RNA-binding protein that inhibits miRNA let-7, by the master regulator Myc is blocked in the presence of RKIP. Myc is activated by the RAF-MERK-ERK cascades, which makes it an RKIP target. Myc and Lin28 blockade results in upregulation of let-7 in cancer cells, which is followed by inhibition of two metastatic transcription factors - BACH1 and HMGA2 [109]. BACH1 and HMGA2 promote metastasis by activating metastatic genes MMP1, OPN, and CXCR4. Rosner and colleagues further extended this RKIP network by identifying downstream gene targets of HMGA2 that plays a role in invasion and metastasis. HMGA2 induces lysine oxidase (LOX), a collagen and elastin crosslinker, and syndecan 2 (SDC2), a transmembrane heparan sulfate proteoglycan that mediates cell adhesion, cell-matrix interactions, signaling [93]. RKIP also increases expresison of the epigenetic regulator ten-eleven translocation 1 (TET1) and developmental gene homeobox A9 (HOXA9) through inhibition of HMGA2, both of which suppress cancer cell invasion, tumor growth, intravasation, extravasation, and metastasis [94]. More recently we established inhibtion of electron transport chain genes as a mechanisms by which BACH1 promotes metastasis (manuscript accepted). All of this previous work represent a metastatic network of extracellular matrix remodelers, signal transducers, and epigenetic modulators, and metabolic rregulators that is downstream of RKIP signaling, and highlights multi-faceted role of RKIP in reprogramming metastatic tumors into a more benign state.

Majority of these mechanistic events happen dowsntream of ERK signaling. In Chapter 1, however, we demonstrated that regulation of metastatic networks by RKIP extends beyond the RAF-MEK-ERK cascade. We have identified p38 and JNK stress MAPK pathways

as targets of RKIP signaling, but the transcriptional networks that lie downstream to these stress-induced signaling cascades are unknown. Here, we shought to reveal clinically-relevant metastatic genes targeted by RKIP through the stress kinases. Moreover, we wanted to investigate whether RKIP-mimicking treatments like the 4-drug MAPKi combination can target these RKIP targets as well. Finding metastatic genes and elucidating their regulation will not only allow us to understand how RKIP blocks metastasis in cancers, but also explore the clinical significance of anti-metastatic therapies that mimic metastasis suppressors.

4.3 Results

4.3.1 Putative target gene discovery guided by patient-derived high-throughput data

We have established that RKIP inhibits invasiveness of TNBC cell lines by blocking stress MAPK signaling. An RKIP mimicking combination of MAPK inhibitors works in the same way by partially reducing the signal intensity within all three axes of the MAPK network. As a next step of understanding metastatic mechanisms, we wanted to investigate the mechanism by which the stress MAPKs inhibit invasion and metastasis. First we wanted to identify metastatic genes that are targeted by RKIP as a result of decreased stress MAPK signaling. We employed RNA-sequencing technology to compare the transcriptional state of metastatic BM1-VC tumors to non-metastatic BM1-RKIP tumors. Tumors in both of the experimental groups grew at a similar rate and when they were isolated for RNA collection, there was no size difference (Figure 4.1, panel A on page 78). This is consistent with the previous observations that RKIP inhibits metastatic progression without significantly effecting primary growth of tumors in vivo.

Principle component analysis of the sequencing data shows that the tumors samples fall into two distinct populations separeted by their RKIP status (Figure 4.1, panel B). Sample-to-sample distances are shorter for samples within the same experimental group,

but overall, the samples in the control group are closer to each other than the samples in the RKIP group are (Figure 4.1, panel C). Differential expression analysis between control and RKIP tumors yielded a total of 5746 differentially expressed genes - 2824 of these were downregulated and 2922 were upregulated. Functional gene set enrichment analysis of the differentially expressed genes demonstrated that RKIP downregulates sets of genes involved in cell motility/invasion, signal transduction, and cell division (Figure 4.2, panel A on page 79). The upregulated genes fall into the categories of mitochondrial components and metabolism, catabolic process and autophagy, and protein targeting (Figure 4.2, panel B).

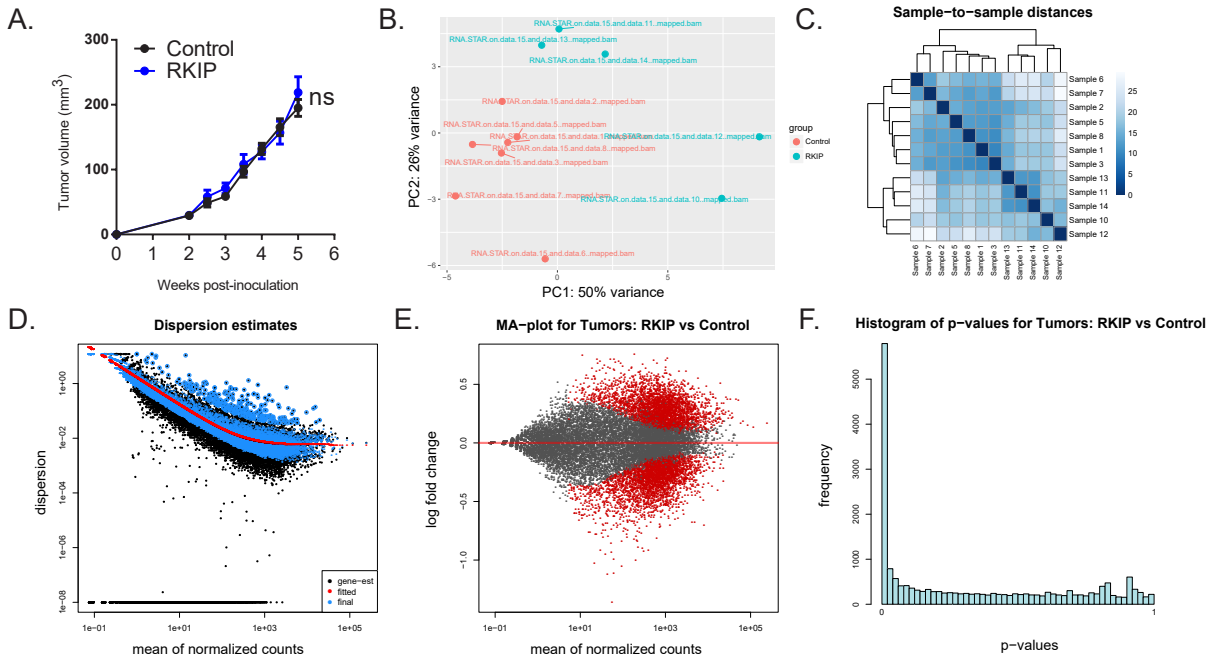

Figure 4.1: RNA-seq analysis of Control vs. RKIP tumors in the xenograft model. (A) Growth curves for the BM1 tumors orthotopically injected into athymic nude mice. Tumor volume was measured with caliper and data are shown as mean ± s.e.m. Significance was tested with 2-way ANOVA. ns - not significant. (B) Principle component analysis of the BM1-VC (Control) and BM1-RKIP (RKIP) tumors based on RNA-seq data. (C) Sample-to-sample distances .(D) Dispersion estimates of the normalized counts. (E) MA plot for the normalized counts. Each dot represents the average normalized mean count for a gene. Red dots are the genes statistically different between Control vs. RKIP tumors. (F) Distribution of p-values for the differential gene expression analysis.

The RNA-seq analysis provided a long list of candidate target genes, which makes experimental validation challenging. In order to narrow down this list, we followed an integrated

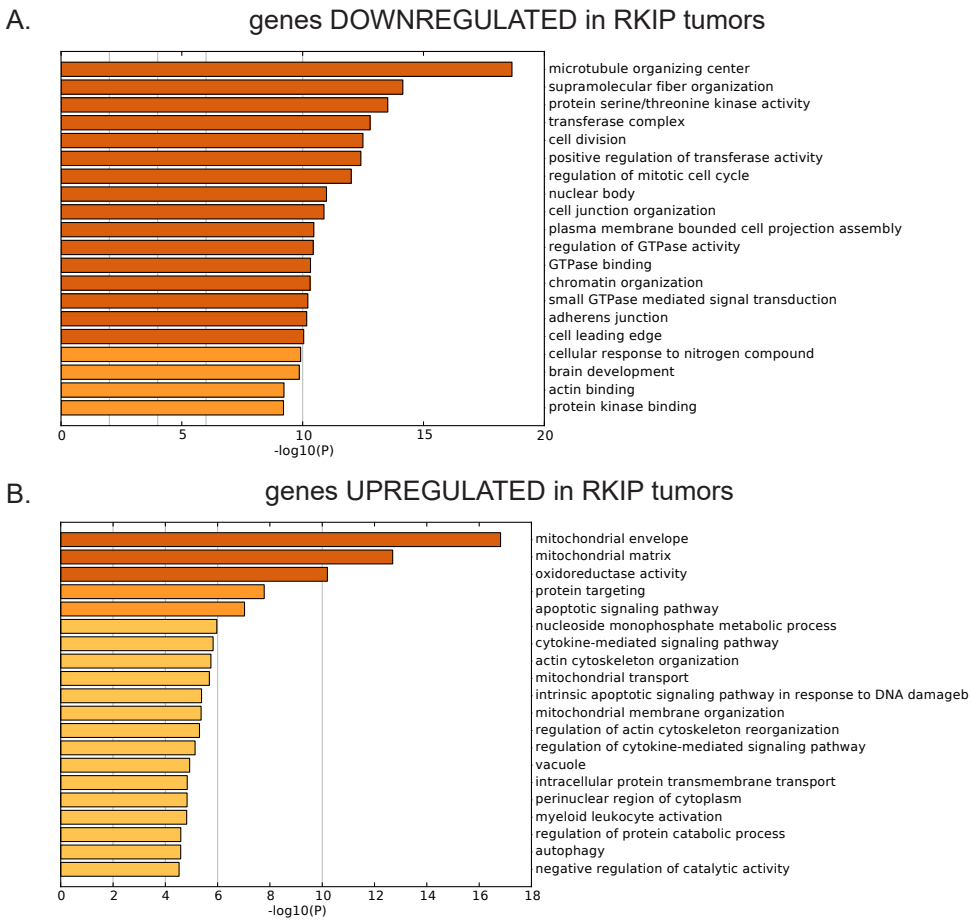

Figure 4.2: Functional gene set enrichment analysis on genes downregulated (A) and upregulated (B) by RKIP in xenograft BM1 tumors based on RNA-seq data.

approach where we used publically available TCGA data to filter RNA-seq data for clinical relevance. We hypothesized that if there is a mechanistic connection between RKIP and a set of putative target genes, expression of these gene sets should correlate with RKIP expression in the patient data as well. Thus, by intersecting RNA-seq-derived gene sets with patient-derived gene sets, we can identify a smaller set of genes that are likely to be RKIP targets.

Metascape (http://metascape.org) [97] is a web-based software that can identify gene sets commonly enriched in multiple datasets. After applying a fold change (log2) threshold of +0.3/-0.3 for the differentially expressed genes in RKIP RNAseq data and a pearson/spearman correlation coefficient cutoff of +0.3/-0.3 for genes correlated with RKIP in

the patient data, we employed Metascape to identify RKIP-associated gene sets common to both of the data sets. Among the GO terms negatively associated with RKIP were cell motility/invasion gene sets (e.g. "cell leading edge", "adherens junction", "regulation of plasma membrane bounded cell projection organization", "actin binding"), signal transduction (e.g. "protein serine/threonine kinase activity", "regulation of GTPase activity", "small GTPase mediated signal transduction") and cell division (e.g. "cell division", "microtubule organizing center", "nuclear body", "regulation of DNA metabolic process") (Figure 4.3, panel A on page 81). Positively associated gene sets were again mitochondrial components and metabolism (e.g. "mitochondrial innermembrane space", "mitochondrion organization", "mitochondrial transmembrane transport", "cytochrome complex assembly"), ribosomal-related gene sets (e.g. " small ribosomal subunit", "ribosomal large subunit biogenesis" , "ribonucleoprotein complex biogenesis"), cytokine signaling (e.g. "cytokine-mediated signaling pathway"), apoptosis (e.g. "intrinsic apoptotic signaling pathway", "regulation of cysteine-type endopeptidase activity involved in apoptotic process"), and autophagy (Figure 4.3, panel B). This analysis demonstrates that our RNA-seq results are similar to the gene associations observed within the patient data, suggesting that these associations we identified are present in patient tumors.

4.3.2 RKIP and MAPKi combo inhibit motility and invasion genes

Since we are interested identifying clinically relevant metastatic genes that are inhibited by RKIP, we decided to focus on downregulated genes in the RNA-seq data. Integration of experimental (RNA-seq) and patient (TCGA) data allowed us to narrow down canditate target gene list. Initial cut-off of -0.3 for the fold change (log2) reduced the number of negatively regulated genes to 1529 (from 2824). Given that RKIP's main function in vitro is to regulate cell invasion, we focused on cell motility / invasion genes that overlapped between the tumor RNA-seq data and the patient data. For this analysis we combined the genes in the "cell leading edge", "adherens junction", "cell junction organization", "regulation of

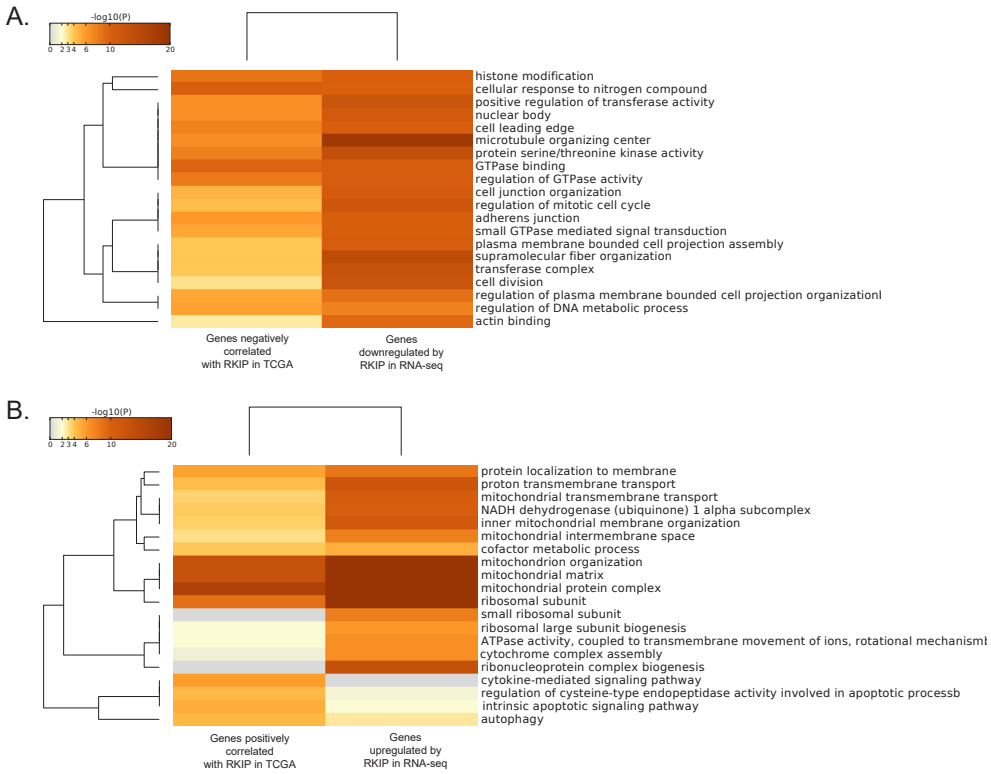

Figure 4.3: Overlapping gene sets between the RNA-seq data and the TCGA gene correlation data. (A) Gene set enrichment analysis for commonly enriched gene sets between genes downregulated by RKIP in xenograft tumors and genes negatively correlated to RKIP expression in TCGA breast cancer patient data. (B) Conversely, commonly enriched gene sets between genes upregulated by RKIP in xenograft tumors and genes positively correlated to RKIP expression in TCGA breast cancer patient data. Heatmap shows the adjusted p-values for the gene sets in -log10 scale.

plasma membrane bounded cell projection organization", "cell adhesion molecule binding", "positive regulation of cell migration", and "cell-substrate adhesion" GO terms. Our integrated aproach yielded 78 motility and invasion genes that were significantly downregulated by RKIP in BM1 tumors and also negatively correlated with RKIP expression in TCGA breast cancer samples.Since our goal is to identify genes that can be regulated by stress signaling, we applied two restrictions on this gene list as a final step: (1) the candidate genes should have previously been validated experimentally to promote migration, invasion, or metastasis in cancers, and (2) these genes should have binding site near their promoter for ATF and JUN family transcription factors that are activated by stress signaling. Out of 78, the following 15 genes met these requirements: ROCK1, ROCK2, DOCK4, DOCK5,

ADAM10, ADAM17, RAPGEF2, RAPGEF6, NFATC2, PIKFYVE, EPC1, DDR2, ITGA1, ARL13B, and APC (Table 4.1 on page 82).

Gene	FC(log2)	P	S	JUN	ATF	MYC	BACH1	Reference for metastatic function
ROCK1	-0.51	-0.43	-0.46	Yes	No	Yes	Yes	[83, 82]
ROCK2	-0.81	-0.34	-0.42	Yes	Yes	Yes	No	[83, 82]
ADAM10	-0.71	-0.39	-0.42	Yes	Yes	Yes	No	[68, 98]
ADAM17	-0.52	-0.34	-0.45	Yes	Yes	Yes	Yes	[84, 115]
EPC1	-0.59	-0.31	-0.31	Yes	Yes	Yes	No	[100]
PIKFYVE	-0.50	-0.39	-0.42	Yes	Yes	Yes	Yes	[73]
DOCK4	-0.48	-0.36	-0.44	Yes	Yes	Yes	Yes	[101, 51, 108]
DOCK5	-0.39	-0.35	-0.42	Yes	Yes	Yes	Yes	[29]
ARL13B	-0.46	-0.30	-0.32	Yes	Yes	Yes	No	[86, 12]
DDR2	-0.45	-0.37	- 0.50	Yes	Yes	Yes	No	[81]
ITGA1	-0.41	-0.31	-0.36	Yes	No	Yes	Yes	[35, 95]
RAPGEF2	-0.35	-0.35	-0.42	Yes	Yes	Yes	Yes	
RAPGEF6	-0.39	-0.31	-0.36	Yes	Yes	Yes	Yes	[62]
NFATC2	-0.85	-0.31	-0.42	Yes	Yes	Yes	Yes	[78, 74, 107, 27, 54]
APC	-0.33	-0.32	-0.34	Yes	Yes	Yes	No	[71]

Table 4.1: List of candidate target genes, their fold change (FC) in RKIP vs. control tumors from the RNA-seq data in log2 scale, their pearson (P) and spearman (S) correlation coefficients with RKIP expression in the TCGA breast cancer patient data, whether they have binding site for the transcription factors JUNs, ATFs, MYC, or BACH1 based on ENCODE CHIP-seq data, and the list of references for studies describing their roles in migration, invasion, and metastasis of cancer cells.

To validate the regulation of these putative target genes by RKIP, we measured relative expression of the target genes in the human cell lines BM1 and MB436 with respect to RKIP expression via quantitative RT-PCR. Overexpressing wild type RKIP or the S153E mutant in both of the cell lines resulted in a significant downregulation of ROCK1, ROCK2, DOCK4, DOCK5, RAPGEF6, NFATC2, ADAM9, ITGA1, and APC in BM1 cells (Figure 4.4, on page 83) and ROCK1, ROCK2, NFATC2 (Figure 4.5 on page 84) in MB436 cells under anisomycin-induced stress conditions in vitro. Similar to RKIP over-expression, the 4-drug MAPKi combination also decreased target gene transcript levels in vitro in 3D culture conditions (Figure 4.6 on page 84). Interestingly, not all of the motility/invasion genes were induced by anisomycin treatment (e.g. RAPGEF6 and PIKFYVE), but the MAPKi combination was still able to reduce the basal level expression for these genes. 4-

drug combination was also much effective than 2-drug combinations, consistent with the observed effects of the 2-drug combinations on the RKIP-network signaling. In some cases, 2-drug combinations, in fact, showed the undesired effect of increasing target gene expression. Treatment of syngenic LMB tumors with the 4-drug MAPKi for 3-weeks downregulated the expression of ROCK1, ROCK2, DOCK4, DOCK5, DDR2, RAPGEF2, RAPGEF6, NFATC2, and APC (Figure 4.7 on page 85). All of these results suggest that cell motility/invasion genes that we have identified in our integrated omics analysis are truly targeted by RKIP and the RKIP-mimicking MAPKi.

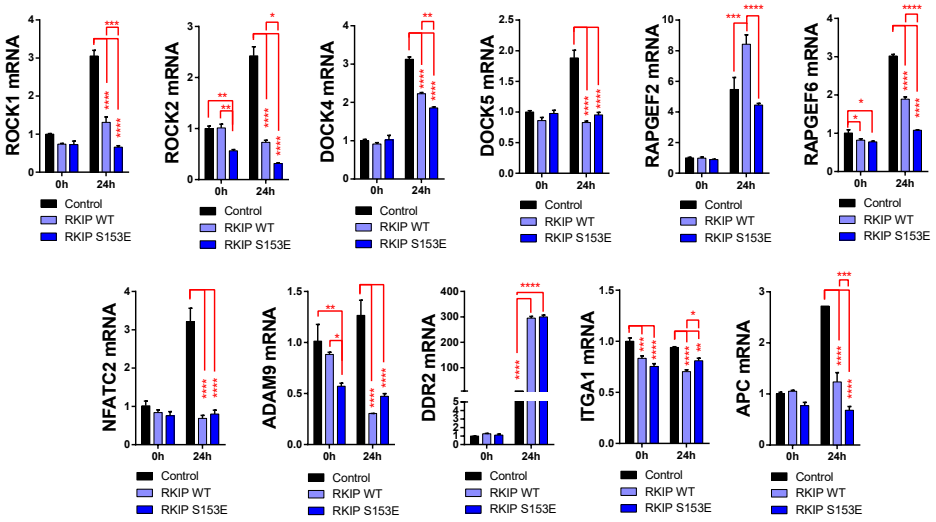

Figure 4.4: RKIP downregulates cell adhesion/motility genes in BM1 cells. BM1-VC, BM1-RKIP, and BM1-RKIP S153E cells were starved overnight, and induced with anisomycin (25ng/ml) for 24 hours. Quantitative RT-PCR data for the expression of the target genes was normalized to the Control cell expression in starved conditions (0h) and plotted as mean ± s.e.m. of the normalized values. Significance was tested for RKIP and RKIP S153E expression with respect to the Control expression at each time point using a two-tailed t-test. (p-values: * $p < 0.05$, ** $p < 0.01$, *** $p < 0.001$, **** $p < 0.0001$)

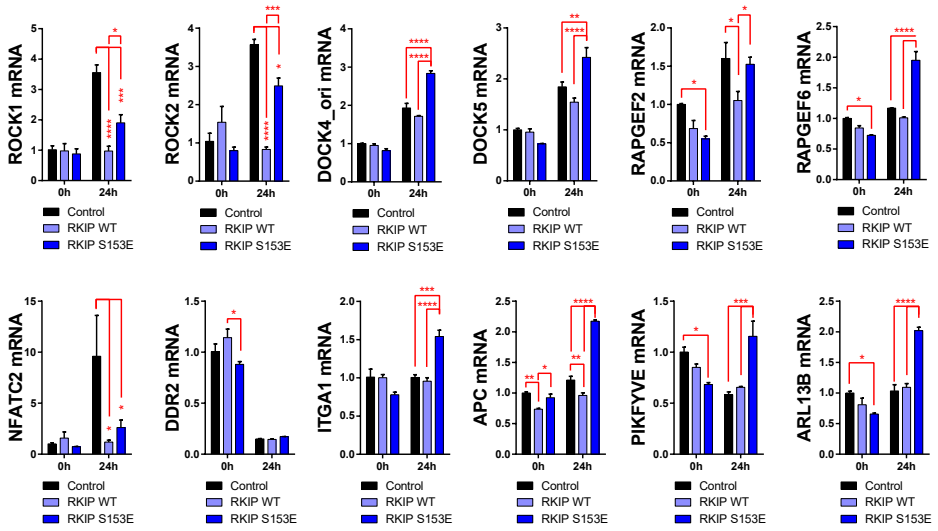

Figure 4.5: RKIP downregulates cell adhesion/motility genes in MB436 cells. MB436-VC, MB436-RKIP, and MB436-RKIP S153E cells were starved overnight, and induced with anisomycin (25ng/ml) for 24 hours. Quantitative RT-PCR data for the expression of the target genes was normalized to the Control cell expression in starved conditions (0h) and plotted as mean ± s.e.m. of the normalized values. Significance was tested for RKIP and RKIP S153E expression with respect to the Control expression at each time point using a two-tailed t-test. (p-values: * $p < 0.05$, ** $p < 0.01$, *** $p < 0.001$, **** $p < 0.0001$)

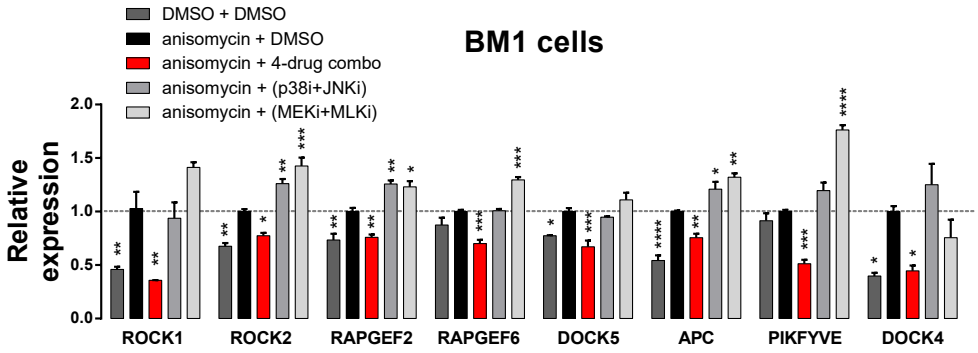

Figure 4.6: 4-drug MAPKi mimics RKIP's regulatatory effect on its downstream target genes in vitro. BM1 cells were starved overnight in 2mg/ml basement membrane extract, pre-treated with DMSO (control), 4-drug MAPKi combination, p38i+JNKi, or MEKi+MLKi for 30 minutes, and induced with anisomycin (25ng/ml) for 24 hours. Barplot shows quantitative RT-PCR data as mean ± s.e.m. of the normalized values. Expression values were calibrated to the anisomycin induction / no treatment sample (black bar). Significance was also tested with respect to the anisomycin induction / no treatment sample using two-tailed t-test. Dotted horizontal black line shows the expression level for each gene after 24 hours of anisomycin treatment in the absence of any inhibitors. (p-values: * $p < 0.05$, ** $p < 0.01$, *** $p < 0.001$, **** $p < 0.0001$)

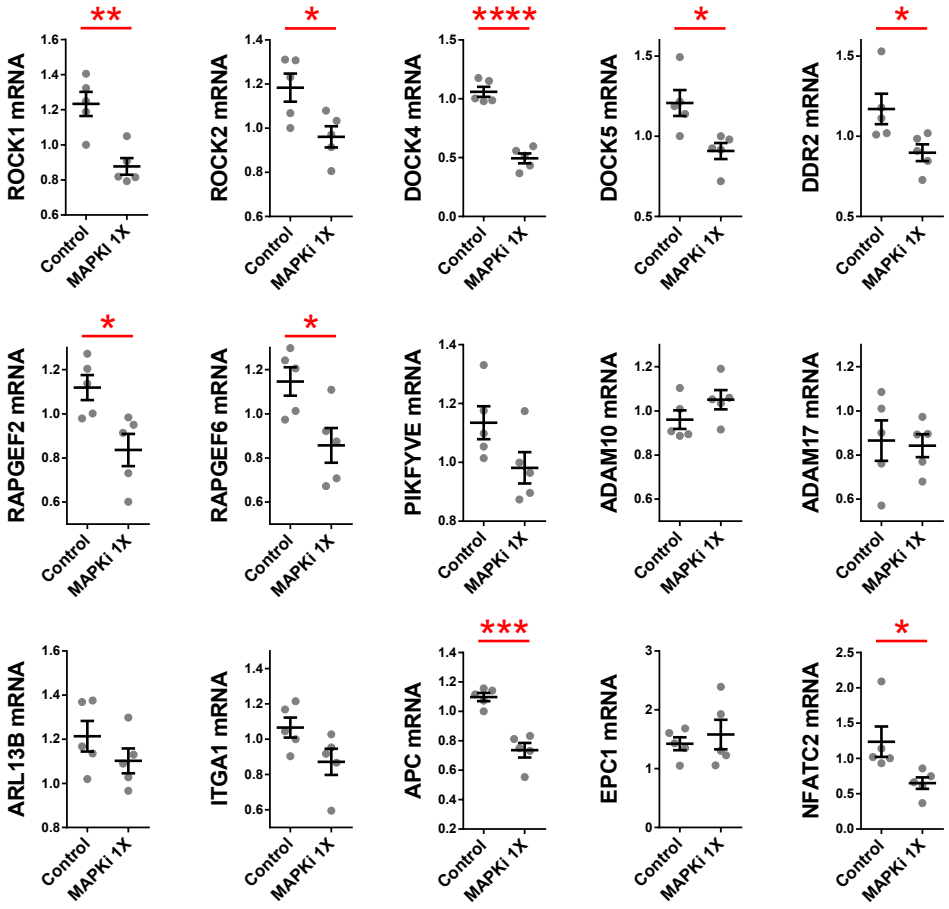

Figure 4.7: 4-drug MAPKi mimics RKIP's regulatatory effect on its downstream target genes in vivo in syngeneic LMB tumors. Quantitative RT-PCR analysis of target gene expression in LMB tumors treated with control vs. 4-drug MAPKi for 3-weeks. Each dot represents the average expression of n=3 technical replicates from a biological replicate. Significance was tested using a two-tailed t-test. (p-values: * $p < 0.05$, ** $p < 0.01$, *** $p < 0.001$, **** $p < 0.0001$)

4.3.3 Stress signaling induces the transcription factor BACH1, a primary target of RKIP

Our previous results have shown that RKIP regulates invasion / metastasis genes via inhibition of the MAPKs, but the mechanism by which these genes are regulated is unclear. Previous studies have implicated BACH1 as a translational target of RKIP via the microRNA let-7 [109]. To see whether RKIP regulates BACH1 at the transcriptional level as well, we

compared BACH1 expression in BM1 RKIP cells under stress conditions. BACH1 transcript levels increased very robustly upon chemical induction of stress by anisomycin, which was dampened partially by wild-type or S153E mutant RKIP over-expression in BM1 cells in vitro (Figure 4.8, panel A on page 86). Comparison of BACH1 expression in the RNA-seq data between BM1-VC and BM1-RKIP tumors also showed a significant downregulation of BACH1 expression in RKIP-expressing tumors (Figure 4.8, panel B).

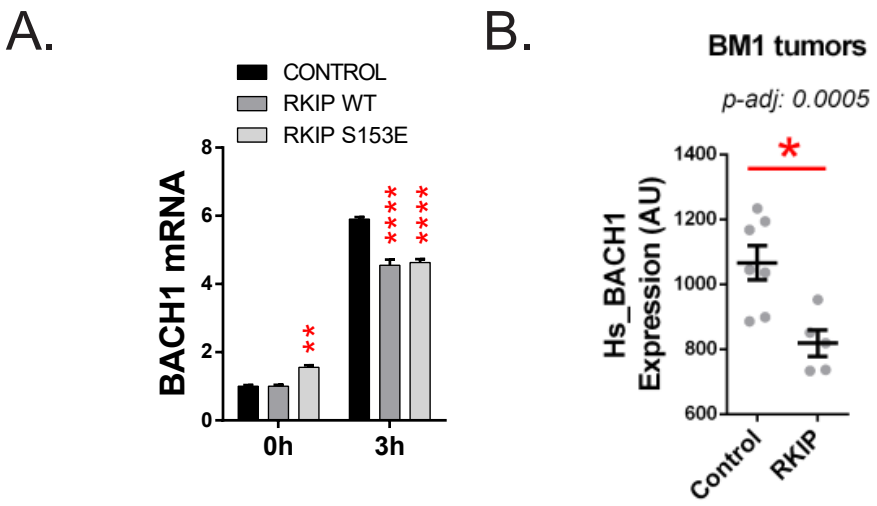

Figure 4.8: RKIP downregulates BACH1 mRNA expression in vitro and in vivo. (A) Quantitative RT-PCR analysis of BACH1 expression in BM1 cells expressing exogenous RKIP or RKIP S153E. Cell are starved overnight and induced with anisomycin (25ng/ml) for 3 hours. Significance was tested with respect to the Control samples using a two-tailed t-test. (B) BACH1 expression from the RNA-seq data replotted as mean ± s.e.m. of the normalized read counts.(p-values: * $p < 0.05$, ** $p < 0.01$, *** $p < 0.001$, **** $p < 0.0001$)

BACH1 is a transcriptional target of the MAPKs as well. In BM1 cells, BACH1 induction upon anisomycin treatment was blocked by the MAPKi combo, and the effect size of the combination treatment was more potent than the individual drugs at the doses used in the combination (Figure 4.9, panel A on page 88). At high doses, however, all four kinase inhibitors (p38i, JNKi, MEKi, and MLKi) inhibited BACH1 expression (Figure 4.9, panel D), suggesting that BACH1 expression can be downstream of all three MAPK axes of signaling. Subsequently, MAPKi combo also reduced BACH1 protein level by about 30% in vitro upon 24h induction with anisomycin (Figure 4.10 on page 89). The combination treat-

ment significantly blocked BACH1 expression at the transcipt and protein level in MB436 and LMB cell lines as well(Figure 4.9 and Figure 4.10), but the signaling axis responsible for the regulation was different in each cell line. Unlike BM1 cells, BACH1 expression was inhibited by p38i, JNKi, and MLKi treatment, but not MEKi, in MB436 cells (Figure 4.9, panel B and E). In the mouse TNBC cell line LMB, the findings were even more interesting, as only JNKi and MEKi were responsible for downregulation of BACH1 induction, while MLKi had no effect and p38 inhibition, in fact, increased BACH1 induction at high doses (Figure 4.9, panel C and F). These findings are critical in demonstrating that targeting individual axes of the MAPK network at high doses can prove inefficient or maybe even have unwanted effects on tumor cells. Conversely, targeting multiple nodes from different axes with inhibitors at low doses can achieve the desired phenotype across more cell lines even though the mechanism of action is unique to each cell line.

Regulation of BACH1 by the MAPK network was not limited to cell culture conditions. LMB syngeneic tumors that have been treated with the MAPKi combo for 3-weeks also demonstrated a signficant reduction in the mouse BACH1 transcript level (Figure 4.11 on page 89).

4.3.4 BACH1 regulates RKIP target genes

Since we have shown that RKIP can regulate BACH1 through the stress kinase network, we hypothesized that some of the metastasis related RKIP target genes (if not all), should also be BACH1 targets as well. BACH1 is a pro-invasive gene, as knocking down BACH1 expression via shRNAs reduces invasion and metastasis in BM1 cells [109]. Therefore, it is possible that this phenotype is mediated by a similar set of downstream genes shared between BACH1 and RKIP. In support of this idea, a subset of the RKIP target genes had binding sites for BACH1 in the ENCODE data (Table 4.1 on page 82).

With this logic, we followed the similar integrated approach discussed in Section 4.3.1 with the addition of a BACH1 filter. We reasoned that the metastatic genes that are in the same

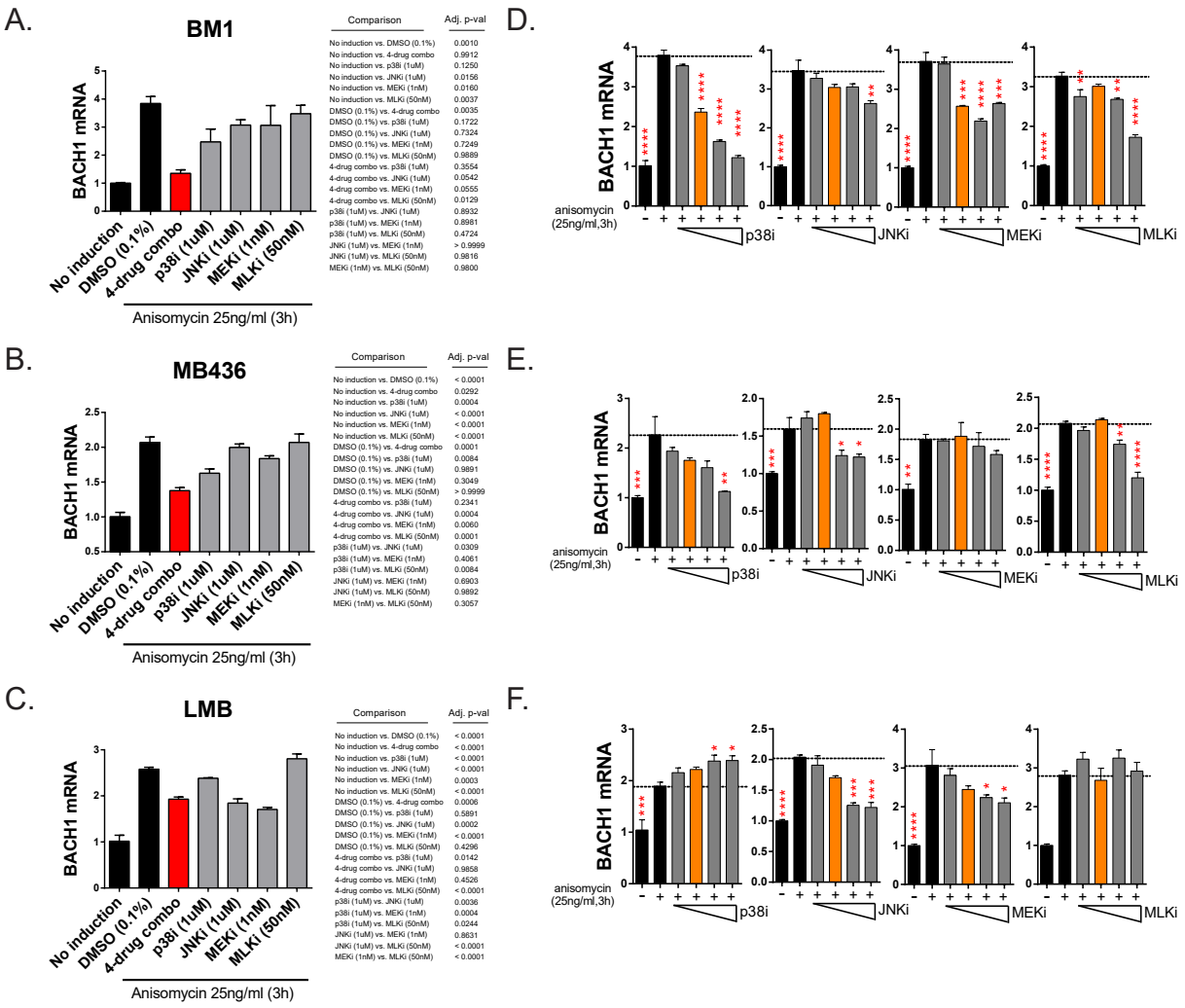

Figure 4.9: BACH1 expression is regulated by a different MAPK axis in each cell line, but the 4-drug MAPKi inhibits its induction in all three cell lines. (A) through (C) shows BACH1 expression after 3 hours induction with anisomycin (25ng/ml) in BM1 (A), MB436 (B), and LMB (C) cells in the presence of the 4-drug MAPKi or the individual inhibitors used at their combination dose. (D) through (F) shows dose-response for BACH1 expression upon treatment with the increasing doses of each MAPK inhibitors individually. Dosage: 0.1,1,10, 25 μM for p38i and JNKi; 0.1,1,10,100 nM for MEKi; 10,50,200,1000nM for MLKi. Orange bars indicate the doses of the drug used in the MAPKi combination, also shown in (A) through (C). All data was shown as mean ± s.e.m. of n=3 technical replicates. (A) through (C) are representative of two independent experiments with similar results. Significance was tested using two-tailed t-test. P-values are listed as exact adjusted p-values for (A) through (C) (right panel) and as interval for (D) through (F) where * $p < 0.05$, ** $p < 0.01$, *** $p < 0.001$, **** $p < 0.0001$

RKIP-BACH1 pathway would be negatively correlated with RKIP, and positively correlated with BACH1 in the TCGA patient data. Overlapping these genes with the experimentally-

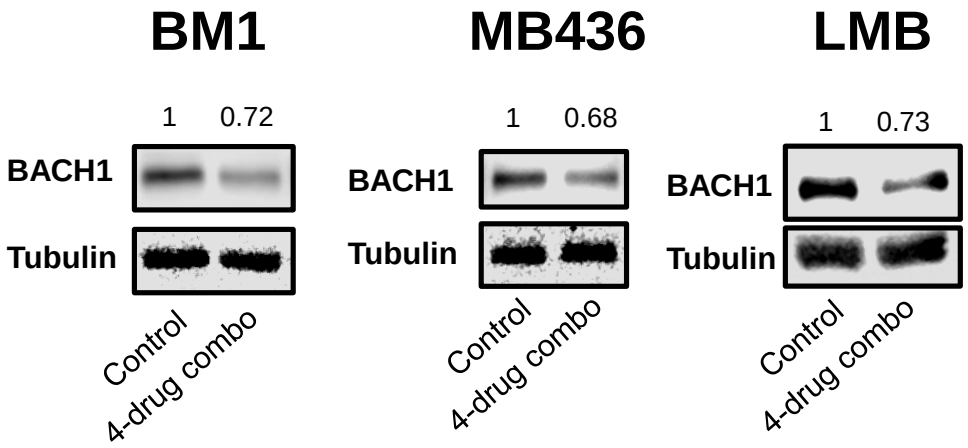

Figure 4.10: 4-drug MAPKi inhibits BACH1 induction by anisomycin (25ng/ml, 24 hour treatment) at the protien level.

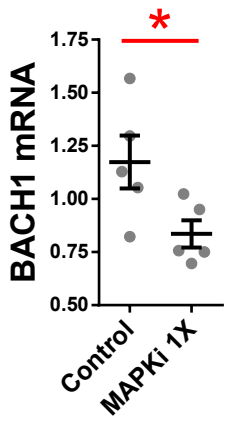

Figure 4.11: 4-drug MAPKi inhibits BACH1 transcripts in syngeneic LMB tumors.Quantitative RT-PCR analysis of target gene expression in LMB tumors treated with control vs. 4-drug MAPKi for 3-weeks. Each dot represents the average expression of n=3 technical replicates from a biological replicate. Significance was tested using a two-tailed t-test. (p-values: * $p < 0.05$, ** $p < 0.01$, *** $p < 0.001$, **** $p < 0.0001$)

derived RKIP target genes would give us a list of putative BACH1 target genes.

Metascape analysis involving genes negatively correlated with RKIP in the TCGA BRCA set, genes positively correlated with BACH1 in the TCGA BRCA set, and the genes that are downregulated by RKIP in the tumor RNA-seq data, revealed that there is a set of target genes shared by BACH1 and RKIP, which fall within the invasion related gene sets such as "cell-substrate adhesion", "cell leading edge", "cell adhesion molecule binding", "actin

cytoskeletal organization", and "actin binding" (Figure 4.12 on page 90). Interestingly, signaling related gene sets such as "kinase binding", "small GTPase mediated signal transduction", "protein serine/threonine kinase ativity" were also common.

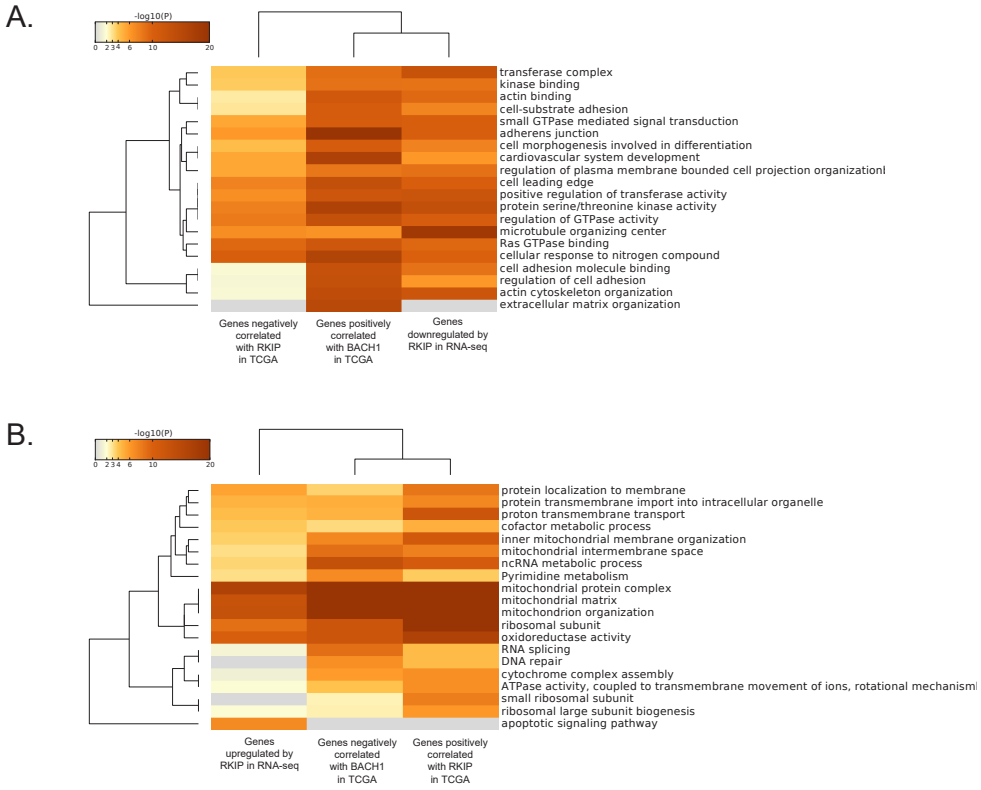

Figure 4.12: Overlapping gene sets between the RNA-seq data and the TCGA gene correlation data, with the addition of the BACH1 filter. (A) Gene set enrichment analysis for commonly enriched gene sets between genes downregulated by RKIP in xenograft tumors and genes negatively correlated with RKIP expression and positively correlated with BACH1 expression in TCGA breast cancer patient data. (B) Conversely, commonly enriched gene sets between genes upregulated by RKIP in xenograft tumors and genes positively correlated with RKIP expression and negatively correlated with BACH1 expression in TCGA breast cancer patient data. Heatmap shows the adjusted p-values for the gene sets in -log10 scale.

Taking a deeper look at the genes that are common between all three filters of the Metascape analysis revealed that the majority of genes that we have identified as RKIP targets in the previous sections, were also highly correlated with BACH1 expression in the patients, suggesting that they can be BACH1 targets as well. Figure 4.13 on page 91 shows that the genes that inversely correlate with RKIP expression are positively correlated with

BACH1 at the individual patient level. To test the regulation of these genes by BACH1, we used two shRNA constructs against human BACH1 in BM1 cells. In BM1 cells that had reduced levels of BACH1, the expression of these adhesion and invasion related genes were also reduced significantly (Figure 4.14 on page 92). CHIP analysis in BM1 cells using an anti-BACH1 antibody showed that BACH1 directly binds upstream of the transcription start site of at least three target genes (ROCK1, DOCK4, and PIKFYVE) (Figure 4.15 on page 93). This suggests that RKIP likely inhibits the expression of thesse invasion / metastasis genes by reducing BACH1 levels.

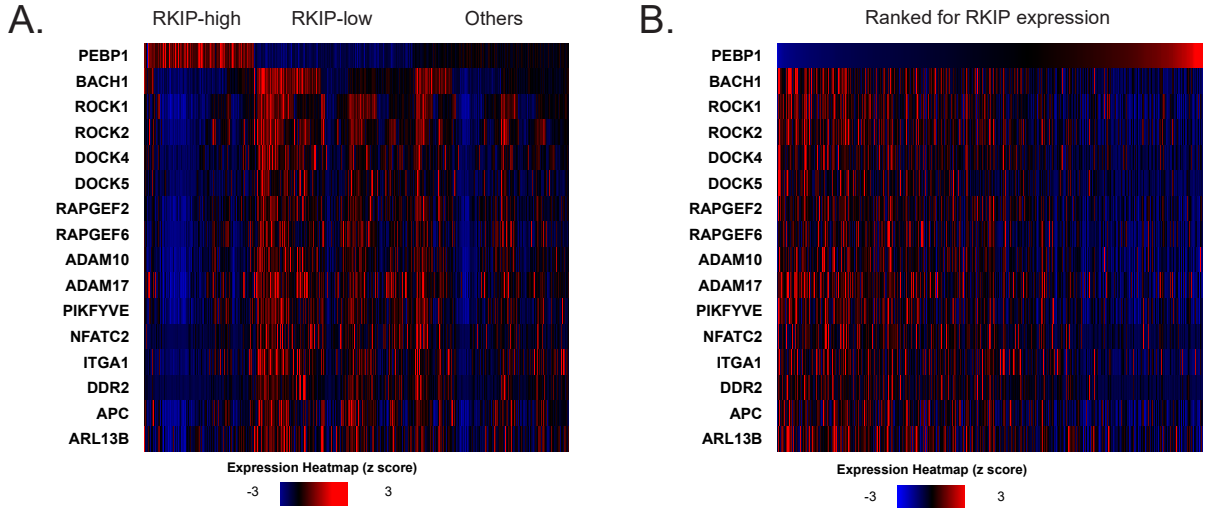

Figure 4.13: Expression heatmap for RKIP, BACH1, and the target genes (rows) in individual patients (columns) in the TCGA breast cancer data set. (A) Normalized counts for the expression of RKIP and its target genes were scaled row-wise to obtain z-scores. The heatmap shows the z-scores for each gene across the patient population. RKIP-high vs. RKIP-low status was determined based on a z-score threshold of -0.5/0.5 in either direction. (B) Patients samples were ranked in increasing order based on their normalized RKIP expression.

4.3.5 RKIP and BACH1 expression correlates with target gene expression in patients across multiple cancer types

Previous work from the Rosner lab elucidated metastatic mechanisms that are targeted by RKIP and BACH1 in TNBCs. Gene signatures based on RKIP-targeted signaling pathways

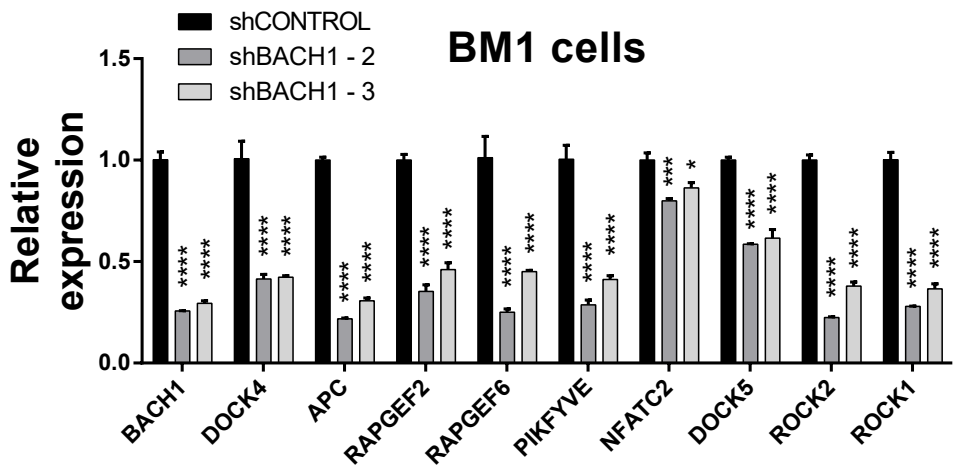

Figure 4.14: BACH1 regulates expression of RKIP target genes. BACH1 was knocked down in BM1 cells using two shRNA constructs. Cells were starved overnight, and induced with anisomycin (25ng/ml) for 24 hours. Expression in the shBACH1 cells for each gene is plotted as mean ± s.e.m. with respect to expression levels in the shCONTROL sample. Significance was determined against the shCONTROL sample using two-tailed t-test.(p-values: * $p < 0.05$, ** $p < 0.01$, *** $p < 0.001$, **** $p < 0.0001$)

can predict metastatic risk of a patient better than most of other gene signatures that are used in the clinic [56]. Moreover, these signatures are specific to the TNBC cases, that is, they stratify patients only within the TNBC/basal subgroup and not in ER(+) or HER2-enriched groups. This is largely becuse genes included in these signatures are identified as RKIP or BACH1 targets in TNBC cells and they are enriched in the TNBC/basal cases versus the remaining tumors.

Comparisons of the expression levels for the 15 metastasis genes between TNBC and non-TNBC patient samples in the TCGA data revealed that most of these genes were not enriched in TNBC tumors (with the exception of ROCK2, ADAM17, DOCK5, and DDR2) (Figure 4.16 on page 94). The results were similar for comparisons between molecular subtypes of breast cancer as well (Figure 4.17 on page 95). These findings suggest that the associations between RKIP and these cell motility related target genes are not specific to TNBCs. In fact, Metascape analysis across different TCGA cancer types, shows that RKIP negatively correlates with the same gene sets related to cellular adhesion, cell-matrix

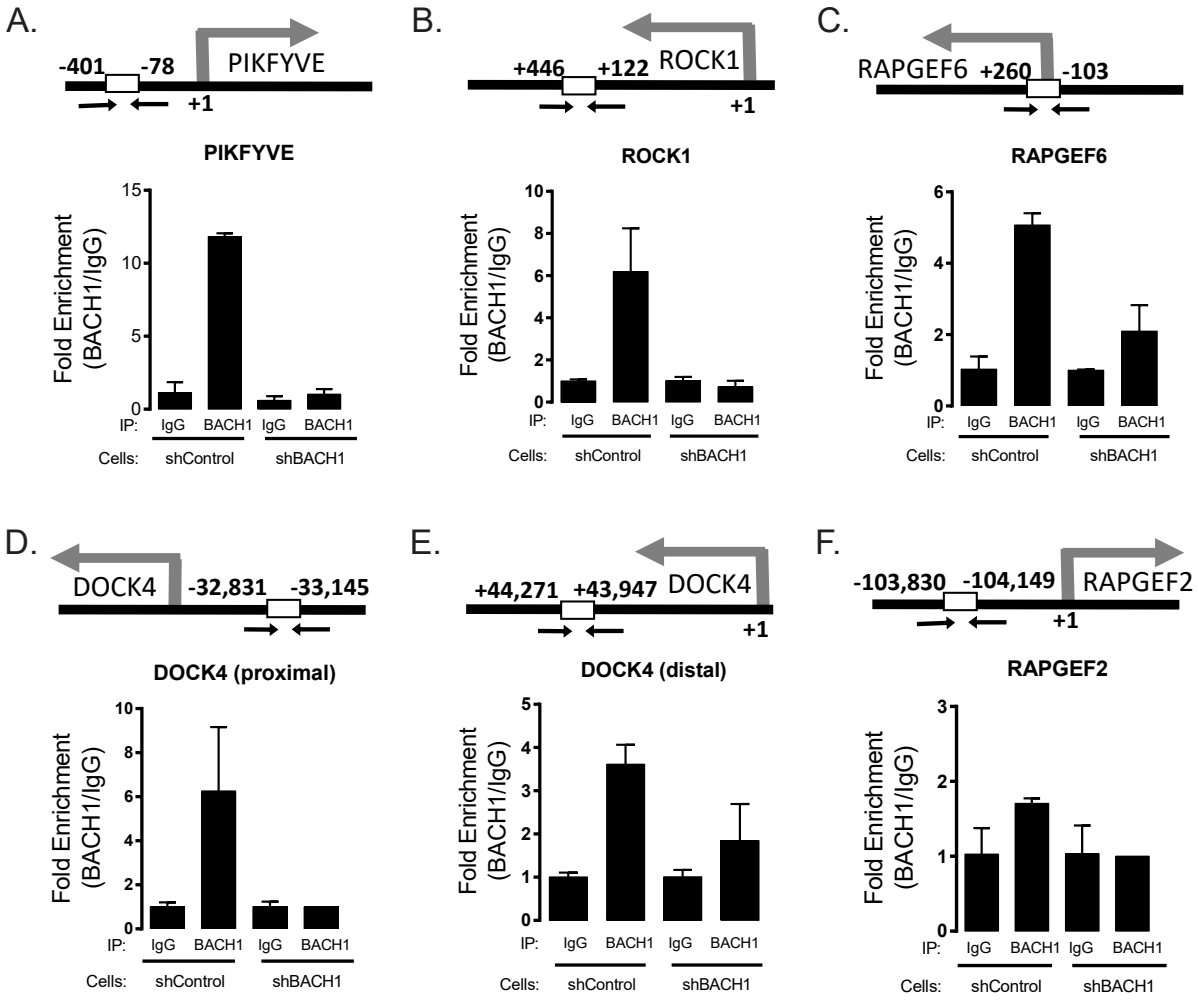

Figure 4.15: BACH1 can regulate a subset of RKIP target genes by directly binding to their promoter region in BM1 cells. BACH1 binding to the promoter regions was determined by CHIP analysis using BACH1-specific antibodies. CHIP from shBACH1 cells were used as a control for BACH1 antibody specificity.

interactions, and extracellular matrix organization in many solid cancers (Figure 4.18 on page 95 and Figure 4.19 on page 96).

Finally, negative associations with genes related to cell motility / invasion, cell-matrix interactions, and GTPase signaling are shared between RKIP and other metastasis suppressorsl (Figure 4.20 on page 97). We have identified at least four other experimentally-validated metastasis suppressors (BRMS1, ARGHDIA, NME1, and DRG1) which correlate negatively with these metastatic gene sets in breast cancers. These findings suggest that downregula-

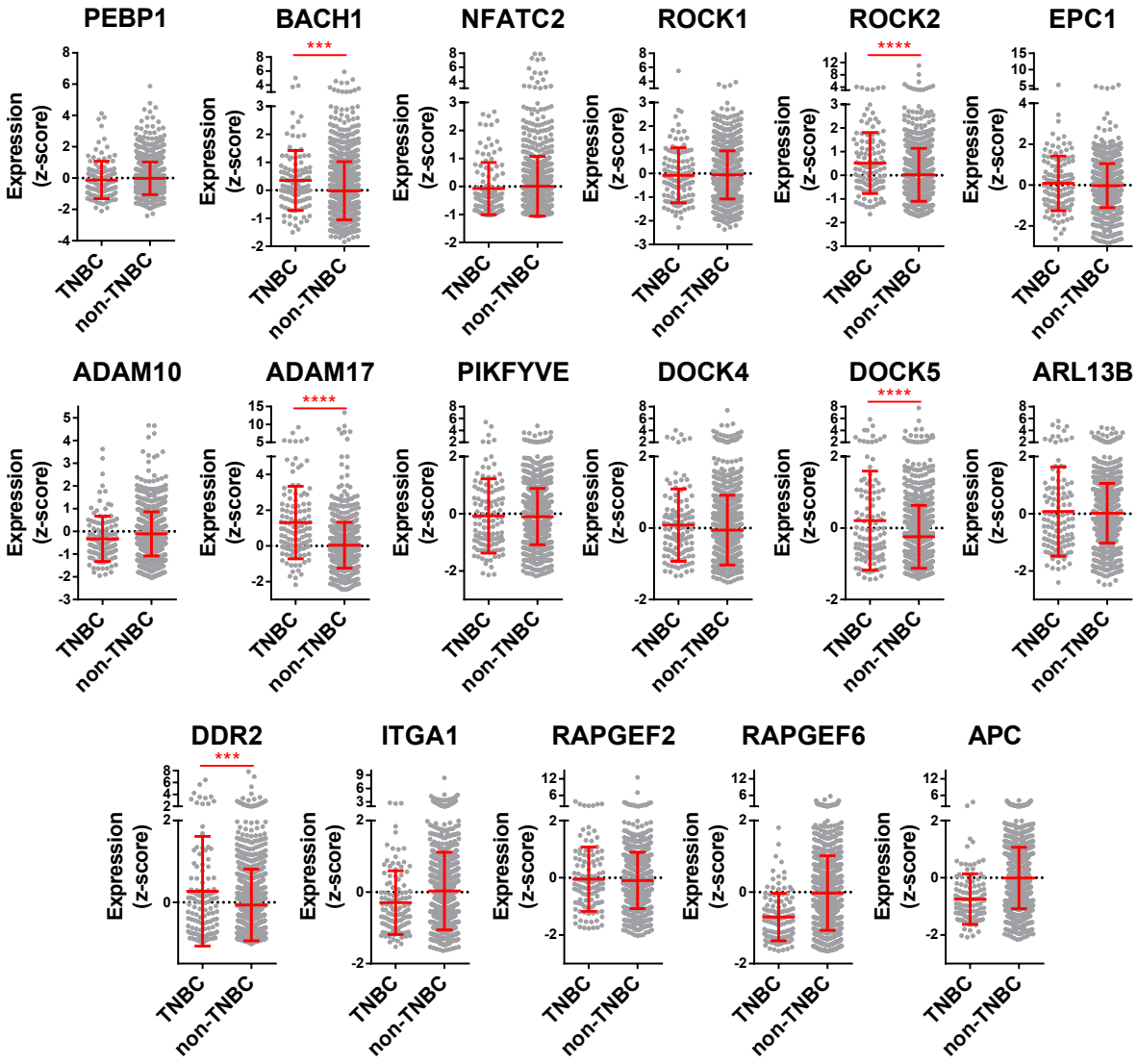

Figure 4.16: RKIP target gene expression in the TNBC sybtype of breast cancer

tion of cell-matrix interactions and cytoskeletal reorganization mechanisms is a hallmark of metastasis suppressors, and can be exploited as a broad-based therapeutic opportunity in metastatic disease.

4.4 Discussion

Our understanding of mechanisms by which RKIP reprograms cancer cell transcriptome is incomplete. Earlier chapters discussed the idea of metastasis as a process whereby cancer cells

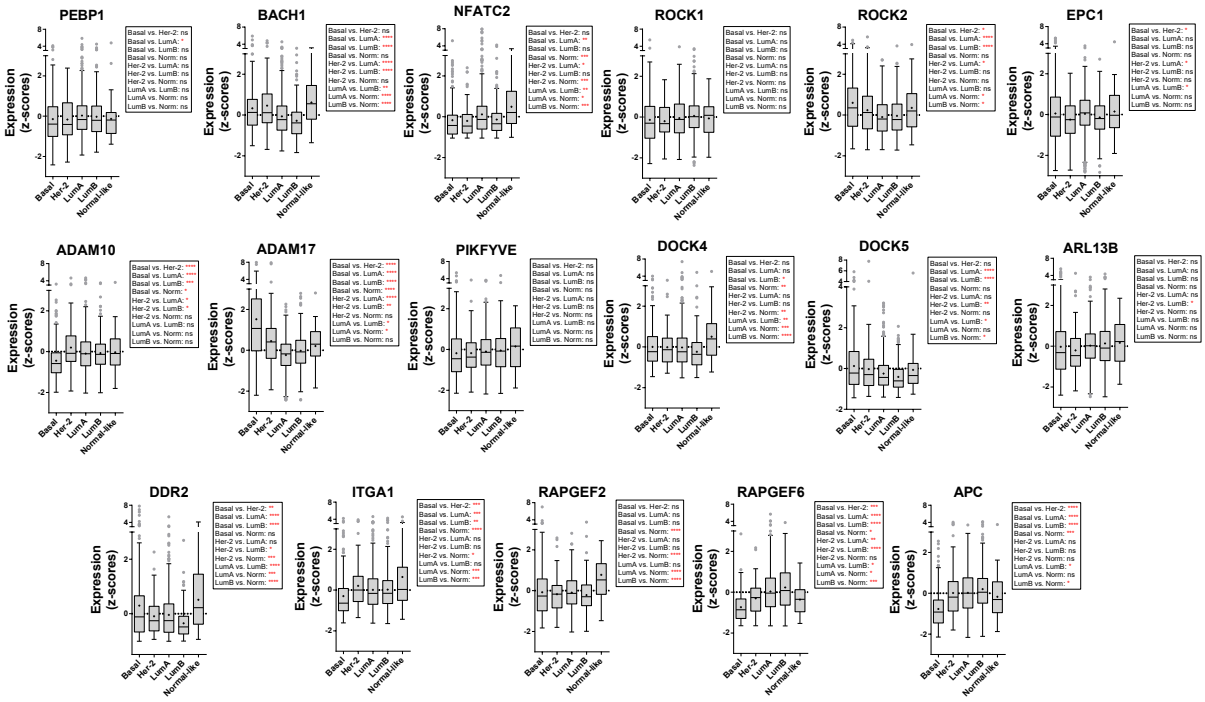

Figure 4.17: RKIP target gene expression based on the molecular subtypes of breast cancer in the TCGA data set.

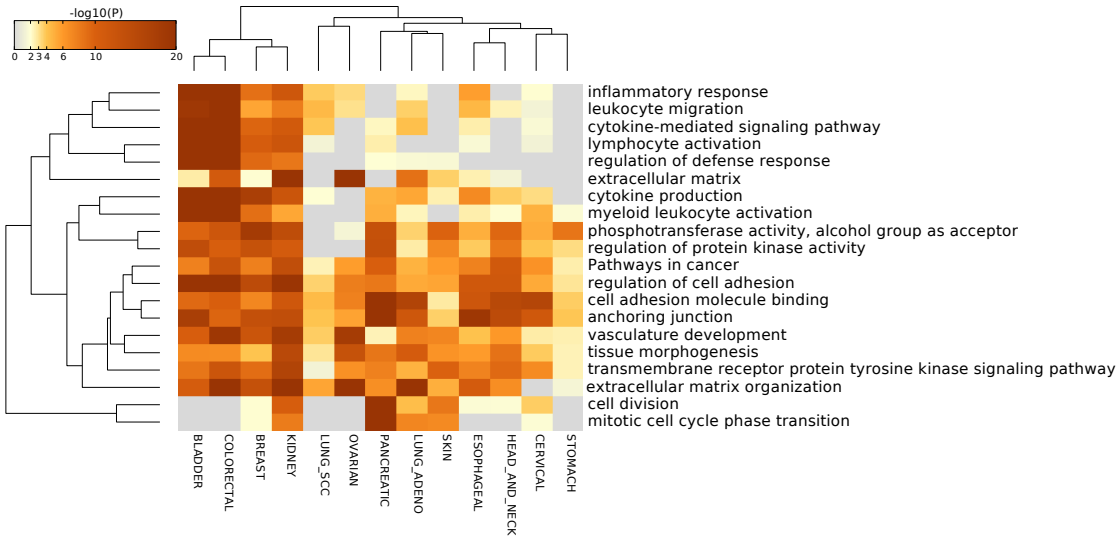

Figure 4.18: RKIP negatively correlates with cell adhesion/motility related gene sets in multiple solid cancer types

experiencing oncogenic and/or microenvironmental stress undergo kinomic and transcriptomic changes in order to gain motility. We have demonstrated that RKIP targets signaling events that mediate this transition by primarily targeting a stress-induced MAPK network.

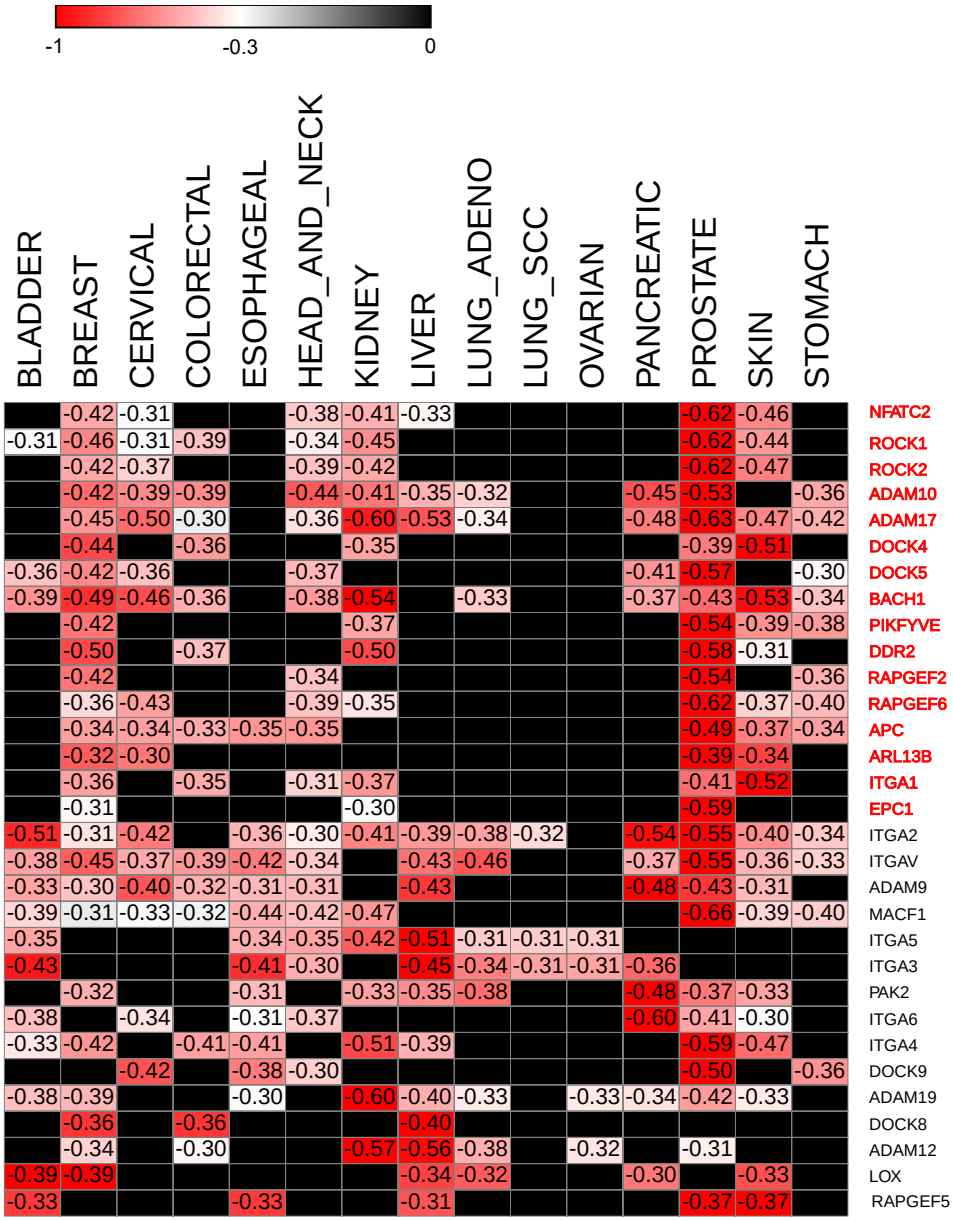

Figure 4.19: RKIP negatively correlates with BACH1 and cell adhesion/motility genes in multiple solid cancer types. Heatmap shows the spearman correlation coefficient for RKIP and each target gene listed. Black box indicates Spearman coefficient higher than -0.3.

The subsequent transcriptomic changes, however, have been elusive. In this chapter, we employ a computational approach to identify a set of metastatic genes that are putatively regulated by RKIP signaling network, and we validate them as RKIP targets in vivo and in vitro. Our focus was on a small set of motility and invasion related genes because of RKIP's anti-invasive role.

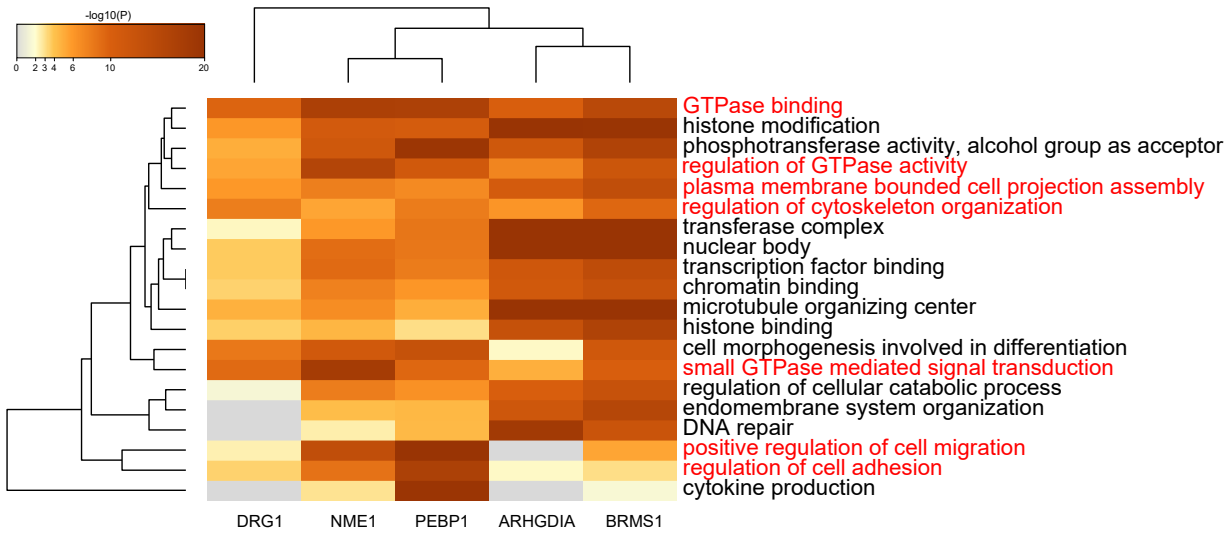

Figure 4.20: Cell adhesion, motility and invasion gene sets are negatively correlated with other metastasis suppressors in breast cancer as well

The RKIP target genes that we identified in this study have been previously shown to play a role in metastatic progression of cancers. For example, NFATC2 (also known as NFAT1) is a calcium sensing transcription factor that is overexpressed in many cancers (reviewed in [78], and it promotes metastatic phenotypes such as migration, invasion, prolfieration, and angiogenesis in breast cancer, melanoma, glioblastoma [107, 27]. Interestingly, NFATC2 directly interacts with p38 and JNK kinases which can enchance its transcriptional activity [74, 54], suggesting that transcriptional inhibition by stress signaling may not be the only mechanism for NFATC2 regulation. ROCKs, DOCKs, and RAPGEFs are directly involved in cell motility, contractility, and protrusion formation by regulating actin/myosin dynamics [82, 4, 32, 110]. DOCK4 is essential for TGF-β-mediated metastasis of lung adenocarcinoma cells into liver and bone [108]. It also promotes migration in MDA-MB-231 cells and BM1 cells by activating Rac1 [51] and knockin down in DOCK4 by shRNA reduces migration . Studies investigating or summarizing the rest of the candidate genes for their function in metastasis progression are listed in Table 4.1 on page 82. Our findings are consistent with the pro-metastatic function of these genes as they are inhibited by the metastasis suppressor RKIP in vivo and in vitro.

Our study supports a recent study by Insua-Rodriguez and colleagues showed that ascites and pleural effusion samples from breast cancer patients demonstrated increased activity of JNK signaling, which correlated with poor clinical outcome [45]. JNK signaling in breast cancer cell lines enhanced the extracellular matrix proteins Osteopontin and Tenascin C, supported stem cell niche, and conferred resistance to chemotherapy. Our experimental results are consistent with these findings that implicate p38 and JNK as mediators of cellular motility, invasion, and metastatic progression of cancers. Interestingly, we have previously identified Osteopontin as a downstream target of RKIP [22, 109] in a cascade involving the Raf-Mek-Erk axis and the transcription factor HMGA2. Insua-Rodriguez's work complements our work by showing that some of the RKIP targets we have identified in our previous studies (like HMGA2) can be regulated not only through ERKs, but also through stress kinases. Chemosensitization role of JNK inhibition is consistent with the same phenotype observed in RKIP-overexpressing cells [15, 9] and argues that RKIP might be sensitizing cancer cells to chemotherapeutic agents by inhibiting JNK signaling in breast cancers. This also highlights the potential for the 4-drug MAPKi to chemosensitize since it targets JNK activity as well. However, we demonstrated that the effect of inhibiting the entire MAPK network is not always additive of inhibiting individual MAPK axes. Therefore, these hypotheses need to be further tested experimentally in breast cancers.

The computational analysis of patient expression data from multiple TGCA data sets implied that our findings are not limited to just triple negative breast cancers. Inverse correlations between RKIP and the cell motility genes identified here (such as ROCKs and DOCKs) are present in other solid tumors as well. This implies that regulation of cell-matrix interactions and invasion related genes can be a common anti-metastatic mechanism for RKIP in cancers. RKIP might have cancer-type specific functions as well, such as regulation of innate immunity, inflammation and cell division, as these gene sets are enriched for certain cancer types but not for others (Figure 4.18 on page 95 and Figure 4.19 on page 96). Other commonly studied metastasis suppressors also share this negative correlation

with motility and invasion genes, demonstrating patient-derived evidence that blocking migration, invasion, and cell-matrix interactions is a hallmark of metastasis suppressors. These findings highlight the clinical relevence and broadness of the RKIP-network, and potential for multicancer applications regarding RKIP-mimicking treatments such as our MAPKi combination.

CHAPTER 5

SUMMARY AND DISCUSSION

Metastasis is the deadliest aspect of cancer. Majority of cancer patients do not die of primary disease, but of metastatic spread of the disease to vital organs. Clinically, metastatic phenotype is associated with treatment resistance, rapid progression, and lower overall survival rates. In most cancers, the standard of care for late stage disease is systemic treatment like chemotherapy, and the treatment is usually used to slow down progression or as palliative care. In most cancer types, more than 80% of patients will eventually succumb to the disease if their cancers are already metastatic at the time of diagnosis. This occasionally prompts cancer patients to opt out of chemotherapy because the toxicity of the treatment can outweigh the benefits of the treatment. Therefore, there is a dire need for less toxic and more effective therapeutic options for metastatic patients.

In this study, we sought to learn from the molecular and physiological functions of the metastasis suppressor RKIP in order to explore novel anti-metastatic strategies. RKIP is a great tool for studying mechanisms of metastasis because it not only inhibits multiple steps of metastasis (e.g. invasion, intravasation, overall metastatic progression), but it also molecularly functions as a kinome modulator, which allows us to focus on metastatic signaling events. This is critical in developing targeted treatments against metastasis because kinases are one of the easiest class of molecules to target, and there is a plethora of inhibitors available for use. Here, we outline a research pipeline that involves (1) identifying signaling networks that are altered by the metastasis suppressor, (2) testing inhibitors that can inhibit this network, (3) identifying downstream gene targets of the network that are clinically relevant, and (4) elucidating the transcriptional regulation that connect the signaling network to the gene expression. What is outside the scope of this study is a final step (5) where the functions of the downstream target genes in metastasis are explored experimentally and (6) development of pathway-based gene signatures that can stratify patients for metastatic risk, or for treatment efficacy. This approach can be customized and applied to other metastasis

suppressors or tumor suppressors that cannot be reintroduced to tumors easily.

By studying RKIP's effect on TNBC kinome, we identified a network of MAP kinases to be essential for invasion and metastasis. Importantly, RKIP inhibited many kinases regardless of their basal activity level, but it inhibited these kinases only partially. This is different from the way targeted therapies are used in the clinic currently, which focuses on hitting a single target at highest dose tolerable. To mimic RKIP we developed a multi-drug combination in which each inhibitor is used at sub-therapeutic doses and collectively they inhibit all three axes of MAPK network only partially. This MAPKi combination effectively blocked invasion in multiple TNBC cell lines without affecting their growth in vitro. It also inhibited expression of stress-induced RKIP targets, mainly the genes involved in cell-matrix interactions, motility, and invasion (e.g. ROCK1/2, DOCK4/5, RAPGEF2/6 and APC), which attests to its anti-metastatic effect. In mouse models of TNBC, the combinatorial treatment functioned as both metastasis suppressor and a tumor supressor. Especially in BM1 tumors, the MAPKi treatment blocked primary tumor growth as well as the metastatic growth. In syngeneic LMB tumors, the effect on metastasis was more robust than the effect on primary tumor growth, highlighting the context-dependent efficacy of the treatment.

Our multi-drug combination targeting MEK, p38, JNK, and MLK is a novel combination. In the clinic, resistance to MEK inhbitors are associated with activation of PI3K and AKT pathways [16, 61], and therefore, most combination attempts have focused PI3K or AKT inhibitors along with MEK inhibitors [63, 61]. Other approaches involve combining receptor tyrosine kinase inhibitors, HDAC inhibitors, and inhibitors of tumor-associated microenvironment, all reviewed by Smith and Wellbrock [89]. p38 and JNK inhibitors as single agents yielded discouraging results in clinical trials [65]. Some studies now focus on combining p38 inhibitors with chemotherapeutic agents such as gemcitibine and carboplatin [18] (e.g. clinical trial NCT01663857) or with EGFR/HER2 inhibitors [67]. To date, very few JNK inhibitors made it to the clinical trial level. An early MLK inhibitor CEP-1347 was tested in PhaseII-III clinical trials for Parkinson's disease and did not show efficacy, but now it is

being considered as anti-cancer treatment for targeting stem cells [72]. A more recent MLK inhibitor URMC-099 is still in its pre-clinical phases. Our approach of targeting these four MAPKs is unique because, to our knowledge, no other study is considering such combination. Our approach is not limited to the use of the four specific inhibitors used in this study (SB203580, SP600125, Trametinib, and URMC-099). We acknowledge that there can be other possible combinations of various number of inhibitors that target the RKIP-network. Our findings would also justify development of multi-target kinase inhibitors that inhibit all three MAPKs p38, JNK, and MEK/ERK.

CHAPTER 6

FUTURE WORK

The fact that RKIP does not change overall growth properties of cancers suggests that RKIP is probably influencing the tissue invasion, intravasation, and extravasation steps of metastasis. Our short term treatment of circulating tumor cells with the RKIP-mimicking MAPKi combo also supports the idea that the RKIP-network is important for tumor cells to move in and out of the circulation. Though unlikely, RKIP might also be inhibiting metastatic growth by influencing the colonization of tumors in the metastatic site. This is a possibility we have not investigated thoroughly. The therapeutic effect of reintroducing RKIP in already established metastases can be tested by using inducible RKIP constructs which allow for activating RKIP expression after the metastatic burden in mice reaches a certain level.

Using an integrated approach, we have identified novel downstream target genes of the RKIP-network which are at least partially regulated by the transcription factor BACH1. Though BACH1 is a major player in the RKIP-network, it is not the only one. In the past, we have identified other transcription factors that can mediate RKIP's effect on metastatic gene expression, such as HMGA2 and MYC. It is possible that these genes are involved in regulation of some of the novel target genes that were not affected by BACH1 inhibition. To test if BACH1 is a major regulator for the RKIP network, phenotypic rescue experiments should be conducted. We anticipate that over-expressing BACH1 in RKIP-high background will be not be sufficient to rescue the RKIP phenotype completely because there are other transcriptional regulators targeted by RKIP. But we do expect to see at least a partial rescue of the invasion as well as downstream gene expression since BACH1 seems to be involved in both of these processes. Previous work also demonstrated that overexpressing a sinlge downstream metastatic target is usually not enough to rescue RKIP's anti-metastatic function, and even partial rescue requires over-expression of multiple target genes. This will likely hold true for the new metastasis target genes we identified in this study. Future studies

should consider strengthening the mechanistic association between RKIP and its target genes involved in cell adhesion and motility

In this study, we only focused on the invasion and cell motility related gene sets because our main interest was to be able to use inhibitors to block the expression of these genes in an attempt to mimic RKIP. However, regulating cell motility is not the only function RKIP has. We have identified a number of other gene sets that is associated with RKIP both in experimental models and in the patient data. Some of these genes are related to cell division and negatively correlated with RKIP expression. We have previously elucidated regulation of cell cycle by RKIP in a mechanism involving Aurora Kinase B [26]. The RNA-seq results suggest that RKIP might be influencing cell cycle through the expression of many other genes.

On the other hand, the RNA-seq data from both the BM1 tumors and the TCGA patients suggested a strong positive correlation between RKIP and ribosomal subunit expression, which associates with proliferative state of the cell. Ribosome biogenesis is essential for growth, proliferation, and differentiation, and it fine-tunes rate of proliferation [85]. Interestingly, intracellular and extracellular factors such as genetic changes in ribosomal genes, treatments with certain chemical agents or radiation, serum/nutrient/glucose starvation, and even hypoxia, result in accumulation of ribosomal subunits that are not in a ribosomal complex - a state called "ribosomal stress" (reviewed in detail by Zhou et al. [116]). These ribosome-free ribosomal proteins (RPs) have been shown to have translation-independent functions, some oncogenic and some tumor-suppressive. Certain RPs can act as tumor suppressors by inactivating c-Myc, downregulating LIN28B, inhibiting PI3K/AKT, ERK, NFκB signaling, and ATF4-mediated transcription of survival genes, or potentially influencing angiogenesis by reducing vascular smooth muscle cell proliferation. Others demonstrate oncogenic activity by inactivating p53, activating NFκB signaling, and induce cell cycle genes such as Cyclin D1, D3 and CDK1. Some can activate JNK signaling, which can be suppressive or oncogenic/metastatic depending on the cellular state. Regarding these non-canonical

roles for RPs, their upregulation by RKIP might serve three potenial purposes: (1) RKIP might be primarily upregulating RPs with suppressive functions to reprogram tumor cells into a more benign state. Downregulation of stress MAPK activity might even be partially a result of ribosomal subunit regulation by RKIP. (2) Alternatively, by upregulating ribosomal subunit expression in general, it induces more normal ribosome assembly and translation, which reduces the ribosomal stress that is present in tumor cells. (3) Finally, it is also possible that different RPs have different affinity for certain mRNA species. An example of this is RPL38, which attracts Hox gene mRNAs to ribosomes and facilitates anterior-posterior patterning of the embryo during development. Some RPs favor IRES-dependent translation, while others mediate cap-dependent translation, which can alter the proteomic state of a cell. Therefore, it is critical that we experimentally elucidate the mechanisms by which RKIP modulates translation as it can be ciritical to the metastatic progression and might constitute another therapeutic avenue.

Another set of genes positively regulated by RKIP is mitochondrial genes. Many mitochondrial / inner-mitochondrial membrane genes are positively correlated with RKIP and negatively correlated with BACH1 in many solid cancer types. Our recent work demonstrated that in breast cancers, high BACH1 expression inhibits oxidative phosphorylation (OXPHOS) by downregulating transcription of inner mitochondrial transmembrane genes that are involved in electron transport chain (ETC). Therefore, it makes sense that RKIP induces a similar set of genes by reducing BACH1 activity. More importantly, decreasing BACH1 expression in tumors by shRNAs or causing its degradation by Heme treatment, pushes cancer cells into a more OXPHOS-dependent state, where the cells are more vulnarable to the mitochondrial respiration complex I inhibitor Metformin. This argues that RKIP expression and the RKIP-mimicking 4-drug combination will synergize with Metformin treatment in cancers as a viable therapeutic option, which should be tested in mouse models.

RKIP is an effective tool in suppressing metastatic progression of cancer, but it does

not provide solutions for already established disease. RKIP itself is not cytotoxic or growth inhibitory to the tumors, suggesting that it needs to be coupled with a cytotoxic treatment for complete eradication of the disases. Same applies to our RKIP-mimicking 4-drug MAPKi combination. Even though it can act as a tumor suppressor in a certain context, we have shown that if the treatment ceases, the tumor growth resumes. This indicates that, though it can be a powerful chronic treatment for late-stage disease, our MAPKi combination is not enough by itself to clear all the tumor from the body. Therefore, next steps for this study involve testing cytotoxic treatments such as chemotherapy, radiation, and immunotherapy along with RKIP-mimicking treatments.

Interestingly, RKIP has previously been shown to sensitize tumors to some of these cytotoxic treatments [15, 9]. Though the mechanisms are not clear, we believe that reintroducing RKIP to tumors reprogams thems to a more homogenous state which is vulnarable to cytotoxic agents. Recent work from the Rosner laboratory has examplified this idea by showing that BACH1 inhibition pushes tumors to a more homogenous state where the cells reactivate oxidative phosphorylation, which then sensitizes them to metabolic inhibitors such as metformin (manuscript accepted). RKIP should work the similar way, if not more robustly than BACH1 inhibition, in homogenizing tumors to cytotoxic agents. Any RKIP-induced phenotypic change that is important for a tumor cell's survival can be leveraged as a therapeutic target. We envision novel 2-phase treatment apporaches where the cancers are reprogrammed by RKIP re-introduction or RKIP-mimicking treatments into a less heterogeneous state, and then hit with an inhibitor that targets this state as a the second line of treatment. Studies testing this idea are currently underway in the Rosner laboratory.

Our lab previously demonstrated that RKIP pathway-based gene signatures are powerful predictors of metastatic potential. RKIP pathway metastasis signature (RPMS) and BACH1 pathway metastasis signature (BPMS) perform better than many gene signatures developed by other groups. We reported theses signatures to be specific to TNBC subtype of breast cancer, as they can identify more aggressive tumors that are likely to metastasize within

the TNBC cohort. This is probably because the RKIP and BACH1 pathway genes used in these signatures are based on experimentally validated mechanistic relationships that were generated using TNBC cell lines and mouse models. In this study we continued to use TNBC as a model to investigate metastatic mechanisms. However, our TCGA patient data analysis suggested that our findings might have more global implications because the correlations we are observing between RKIP, BACH1, and the downstream target genes are present across multiple cancer types. Therefore, it might be possible to develop a gene signature using the RKIP-network genes identified in this study which can predict metastasis-free survival, or even overall survival, in multiple cancer types. Such signature could also predict which patients are more likely to respond to an RKIP-mimicking treatment. Those patients scoring high for this signature (high expression for metastatic genes, low RKIP expression) would be more likely to respond to a treatment that targets RKIP-network genes. Therefor, it is critical that we experimentally validate the regulation of metastatic genes involved in cell-matrix adhesion, cell motility / invasion, ribosome biogenesis, and mitochondrial respiration by RKIP, BACH1, and MAPKi combination in other cancer types as well.

REFERENCES

[1] J. A. Aguirre-Ghiso. Models, mechanisms and clinical evidence for cancer dormancy. *Nat. Rev. Cancer*, 7(11):834–846, Nov 2007.

[2] F. Al-Mulla, M. S. Bitar, M. Al-Maghrebi, A. I. Behbehani, W. Al-Ali, O. Rath, B. Doyle, K. Y. Tan, A. Pitt, and W. Kolch. Raf kinase inhibitor protein RKIP enhances signaling by glycogen synthase kinase-3β. *Cancer Res.*, 71(4):1334–1343, Feb 2011.

[3] F. Al-Mulla, M. S. Bitar, J. P. Thiery, T. T. Zea, D. Chatterjee, L. Bennett, S. Park, J. Edwards, and K. C. Yeung. Clinical implications for loss or diminution of expression of Raf-1 kinase inhibitory protein and its phosphorylated form in ductal breast cancer. *Am J Cancer Res*, 3(5):446–464, 2013.

[4] M. Amano, M. Nakayama, and K. Kaibuchi. Rho-kinase/ROCK: A key regulator of the cytoskeleton and cell polarity. *Cytoskeleton (Hoboken)*, 67(9):545–554, Sep 2010.

[5] C. K. Anders and L. A. Carey. Biology, metastatic patterns, and treatment of patients with triple-negative breast cancer. *Clin. Breast Cancer*, 9 Suppl 2:73–81, Jun 2009.

[6] R. Bainer, C. Frankenberger, D. Rabe, G. An, Y. Gilad, and M. R. Rosner. Gene expression in local stroma reflects breast tumor states and predicts patient outcome. *Sci Rep*, 6:39240, 12 2016.

[7] S. Beach, H. Tang, S. Park, A. S. Dhillon, E. T. Keller, W. Kolch, and K. C. Yeung. Snail is a repressor of RKIP transcription in metastatic prostate cancer cells. *Oncogene*, 27(15):2243–2248, Apr 2008.

[8] N. R. Bertos and M. Park. Breast cancer - one term, many entities? *J. Clin. Invest.*, 121(10):3789–3796, Oct 2011.

[9] B. Bonavida. RKIP-mediated chemo-immunosensitization of resistant cancer cells via disruption of the NF-ÎºB/Snail/YY1/RKIP resistance-driver loop. *Crit Rev Oncog*, 19(6):431–445, 2014.

[10] T. Brabletz, D. Lyden, P. S. Steeg, and Z. Werb. Roadblocks to translational advances on metastasis research. *Nat. Med.*, 19(9):1104–1109, Sep 2013.

[11] S. W. Brady, J. A. McQuerry, Y. Qiao, S. R. Piccolo, G. Shrestha, D. F. Jenkins, R. M. Layer, B. S. Pedersen, R. H. Miller, A. Esch, S. R. Selitsky, J. S. Parker, L. A. Anderson, B. K. Dalley, R. E. Factor, C. B. Reddy, J. P. Boltax, D. Y. Li, P. J. Moos, J. W. Gray, L. M. Heiser, S. S. Buys, A. L. Cohen, W. E. Johnson, A. R. Quinlan, G. Marth, T. L. Werner, and A. H. Bild. Combating subclonal evolution of resistant cancer phenotypes. *Nat Commun*, 8(1):1231, 11 2017.

[12] C. Casalou, A. Faustino, and D. C. Barral. Arf proteins in cancer cell migration. *Small GTPases*, 7(4):270–282, 10 2016.

[13] E. Cerami, J. Gao, U. Dogrusoz, B. E. Gross, S. O. Sumer, B. A. Aksoy, A. Jacobsen, C. J. Byrne, M. L. Heuer, E. Larsson, Y. Antipin, B. Reva, A. P. Goldberg, C. Sander, and N. Schultz. The cBio cancer genomics portal: an open platform for exploring multidimensional cancer genomics data. *Cancer Discov*, 2(5):401–404, May 2012.

[14] C. L. Chaffer and R. A. Weinberg. A perspective on cancer cell metastasis. *Science*, 331(6024):1559–1564, Mar 2011.

[15] D. Chatterjee, Y. Bai, Z. Wang, S. Beach, S. Mott, R. Roy, C. Braastad, Y. Sun, A. Mukhopadhyay, B. B. Aggarwal, J. Darnowski, P. Pantazis, J. Wyche, Z. Fu, Y. Kitagwa, E. T. Keller, J. M. Sedivy, and K. C. Yeung. RKIP sensitizes prostate and breast cancer cells to drug-induced apoptosis. *J. Biol. Chem.*, 279(17):17515–17523, Apr 2004.

[16] C. H. Chen, T. C. Hsia, M. H. Yeh, T. W. Chen, Y. J. Chen, J. T. Chen, Y. L. Wei, C. Y. Tu, and W. C. Huang. MEK inhibitors induce Akt activation and drug resistance by suppressing negative feedback ERK-mediated HER2 phosphorylation at Thr701. *Mol Oncol*, 11(9):1273–1287, 09 2017.

[17] Y. Choi, Y. S. Ko, J. Park, Y. Choi, Y. Kim, J. S. Pyo, B. G. Jang, D. H. Hwang, W. H. Kim, and B. L. Lee. HER2-induced metastasis is mediated by AKT/JNK/EMT signaling pathway in gastric cancer. *World J. Gastroenterol.*, 22(41):9141–9153, Nov 2016.

[18] J. Cicenas, E. Zalyte, A. Rimkus, D. Dapkus, R. Noreika, and S. Urbonavicius. JNK, p38, ERK, and SGK1 Inhibitors in Cancer. *Cancers (Basel)*, 10(1), Dec 2017.

[19] A. Colaprico, T. C. Silva, C. Olsen, L. Garofano, C. Cava, D. Garolini, T. S. Sabedot, T. M. Malta, S. M. Pagnotta, I. Castiglioni, M. Ceccarelli, G. Bontempi, and H. Noushmehr. TCGAbiolinks: an R/Bioconductor package for integrative analysis of TCGA data. *Nucleic Acids Res.*, 44(8):e71, 05 2016.

[20] E. Comen, L. Norton, and J. Massague. Clinical implications of cancer self-seeding. *Nat Rev Clin Oncol*, 8(6):369–377, Jun 2011.

[21] K. C. Corbit, N. Trakul, E. M. Eves, B. Diaz, M. Marshall, and M. R. Rosner. Activation of Raf-1 signaling by protein kinase C through a mechanism involving Raf kinase inhibitory protein. *J. Biol. Chem.*, 278(15):13061–13068, Apr 2003.

[22] S. Dangi-Garimella, J. Yun, E. M. Eves, M. Newman, S. J. Erkeland, S. M. Hammond, A. J. Minn, and M. R. Rosner. Raf kinase inhibitory protein suppresses a metastasis signalling cascade involving LIN28 and let-7. *EMBO J.*, 28(4):347–358, Feb 2009.

[23] A. S. Dhillon, S. Hagan, O. Rath, and W. Kolch. MAP kinase signalling pathways in cancer. *Oncogene*, 26(22):3279–3290, May 2007.

[24] B. Doyle, S. Hagan, F. Al-Mulla, L. Scott, S. Harden, J. Paul, H. Mulcahy, G. I. Murray, K. Sheahan, J. O'Sullivan, and W. Kolch. Raf kinase inhibitor protein expression

combined with peritoneal involvement and lymphovascular invasion predicts prognosis in Dukes' B colorectal cancer patients. *Histopathology*, 62(3):505–510, Feb 2013.

[25] J. S. Duncan, M. C. Whittle, K. Nakamura, A. N. Abell, A. A. Midland, J. S. Zawistowski, N. L. Johnson, D. A. Granger, N. V. Jordan, D. B. Darr, J. Usary, P. F. Kuan, D. M. Smalley, B. Major, X. He, K. A. Hoadley, B. Zhou, N. E. Sharpless, C. M. Perou, W. Y. Kim, S. M. Gomez, X. Chen, J. Jin, S. V. Frye, H. S. Earp, L. M. Graves, and G. L. Johnson. Dynamic reprogramming of the kinome in response to targeted MEK inhibition in triple-negative breast cancer. *Cell*, 149(2):307–321, Apr 2012.

[26] E. M. Eves, P. Shapiro, K. Naik, U. R. Klein, N. Trakul, and M. R. Rosner. Raf kinase inhibitory protein regulates aurora B kinase and the spindle checkpoint. *Mol. Cell*, 23(4):561–574, Aug 2006.

[27] R. J. Flockhart, J. L. Armstrong, N. J. Reynolds, and P. E. Lovat. NFAT signalling is a novel target of oncogenic BRAF in metastatic melanoma. *Br. J. Cancer*, 101(8):1448–1455, Oct 2009.

[28] W. D. Foulkes, I. E. Smith, and J. S. Reis-Filho. Triple-negative breast cancer. *N. Engl. J. Med.*, 363(20):1938–1948, Nov 2010.

[29] S. R. Frank, C. P. Kollmann, J. F. van Lidth de Jeude, J. R. Thiagarajah, L. H. Engelholm, M. Frodin, and S. H. Hansen. The focal adhesion-associated proteins DOCK5 and GIT2 comprise a rheostat in control of epithelial invasion. *Oncogene*, 36(13):1816–1828, 03 2017.

[30] C. Frankenberger, D. Rabe, R. Bainer, D. Sankarasharma, K. Chada, T. Krausz, Y. Gilad, L. Becker, and M. R. Rosner. Metastasis Suppressors Regulate the Tumor Microenvironment by Blocking Recruitment of Prometastatic Tumor-Associated Macrophages. *Cancer Res.*, 75(19):4063–4073, Oct 2015.

[31] Z. Fu, P. C. Smith, L. Zhang, M. A. Rubin, R. L. Dunn, Z. Yao, and E. T. Keller. Effects of raf kinase inhibitor protein expression on suppression of prostate cancer metastasis. *J. Natl. Cancer Inst.*, 95(12):878–889, Jun 2003.

[32] G. Gadea and A. Blangy. Dock-family exchange factors in cell migration and disease. *Eur. J. Cell Biol.*, 93(10-12):466–477, Oct 2014.

[33] A. Gandalovičová, D. Rosel, M. Fernandes, P. Veselý, P. Heneberg, V. Čermák, L. Petruželka, S. Kumar, V. Sanz-Moreno, and J. Brábek. Migrastatics-Anti-metastatic and Anti-invasion Drugs: Promises and Challenges. *Trends Cancer*, 3(6):391–406, 06 2017.

[34] J. Gao, B. A. Aksoy, U. Dogrusoz, G. Dresdner, B. Gross, S. O. Sumer, Y. Sun, A. Jacobsen, R. Sinha, E. Larsson, E. Cerami, C. Sander, and N. Schultz. Integrative analysis of complex cancer genomics and clinical profiles using the cBioPortal. *Sci Signal*, 6(269):pl1, Apr 2013.

[35] A. Gharibi, S. La Kim, J. Molnar, D. Brambilla, Y. Adamian, M. Hoover, J. Hong, J. Lin, L. Wolfenden, and J. A. Kelber. ITGA1 is a pre-malignant biomarker that promotes therapy resistance and metastatic potential in pancreatic cancer. *Sci Rep*, 7(1):10060, Aug 2017.

[36] A. E. Granovsky, M. C. Clark, D. McElheny, G. Heil, J. Hong, X. Liu, Y. Kim, G. Joachimiak, A. Joachimiak, S. Koide, and M. R. Rosner. Raf kinase inhibitory protein function is regulated via a flexible pocket and novel phosphorylation-dependent mechanism. *Mol. Cell. Biol.*, 29(5):1306–1320, Mar 2009.

[37] F. H. Groenendijk and R. Bernards. Drug resistance to targeted therapies: déjà vu all over again. *Mol Oncol*, 8(6):1067–1083, Sep 2014.

[38] C. A. Hazzalin, R. Le Panse, E. Cano, and L. C. Mahadevan. Anisomycin selectively desensitizes signalling components involved in stress kinase activation and fos and jun induction. *Mol. Cell. Biol.*, 18(4):1844–1854, Apr 1998.

[39] S. Hipp, D. Berg, B. Ergin, T. Schuster, A. Hapfelmeier, A. Walch, S. Avril, B. Schmalfeldt, H. Hofler, and K. F. Becker. Interaction of Snail and p38 mitogen-activated protein kinase results in shorter overall survival of ovarian cancer patients. *Virchows Arch.*, 457(6):705–713, Dec 2010.

[40] A. Hollestelle, F. Elstrodt, J. H. Nagel, W. W. Kallemeijn, and M. Schutte. Phosphatidylinositol-3-OH kinase or RAS pathway mutations in human breast cancer cell lines. *Mol. Cancer Res.*, 5(2):195–201, Feb 2007.

[41] R. G. Holzer, C. MacDougall, G. Cortright, K. Atwood, J. E. Green, and C. L. Jorcyk. Development and characterization of a progressive series of mammary adenocarcinoma cell lines derived from the C3(1)/SV40 Large T-antigen transgenic mouse model. *Breast Cancer Res. Treat.*, 77(1):65–76, Jan 2003.

[42] J. Hong, J. Zhou, J. Fu, T. He, J. Qin, L. Wang, L. Liao, and J. Xu. Phosphorylation of serine 68 of Twist1 by MAPKs stabilizes Twist1 protein and promotes breast cancer cell invasiveness. *Cancer Res.*, 71(11):3980–3990, Jun 2011.

[43] G. Housman, S. Byler, S. Heerboth, K. Lapinska, M. Longacre, N. Snyder, and S. Sarkar. Drug resistance in cancer: an overview. *Cancers (Basel)*, 6(3):1769–1792, Sep 2014.

[44] T. Ideker, J. Dutkowski, and L. Hood. Boosting signal-to-noise in complex biology: prior knowledge is power. *Cell*, 144(6):860–863, Mar 2011.

[45] J. Insua-Rodriguez, M. Pein, T. Hongu, J. Meier, A. Descot, C. M. Lowy, E. De Braekeleer, H. P. Sinn, S. Spaich, M. Sutterlin, A. Schneeweiss, and T. Oskarsson. Stress signaling in breast cancer cells induces matrix components that promote chemoresistant metastasis. *EMBO Mol Med*, 10(10), Oct 2018.

[46] C. N. Johnstone, Y. E. Smith, Y. Cao, A. D. Burrows, R. S. Cross, X. Ling, R. P. Redvers, J. P. Doherty, B. L. Eckhardt, A. L. Natoli, C. M. Restall, E. Lucas, H. B. Pearson, S. Deb, K. L. Britt, A. Rizzitelli, J. Li, J. H. Harmey, N. Pouliot, and R. L. Anderson. Functional and molecular characterisation of EO771.LMB tumours, a new C57BL/6-mouse-derived model of spontaneously metastatic mammary cancer. *Dis Model Mech*, 8(3):237–251, Mar 2015.

[47] M. R. Junttila, S. P. Li, and J. Westermarck. Phosphatase-mediated crosstalk between MAPK signaling pathways in the regulation of cell survival. *FASEB J.*, 22(4):954–965, Apr 2008.

[48] Y. Kang, P. M. Siegel, W. Shu, M. Drobnjak, S. M. Kakonen, C. Cordon-Cardo, T. A. Guise, and J. Massague. A multigenic program mediating breast cancer metastasis to bone. *Cancer Cell*, 3(6):537–549, Jun 2003.

[49] T. G. Karrison, D. J. Ferguson, and P. Meier. Dormancy of mammary carcinoma after mastectomy. *J. Natl. Cancer Inst.*, 91(1):80–85, Jan 1999.

[50] G. E. Kim, N. I. Kim, J. S. Lee, M. H. Park, and J. H. Yoon. Reduced RKIP Expression is Associated With Breast Neoplastic Progression and is Correlated With Poor Outcomes and Aberrant Methylation in Breast Carcinoma. *Appl. Immunohistochem. Mol. Morphol.*, 25(7):467–474, 08 2017.

[51] M. Kobayashi, K. Harada, M. Negishi, and H. Katoh. Dock4 forms a complex with SH3YL1 and regulates cancer cell migration. *Cell. Signal.*, 26(5):1082–1088, May 2014.

[52] D. C. Koboldt, R. S. Fulton, M. D. McLellan, H. Schmidt, J. Kalicki-Veizer, J. F. McMichael, L. L. Fulton, D. J. Dooling, L. Ding, E. R. Mardis, R. K. Wilson, A. Ally, M. Balasundaram, Y. S. Butterfield, R. Carlsen, C. Carter, A. Chu, E. Chuah, H. J. Chun, R. J. Coope, N. Dhalla, R. Guin, C. Hirst, M. Hirst, R. A. Holt, D. Lee, H. I. Li, M. Mayo, R. A. Moore, A. J. Mungall, E. Pleasance, A. Robertson, J. E. Schein, A. Shafiei, P. Sipahimalani, J. R. Slobodan, D. Stoll, A. Tam, N. Thiessen, R. J. Varhol, N. Wye, T. Zeng, Y. Zhao, I. Birol, S. J. Jones, M. A. Marra, A. D. Cherniack, G. Saksena, R. C. Onofrio, N. H. Pho, S. L. Carter, S. E. Schumacher, B. Tabak, B. Hernandez, J. Gentry, H. Nguyen, A. Crenshaw, K. Ardlie, R. Beroukhim, W. Winckler, G. Getz, S. B. Gabriel, M. Meyerson, L. Chin, P. J. Park, R. Kucherlapati, K. A. Hoadley, J. Auman, C. Fan, Y. J. Turman, Y. Shi, L. Li, M. D. Topal, X. He, H. H. Chao, A. Prat, G. O. Silva, M. D. Iglesia, W. Zhao, J. Usary, J. S. Berg, M. Adams, J. Booker, J. Wu, A. Gulabani, T. Bodenheimer, A. P. Hoyle, J. V. Simons, M. G. Soloway, L. E. Mose, S. R. Jefferys, S. Balu, J. S. Parker, D. Hayes, C. M. Perou, S. Malik, S. Mahurkar, H. Shen, D. J. Weisenberger, T. Triche, P. H. Lai, M. S. Bootwalla, D. T. Maglinte, B. P. Berman, D. J. Van Den Berg, S. B. Baylin, P. W. Laird, C. J. Creighton, L. A. Donehower, G. Getz, M. Noble, D. Voet, G. Saksena, N. Gehlenborg, D. DiCara, J. Zhang, H. Zhang, C. J. Wu, S. Y. Liu, M. S. Lawrence, L. Zou, A. Sivachenko, P. Lin, P. Stojanov, R. Jing, J. Cho, R. Sinha, R. W. Park, M. D. Nazaire, J. Robinson, H. Thorvaldsdottir, J. Mesirov, P. J. Park, L. Chin, S. Reynolds, R. B. Kreisberg, B. Bernard, R. Bressler, T. Erkkila, J. Lin, V. Thorsson,

W. Zhang, I. Shmulevich, G. Ciriello, N. Weinhold, N. Schultz, J. Gao, E. Cerami, B. Gross, A. Jacobsen, R. Sinha, B. Aksoy, Y. Antipin, B. Reva, R. Shen, B. S. Taylor, M. Ladanyi, C. Sander, P. Anur, P. T. Spellman, Y. Lu, W. Liu, R. R. Verhaak, G. B. Mills, R. Akbani, N. Zhang, B. M. Broom, T. D. Casasent, C. Wakefield, A. K. Unruh, K. Baggerly, K. Coombes, J. N. Weinstein, D. Haussler, C. C. Benz, J. M. Stuart, S. C. Benz, J. Zhu, C. C. Szeto, G. K. Scott, C. Yau, E. O. Paull, D. Carlin, C. Wong, A. Sokolov, J. Thusberg, S. Mooney, S. Ng, T. C. Goldstein, K. Ellrott, M. Grifford, C. Wilks, S. Ma, B. Craft, C. Yan, Y. Hu, D. Meerzaman, J. M. Gastier-Foster, J. Bowen, N. C. Ramirez, A. D. Black, R. E. Pyatt, P. White, E. J. Zmuda, J. Frick, T. M. Lichtenberg, R. Brookens, M. M. George, M. A. Gerken, H. A. Harper, K. M. Leraas, L. J. Wise, T. R. Tabler, C. McAllister, T. Barr, M. Hart-Kothari, K. Tarvin, C. Saller, G. Sandusky, C. Mitchell, M. V. Iacocca, J. Brown, B. Rabeno, C. Czerwinski, N. Petrelli, O. Dolzhansky, M. Abramov, O. Voronina, O. Potapova, J. R. Marks, W. M. Suchorska, D. Murawa, W. Kycler, M. Ibbs, K. Korski, A. Spycha?a, P. Murawa, J. J. Brzezi?ski, H. Perz, R. ?a?niak, M. Teresiak, H. Tatka, E. Leporowska, M. Bogusz-Czerniewicz, J. Malicki, A. Mackiewicz, M. Wiznerowicz, X. V. Le, B. Kohl, V. T. Nguyen, R. Thorp, V. B. Nguyen, H. Sussman, D. P. Bui, R. Hajek, P. H. Nguyen, V. T. Tran, Q. T. Huynh, K. Z. Khan, R. Penny, D. Mallery, E. Curley, C. Shelton, P. Yena, J. N. Ingle, F. J. Couch, W. L. Lingle, T. A. King, A. M. Gonzalez-Angulo, G. B. Mills, M. D. Dyer, S. Liu, X. Meng, M. Patangan, F. Waldman, H. Stoppler, W. Rathmell, L. Thorne, M. Huang, L. Boice, A. Hill, C. Morrison, C. Gaudioso, W. Bshara, K. Daily, S. C. Egea, M. Pegram, C. Gomez-Fernandez, R. Dhir, R. Bhargava, A. Brufsky, C. D. Shriver, J. A. Hooke, J. L. Campbell, R. J. Mural, H. Hu, S. Somiari, C. Larson, B. Deyarmin, L. Kvecher, A. J. Kovatich, M. J. Ellis, T. A. King, H. Hu, F. J. Couch, R. J. Mural, T. Stricker, K. White, O. Olopade, J. N. Ingle, C. Luo, Y. Chen, J. R. Marks, F. Waldman, M. Wiznerowicz, R. Bose, L. W. Chang, A. H. Beck, A. M. Gonzalez-Angulo, T. Pihl, M. Jensen, R. Sfeir, A. Kahn, A. Chu, P. Kothiyal, Z. Wang, E. Snyder, J. Pontius, B. Ayala, M. Backus, J. Walton, J. Baboud, D. Berton, M. Nicholls, D. Srinivasan, R. Raman, S. Girshik, P. Kigonya, S. Alonso, R. Sanbhadti, S. Barletta, D. Pot, M. Sheth, J. A. Demchok, K. R. Shaw, L. Yang, G. Eley, M. L. Ferguson, R. W. Tarnuzzer, J. Zhang, L. A. Dillon, K. Buetow, P. Fielding, B. A. Ozenberger, M. S. Guyer, H. J. Sofia, and J. D. Palchik. Comprehensive molecular portraits of human breast tumours. *Nature*, 490(7418):61–70, Oct 2012.

[53] K. Lamiman, J. M. Keller, A. Mizokami, J. Zhang, and E. T. Keller. Survey of Raf kinase inhibitor protein (RKIP) in multiple cancer types. *Crit Rev Oncog*, 19(6):455–468, 2014.

[54] M. C. Lawrence, N. Borenstein-Auerbach, K. McGlynn, F. Kunnathodi, R. Shahbazov, I. Syed, M. Kanak, M. Takita, M. F. Levy, and B. Naziruddin. NFAT targets signaling molecules to gene promoters in pancreatic β-cells. *Mol. Endocrinol.*, 29(2):274–288, Feb 2015.

[55] J. Lee, J. Lee, K. S. Farquhar, J. Yun, C. A. Frankenberger, E. Bevilacqua, K. Yeung, E. J. Kim, G. Balazsi, and M. R. Rosner. Network of mutually repressive metastasis

regulators can promote cell heterogeneity and metastatic transitions. *Proc. Natl. Acad. Sci. U.S.A.*, 111(3):E364–373, Jan 2014.

[56] U. Lee, C. Frankenberger, J. Yun, E. Bevilacqua, C. Caldas, S. F. Chin, O. M. Rueda, J. Reinitz, and M. R. Rosner. A prognostic gene signature for metastasis-free survival of triple negative breast cancer patients. *PLoS ONE*, 8(12):e82125, 2013.

[57] K. Lorenz, M. J. Lohse, and U. Quitterer. Protein kinase C switches the Raf kinase inhibitor from Raf-1 to GRK-2. *Nature*, 426(6966):574–579, Dec 2003.

[58] O. Martinho, S. Granja, T. Jaraquemada, C. Caeiro, V. Miranda-Goncalves, M. Honavar, P. Costa, M. Damasceno, M. R. Rosner, J. M. Lopes, and R. M. Reis. Downregulation of RKIP is associated with poor outcome and malignant progression in gliomas. *PLoS ONE*, 7(1):e30769, 2012.

[59] O. Martinho, F. Pinto, S. Granja, V. Miranda-Goncalves, M. A. Moreira, L. F. Ribeiro, C. di Loreto, M. R. Rosner, A. Longatto-Filho, and R. M. Reis. RKIP inhibition in cervical cancer is associated with higher tumor aggressive behavior and resistance to cisplatin therapy. *PLoS ONE*, 8(3):e59104, 2013.

[60] C. S. Mason, C. J. Springer, R. G. Cooper, G. Superti-Furga, C. J. Marshall, and R. Marais. Serine and tyrosine phosphorylations cooperate in Raf-1, but not B-Raf activation. *EMBO J.*, 18(8):2137–2148, Apr 1999.

[61] R. S. McNeill, D. A. Canoutas, T. J. Stuhlmiller, H. D. Dhruv, D. M. Irvin, R. E. Bash, S. P. Angus, L. E. Herring, J. M. Simon, K. R. Skinner, J. C. Limas, X. Chen, R. S. Schmid, M. B. Siegel, A. E. D. Van Swearingen, M. J. Hadler, E. P. Sulman, J. N. Sarkaria, C. K. Anders, L. M. Graves, M. E. Berens, G. L. Johnson, and C. R. Miller. Combination therapy with potent PI3K and MAPK inhibitors overcomes adaptive kinome resistance to single agents in preclinical models of glioblastoma. *Neuro-oncology*, 19(11):1469–1480, Oct 2017.

[62] E. A. McSherry, K. Brennan, L. Hudson, A. D. Hill, and A. M. Hopkins. Breast cancer cell migration is regulated through junctional adhesion molecule-A-mediated activation of Rap1 GTPase. *Breast Cancer Res.*, 13(2):R31, Mar 2011.

[63] J. Meng, B. Dai, B. Fang, B. N. Bekele, W. G. Bornmann, D. Sun, Z. Peng, R. S. Herbst, V. Papadimitrakopoulou, J. D. Minna, M. Peyton, and J. A. Roth. Combination treatment with MEK and AKT inhibitors is more effective than each drug alone in human non-small cell lung cancer in vitro and in vivo. *PLoS ONE*, 5(11):e14124, Nov 2010.

[64] S. Meng, D. Tripathy, E. P. Frenkel, S. Shete, E. Z. Naftalis, J. F. Huth, P. D. Beitsch, M. Leitch, S. Hoover, D. Euhus, B. Haley, L. Morrison, T. P. Fleming, D. Herlyn, L. W. Terstappen, T. Fehm, T. F. Tucker, N. Lane, J. Wang, and J. W. Uhr. Circulating tumor cells in patients with breast cancer dormancy. *Clin. Cancer Res.*, 10(24):8152–8162, Dec 2004.

[65] A. Messoussi, C. Feneyrolles, A. Bros, A. Deroide, B. Dayde-Cazals, G. Cheve, N. Van Hijfte, B. Fauvel, K. Bougrin, and A. Yasri. Recent progress in the design, study, and development of c-Jun N-terminal kinase inhibitors as anticancer agents. *Chem. Biol.*, 21(11):1433–1443, Nov 2014.

[66] E. L. Moen, S. Wen, T. Anwar, S. Cross-Knorr, K. Brilliant, F. Birnbaum, S. Rahaman, J. M. Sedivy, S. F. Moss, and D. Chatterjee. Regulation of RKIP function by Helicobacter pylori in gastric cancer. *PLoS ONE*, 7(5):e37819, 2012.

[67] R. Mora Vidal, S. Regufe da Mota, A. Hayden, H. Markham, J. Douglas, G. Packham, and S. J. Crabb. Epidermal Growth Factor Receptor Family Inhibition Identifies P38 Mitogen-activated Protein Kinase as a Potential Therapeutic Target in Bladder Cancer. *Urology*, 112:1–225, Feb 2018.

[68] M. Mullooly, P. M. McGowan, S. A. Kennedy, S. F. Madden, J. Crown, N. O' Donovan, and M. J. Duffy. ADAM10: a new player in breast cancer progression? *Br. J. Cancer*, 113(6):945–951, Sep 2015.

[69] F. Mundt, S. Rajput, S. Li, K. V. Ruggles, A. D. Mooradian, P. Mertins, M. A. Gillette, K. Krug, Z. Guo, J. Hoog, P. Erdmann-Gilmore, T. Primeau, S. Huang, D. P. Edwards, X. Wang, X. Wang, E. Kawaler, D. R. Mani, K. R. Clauser, F. Gao, J. Luo, S. R. Davies, G. L. Johnson, K. L. Huang, C. J. Yoon, L. Ding, D. Fenyo, M. J. Ellis, R. R. Townsend, J. M. Held, S. A. Carr, and C. X. Ma. Mass Spectrometry-Based Proteomics Reveals Potential Roles of NEK9 and MAP2K4 in Resistance to PI3K Inhibition in Triple-Negative Breast Cancers. *Cancer Res.*, 78(10):2732–2746, May 2018.

[70] R. Noy and J. W. Pollard. Tumor-associated macrophages: from mechanisms to therapy. *Immunity*, 41(1):49–61, Jul 2014.

[71] M. A. Odenwald, J. R. Prosperi, and K. H. Goss. APC/β-catenin-rich complexes at membrane protrusions regulate mammary tumor cell migration and mesenchymal morphology. *BMC Cancer*, 13:12, Jan 2013.

[72] M. Okada, H. Takeda, H. Sakaki, K. Kuramoto, S. Suzuki, T. Sanomachi, K. Togashi, S. Seino, and C. Kitanaka. Repositioning CEP-1347, a chemical agent originally developed for the treatment of Parkinson's disease, as an anti-cancer stem cell drug. *Oncotarget*, 8(55):94872–94882, Nov 2017.

[73] A. Oppelt, E. M. Haugsten, T. Zech, H. E. Danielsen, A. Sveen, V. H. Lobert, R. I. Skotheim, and J. Wesche. PIKfyve, MTMR3 and their product PtdIns5P regulate cancer cell migration and invasion through activation of Rac1. *Biochem. J.*, 461(3):383–390, Aug 2014.

[74] I. Ortega-Perez, E. Cano, F. Were, M. Villar, J. Vazquez, and J. M. Redondo. c-Jun N-terminal kinase (JNK) positively regulates NFATc2 transactivation through phosphorylation within the N-terminal regulatory domain. *J. Biol. Chem.*, 280(21):20867–20878, May 2005.

[75] H. Peinado, H. Zhang, I. R. Matei, B. Costa-Silva, A. Hoshino, G. Rodrigues, B. Psaila, R. N. Kaplan, J. F. Bromberg, Y. Kang, M. J. Bissell, T. R. Cox, A. J. Giaccia, J. T. Erler, S. Hiratsuka, C. M. Ghajar, and D. Lyden. Pre-metastatic niches: organ-specific homes for metastases. *Nat. Rev. Cancer*, 17(5):302–317, 05 2017.

[76] C. M. Perou. Molecular stratification of triple-negative breast cancers. *Oncologist*, 16 Suppl 1:61–70, 2011.

[77] A. T. Piala, R. Akella, M. B. Potts, S. A. Dudics-Giagnocavo, H. He, S. Wei, M. A. White, B. A. Posner, and E. J. Goldsmith. Discovery of novel TAOK2 inhibitor scaffolds from high-throughput screening. *Bioorg. Med. Chem. Lett.*, 26(16):3923–3927, 08 2016.

[78] J. J. Qin, S. Nag, W. Wang, J. Zhou, W. D. Zhang, H. Wang, and R. Zhang. NFAT as cancer target: mission possible? *Biochim. Biophys. Acta*, 1846(2):297–311, Dec 2014.

[79] M. Radu and J. Chernoff. Recent advances in methods to assess the activity of the kinome. *F1000Res*, 6:1004, 2017.

[80] A. Rana, B. Rana, R. Mishra, G. Sondarva, V. Rangasamy, S. Das, N. Viswakarma, and A. Kanthasamy. Mixed Lineage Kinase-c-Jun N-Terminal Kinase Axis: A Potential Therapeutic Target in Cancer. *Genes Cancer*, 4(9-10):334–341, Sep 2013.

[81] T. Ren, W. Zhang, X. Liu, H. Zhao, J. Zhang, J. Zhang, X. Li, Y. Zhang, X. Bu, M. Shi, L. Yao, and J. Su. Discoidin domain receptor 2 (DDR2) promotes breast cancer cell metastasis and the mechanism implicates epithelial-mesenchymal transition programme under hypoxia. *J. Pathol.*, 234(4):526–537, Dec 2014.

[82] K. Riento and A. J. Ridley. Rocks: multifunctional kinases in cell behaviour. *Nat. Rev. Mol. Cell Biol.*, 4(6):446–456, Jun 2003.

[83] I. Rodriguez-Hernandez, G. Cantelli, F. Bruce, and V. Sanz-Moreno. Rho, ROCK and actomyosin contractility in metastasis as drug targets. *F1000Res*, 5, 2016.

[84] A. Rossello, E. Nuti, S. Ferrini, and M. Fabbi. Targeting ADAM17 Sheddase Activity in Cancer. *Curr Drug Targets*, 17(16):1908–1927, 2016.

[85] D. Ruggero and P. P. Pandolfi. Does the ribosome translate cancer? *Nat. Rev. Cancer*, 3(3):179–192, Mar 2003.

[86] J. Shao, L. Xu, L. Chen, Q. Lu, X. Xie, W. Shi, H. Xiong, C. Shi, X. Huang, J. Mei, H. Rao, H. Lu, N. Lu, and S. Luo. Arl13b Promotes Gastric Tumorigenesis by Regulating Smo Trafficking and Activation of the Hedgehog Signaling Pathway. *Cancer Res.*, 77(15):4000–4013, 08 2017.

[87] J. J. Skinner and M. R. Rosner. RKIP structure drives its function: a three-state model for regulation of RKIP. *Crit Rev Oncog*, 19(6):483–488, 2014.

[88] J. J. Skinner, S. Wang, J. Lee, C. Ong, R. Sommese, S. Sivaramakrishnan, W. Koelmel, M. Hirschbeck, H. Schindelin, C. Kisker, K. Lorenz, T. R. Sosnick, and M. R. Rosner. Conserved salt-bridge competition triggered by phosphorylation regulates the protein interactome. *Proc. Natl. Acad. Sci. U.S.A.*, 114(51):13453–13458, 12 2017.

[89] M. P. Smith and C. Wellbrock. Molecular Pathways: Maintaining MAPK Inhibitor Sensitivity by Targeting Nonmutational Tolerance. *Clin. Cancer Res.*, 22(24):5966–5970, Dec 2016.

[90] P. S. Steeg. Targeting metastasis. *Nat. Rev. Cancer*, 16(4):201–218, Apr 2016.

[91] T. J. Stuhlmiller, H. S. Earp, and G. L. Johnson. Adaptive reprogramming of the breast cancer kinome. *Clin. Pharmacol. Ther.*, 95(4):413–415, Apr 2014.

[92] T. J. Stuhlmiller, S. M. Miller, J. S. Zawistowski, K. Nakamura, A. S. Beltran, J. S. Duncan, S. P. Angus, K. A. Collins, D. A. Granger, R. A. Reuther, L. M. Graves, S. M. Gomez, P. F. Kuan, J. S. Parker, X. Chen, N. Sciaky, L. A. Carey, H. S. Earp, J. Jin, and G. L. Johnson. Inhibition of Lapatinib-Induced Kinome Reprogramming in ERBB2-Positive Breast Cancer by Targeting BET Family Bromodomains. *Cell Rep*, 11(3):390–404, Apr 2015.

[93] M. Sun, S. Gomes, P. Chen, C. A. Frankenberger, D. Sankarasharma, C. H. Chung, K. K. Chada, and M. R. Rosner. RKIP and HMGA2 regulate breast tumor survival and metastasis through lysyl oxidase and syndecan-2. *Oncogene*, 33(27):3528–3537, Jul 2014.

[94] M. Sun, C. X. Song, H. Huang, C. A. Frankenberger, D. Sankarasharma, S. Gomes, P. Chen, J. Chen, K. K. Chada, C. He, and M. R. Rosner. HMGA2/TET1/HOXA9 signaling pathway regulates breast cancer growth and metastasis. *Proc. Natl. Acad. Sci. U.S.A.*, 110(24):9920–9925, Jun 2013.

[95] X. Tan, P. Banerjee, X. Liu, J. Yu, D. L. Gibbons, P. Wu, K. L. Scott, L. Diao, X. Zheng, J. Wang, A. Jalali, M. Suraokar, J. Fujimoto, C. Behrens, X. Liu, C. G. Liu, C. J. Creighton, I. I. Wistuba, and J. M. Kurie. The epithelial-to-mesenchymal transition activator ZEB1 initiates a prometastatic competing endogenous RNA network. *J. Clin. Invest.*, 128(4):1267–1282, Apr 2018.

[96] N. Trakul, R. E. Menard, G. R. Schade, Z. Qian, and M. R. Rosner. Raf kinase inhibitory protein regulates Raf-1 but not B-Raf kinase activation. *J. Biol. Chem.*, 280(26):24931–24940, Jul 2005.

[97] S. Tripathi, M. O. Pohl, Y. Zhou, A. Rodriguez-Frandsen, G. Wang, D. A. Stein, H. M. Moulton, P. DeJesus, J. Che, L. C. Mulder, E. Yanguez, D. Andenmatten, L. Pache, B. Manicassamy, R. A. Albrecht, M. G. Gonzalez, Q. Nguyen, A. Brass, S. Elledge, M. White, S. Shapira, N. Hacohen, A. Karlas, T. F. Meyer, M. Shales, A. Gatorano, J. R. Johnson, G. Jang, T. Johnson, E. Verschueren, D. Sanders, N. Krogan, M. Shaw, R. Konig, S. Stertz, A. Garcia-Sastre, and S. K. Chanda. Meta- and Orthogonal

Integration of Influenza "OMICs" Data Defines a Role for UBR4 in Virus Budding. *Cell Host Microbe*, 18(6):723–735, Dec 2015.

[98] J. Y. S. Tsang, M. A. Lee, T. H. Chan, J. Li, Y. B. Ni, Y. Shao, S. K. Chan, S. Y. Cheungc, K. F. Lau, and G. M. K. Tse. Proteolytic cleavage of amyloid precursor protein by ADAM10 mediates proliferation and migration in breast cancer. *EBioMedicine*, 38:89–99, Dec 2018.

[99] S. Vanharanta and J. Massague. Origins of metastatic traits. *Cancer Cell*, 24(4):410–421, Oct 2013.

[100] Y. Wang, V. Alla, D. Goody, S. K. Gupta, A. Spitschak, O. Wolkenhauer, B. M. Putzer, and D. Engelmann. Epigenetic factor EPC1 is a master regulator of DNA damage response by interacting with E2F1 to silence death and activate metastasis-related gene signatures. *Nucleic Acids Res.*, 44(1):117–133, Jan 2016.

[101] J. A. Westbrook, S. L. Wood, D. A. Cairns, K. McMahon, R. Gahlaut, H. Thygesen, M. Shires, S. Roberts, H. Marshall, M. R. Oliva, M. J. Dunning, A. M. Hanby, P. J. Selby, V. Speirs, G. Mavria, R. E. Coleman, and J. E. Brown. Identification and validation of DOCK4 as a potential biomarker for risk of bone metastasis development in patients with early breast cancer. *J. Pathol.*, Nov 2018.

[102] A. E. Yesilkanal and M. R. Rosner. Raf kinase inhibitory protein (RKIP) as a metastasis suppressor: regulation of signaling networks in cancer. *Crit Rev Oncog*, 19(6):447–454, 2014.

[103] A. E. Yesilkanal and M. R. Rosner. Targeting Raf Kinase Inhibitory Protein Regulation and Function. *Cancers (Basel)*, 10(9), Sep 2018.

[104] K. Yeung, P. Janosch, B. McFerran, D. W. Rose, H. Mischak, J. M. Sedivy, and W. Kolch. Mechanism of suppression of the Raf/MEK/extracellular signal-regulated kinase pathway by the raf kinase inhibitor protein. *Mol. Cell. Biol.*, 20(9):3079–3085, May 2000.

[105] K. Yeung, T. Seitz, S. Li, P. Janosch, B. McFerran, C. Kaiser, F. Fee, K. D. Katsanakis, D. W. Rose, H. Mischak, J. M. Sedivy, and W. Kolch. Suppression of Raf-1 kinase activity and MAP kinase signalling by RKIP. *Nature*, 401(6749):173–177, Sep 1999.

[106] K. C. Yeung, D. W. Rose, A. S. Dhillon, D. Yaros, M. Gustafsson, D. Chatterjee, B. McFerran, J. Wyche, W. Kolch, and J. M. Sedivy. Raf kinase inhibitor protein interacts with NF-kappaB-inducing kinase and TAK1 and inhibits NF-kappaB activation. *Mol. Cell. Biol.*, 21(21):7207–7217, Nov 2001.

[107] M. Yoeli-Lerner, G. K. Yiu, I. Rabinovitz, P. Erhardt, S. Jauliac, and A. Toker. Akt blocks breast cancer cell motility and invasion through the transcription factor NFAT. *Mol. Cell*, 20(4):539–550, Nov 2005.

[108] J. R. Yu, Y. Tai, Y. Jin, M. C. Hammell, J. E. Wilkinson, J. S. Roe, C. R. Vakoc, and L. Van Aelst. TGF-β/Smad signaling through DOCK4 facilitates lung adenocarcinoma metastasis. *Genes Dev.*, 29(3):250–261, Feb 2015.

[109] J. Yun, C. A. Frankenberger, W. L. Kuo, M. C. Boelens, E. M. Eves, N. Cheng, H. Liang, W. H. Li, H. Ishwaran, A. J. Minn, and M. R. Rosner. Signalling pathway for RKIP and Let-7 regulates and predicts metastatic breast cancer. *EMBO J.*, 30(21):4500–4514, Aug 2011.

[110] Y. L. Zhang, R. C. Wang, K. Cheng, B. Z. Ring, and L. Su. Roles of Rap1 signaling in tumor cell migration and invasion. *Cancer Biol Med*, 14(1):90–99, Feb 2017.

[111] J. Zhao and S. Wenzel. Interactions of RKIP with inflammatory signaling pathways. *Crit Rev Oncog*, 19(6):497–504, 2014.

[112] M. Zhao, P. Kim, R. Mitra, J. Zhao, and Z. Zhao. TSGene 2.0: an updated literature-based knowledgebase for tumor suppressor genes. *Nucleic Acids Res.*, 44(D1):D1023–1031, Jan 2016.

[113] M. Zhao, Z. Li, and H. Qu. An evidence-based knowledgebase of metastasis suppressors to identify key pathways relevant to cancer metastasis. *Sci Rep*, 5:15478, Oct 2015.

[114] M. Zhao, J. Sun, and Z. Zhao. TSGene: a web resource for tumor suppressor genes. *Nucleic Acids Res.*, 41(Database issue):D970–976, Jan 2013.

[115] X. Zheng, F. Jiang, M. Katakowski, Z. G. Zhang, Q. E. Lu, and M. Chopp. ADAM17 promotes breast cancer cell malignant phenotype through EGFR-PI3K-AKT activation. *Cancer Biol. Ther.*, 8(11):1045–1054, Jun 2009.

[116] X. Zhou, W. J. Liao, J. M. Liao, P. Liao, and H. Lu. Ribosomal proteins: functions beyond the ribosome. *J Mol Cell Biol*, 7(2):92–104, Apr 2015.